EFFECT OF HIGH-PRESSURE COOLANT ON MILLING Ti-6Al-4V ALLOY WITH EXTERNAL ROTARY LIQUID APPLICATOR

By

Mst. Nazma Sultana

A Thesis
Submitted to the
Department of Industrial & Production Engineering
in Partial Fulfilment of the
Requirements for the Degree
of
DOCTOR OF PHILOSOPHY IN INDUSTRIAL & PRODUCTION ENGINEERING

DEPARTMENT OF INDUSTRIAL & PRODUCTION ENGINEERING
BANGLADESH UNIVERSITY OF ENGINEERING & TECHNOLOGY
DHAKA, BANGLADESH

August 2023

The thesis titled "**Effect of High-Pressure Coolant on Milling Ti-6Al-4V Alloy with External Rotary Liquid Applicator**" submitted by **Mst. Nazma Sultana**, Student No. 0418084002P, Session-April 2018, has been accepted as satisfactory in partial fulfillment of the requirement for the degree of Doctor of Philosophy in Industrial & Production Engineering on August 9, 2023.

BOARD OF EXAMINERS

1.	Dr. Nikhil Ranjan Dhar Professor Department of Industrial & Production Engineering BUET, Dhaka	Chairman
2.	Dr. Ferdous Sarwar Professor and Head Department of Industrial & Production Engineering BUET, Dhaka.	Member (Ex-officio)
3.	Dr. A. K. M. Masud Professor Department of Industrial & Production Engineering BUET, Dhaka.	Member
4.	Dr. Shuva Ghosh Associate Professor Department of Industrial & Production Engineering BUET, Dhaka.	Member
5.	Dr. Fahmida Gulshan Professor Department of Materials and Metallurgical Engineering BUET, Dhaka	Member
6.	Dr. Sukhomay Pal Professor Department of Mechanical Engineering IIT, Guwahati, India	Member (External)

Declaration

It is hereby declared that this thesis or any part of it has not been submitted elsewhere for the award of any degree or diploma.

Mst. Nazma Sultana

This work is dedicated

to my 'loving parents'

Md. Nazrul Islam

And

Lovely Islam

Table of Contents

List of Tables		**vi**
List of Figures		**vii**
List of Symbols		**x**
Acknowledgements		**xiv**
Abstract		**xv**
Chapter 1	**Introduction**	**1**
	1.1 Dry Machining of Ti-6Al-4V Alloy	2
	1.2 Effects of High Cutting Temperature	3
	1.3 Literature Review	5
	1.3.1 Controlling Cutting Temperature in Machining	5
	1.3.2 Effects of HPC in Machining Ti-6Al-4V Alloy	9
	1.3.3 Modelling of Machining Responses	12
	1.3.4 Summary of the Review	20
	1.4 Scope of the Thesis	21
	1.5 Objectives of the Present Work	22
	1.6 Methodology	23
Chapter 2	**Experimental Investigations**	**24**
	2.1 Experimental Procedures and Conditions	24
	2.2 Design and Fabrication of External Rotary Liquid Applicator	30
	2.3 Experimental Results	41
	2.3.1 Chips Morphology	41
	2.3.2 Cutting Temperature	43
	2.3.3 Cutting Force	44
	2.3.4 Surface Roughness	45
	2.3.5 Tool Wear and Tool Life	46
	2.4 Costs Analysis	48
Chapter 3	**Discussions on Experimental Results**	**52**
	3.1 Chips Morphology	52
	3.2 Cutting Temperature	53
	3.3 Cutting Force	55
	3.4 Surface Roughness	56
	3.5 Tool Wear and Tool Life	57
Chapter 4	**Modelling of Machining Responses**	**60**
	4.1 Empirical Modelling of Temperature, Force, and Roughness	60
	4.2 Temperature Modelling using FEM	79
	4.3 Modelling of Cutting Forces	88
	4.4 Validation of the Models	95
Chapter 5	**Conclusions and Recommendations**	**101**
	5.1 Conclusions	101
	5.2 Recommendations	103
References		**104**
List of publications		**123**

List of Tables

Table 2.1	:	Thermo-physical properties of Ti-6Al-4V alloy (Grade 5)	25
Table 2.2	:	Experimental conditions	27
Table 2.3	:	L8 orthogonal array of fluid flow parameters	32
Table 2.4	:	Different cooling configurations for CFD	32
Table 2.5	:	Numerical set up parameters for HPC and RHPC	35
Table 2.6	:	Ranking of process parameters based on Taguchi S/N ratio	40
Table 2.7	:	Costs analysis of milling Ti-6Al-4V alloy with HSS end mill tool under three different cooling conditions	50
Table 2.8	:	Comparative analysis of enhanced machinability with RHPC in milling Ti-6Al-4V alloy with the published literature	51
Table 3.1	:	Percentage reduction of cutting temperature, cutting force, and surface roughness under HPC and RHPC over dry milling	54
Table 4.1	:	Input variables and their corresponding levels	62
Table 4.2	:	BBD based design matrix with corresponding responses	62
Table 4.3	:	Selection of appropriate models for cutting temperature, cutting force, and surface roughness based on model summary	63
Table 4.4	:	Statistical fit values for cutting temperature, cutting force, and surface roughness	64
Table 4.5	:	ANOVA for Reduced Quadratic model of cutting temperature, cutting force, and surface roughness	67
Table 4.6	:	Optimization criteria and constraints for desirability approach	77
Table 4.7	:	Validation test results	77
Table 4.8	:	Physical, mechanical, and thermal properties of Ti-6Al-4V alloy and HSS cutting tool	80
Table 4.9	:	J-C plastic flow stress model parameters for Ti-6Al-4V alloy	80
Table 4.10	:	J-C damage model parameters for Ti-6Al-4V alloy	81
Table 4.11	:	Characteristic values of high-pressure coolant jets in HPC and RHPC	84
Table 4.12	:	APE and MAPE for predicted values of cutting temperature, cutting force, and surface roughness by RSM	96
Table 4.13	:	Experimental and numerically predicted results of average cutting temperature using FEM with their corresponding APE	97
Table 4.14	:	Experimental and predicted values of cutting forces at different cutting conditions	99
Table 4.15	:	Comparative analysis of prediction accuracy of RSM and FEM models	100

List of Figures

Fig. 1.1	:	Types of conventional cutting fluids with their corresponding characteristics	6
Fig. 2.1	:	EDX results of the used Ti-6Al-4V alloy	25
Fig. 2.2	:	Photographic view of experimental set up with embedded nozzles	25
Fig. 2.3	:	Schematic diagram of experimental set up with embedded nozzles	26
Fig. 2.4	:	Tool-work thermocouple set up	28
Fig. 2.5	:	Temperature measurement using tool-work thermocouple method	29
Fig. 2.6	:	CAD drawing of the designed rotary liquid applicator	31
Fig. 2.7	:	Physical model of (a) single nozzle, and (b) multiple embedded nozzles	33
Fig. 2.8	:	Mesh model of (a) single nozzle, and (b) multiple embedded nozzles	33
Fig. 2.9	:	Mesh model with boundary conditions of (a) single nozzle, and (b) multiple embedded nozzles	34
Fig. 2.10	:	Velocity contours of (a) HPC and (b) RHPC	36
Fig. 2.11	:	Temperature contour plot under (a) HPC, and (b) RHPC	37
Fig. 2.12	:	Temperature distribution along the path of a reference line (shown in Fig. 2.11) under (a) HPC, and (b) RHPC	37
Fig. 2.13	:	Influence of oil flow pressure on T in RHPC along the path of a reference a line	38
Fig. 2.14	:	Influence of the flow rate on T in RHPC along the path of a reference line	38
Fig. 2.15	:	Influence of nozzle dia. on T in RHPC along the path of a reference line	38
Fig. 2.16	:	CFD results of cutting temperature under different cooling configurations	39
Fig. 2.17	:	Main effect plot for S/N ratios of temperature with changing input variables	40
Fig. 2.18	:	Photographic views of chips under (a) Dry, (b) HPC, and (c) RHPC conditions in milling at V_c=24 m/min, f=44 mm/min and a_p=0.75 mm	41
Fig. 2.19	:	SEM views of chips under (a) Dry, (b) HPC, and (c) RHPC conditions in milling at V_c=24 m/min, f=44 mm/min and a_p=0.75 mm	42
Fig. 2.20	:	Cross-sectional views of chips under (a) Dry, (b) HPC, and (c) RHPC conditions in milling at V_c=24 m/min, f=44 mm/min and a_p=0.75 mm	42
Fig. 2.21	:	Free layer of chips under (a) Dry, (b) HPC, and (c) RHPC conditions in milling at V_c=24 m/min, f=44 mm/min and a_p=0.75 mm	42
Fig. 2.22	:	Variation of cutting temperature with cutting velocity at different feed rates and depth of cuts under various machining conditions	43
Fig. 2.23	:	Variation of cutting force with cutting velocity at different feed rates and depth of cuts under various machining conditions	44

Fig. 2.24	:	Variation of surface roughness with cutting velocity at different feed rates and depth of cuts under various machining conditions	45
Fig. 2.25	:	Growth of average flank wear with machining time while machining Ti-6Al-4V alloy under different cooling conditions	46
Fig. 2.26	:	Photographic view and SEM image of tool wear under different cooling conditions at V_c=32 m/min, f=68 mm/min, and a_p=1.0 mm	47
Fig. 2.27	:	EDX analysis of the worn tools under different cooling conditions	48
Fig. 3.1	:	Percentage reduction of (a) cutting temperature, (b) cutting force, and (c) surface roughness under HPC and RHPC over dry milling	55
Fig. 4.1	:	Normal probability plots for (a) cutting temperature, (b) cutting force, and (c) surface roughness	65
Fig. 4.2	:	Residual plots for (a) cutting temperature, (b) cutting force, and (c) surface roughness	66
Fig. 4.3	:	Perturbation plots for cutting temperature under (a) Dry, (b) HPC and (c) RHPC conditions [A: cutting velocity, B: table feed, C: depth of cut]	68
Fig. 4.4	:	Perturbation plots for cutting force under (a) Dry, (b) HPC and (c) RHPC conditions [A: cutting velocity, B: table feed, C: depth of cut]	69
Fig. 4.5	:	Perturbation plots for surface roughness under (a) Dry, (b) HPC and (c) RHPC conditions [A: cutting velocity, B: table feed, C: depth of cut]	70
Fig. 4.6	:	3D response surface plots showing the interaction effects of V_c and f on T at 0.75 mm depth of cut under (a) Dry, (b) HPC, and (c) RHPC	71
Fig. 4.7	:	3D response surface plots showing the interaction effects of a_p and f on T at 24 m/min cutting velocity under (a) Dry, (b) HPC, and (c) RHPC	72
Fig. 4.8	:	3D response surface plots showing the interaction effects of V_c and f on F_c at 0.75 mm depth of cut under (a) Dry, (b) HPC, and (c) RHPC	73
Fig. 4.9	:	3D response surface plots showing the interaction effects of a_p and f on F_c at 24 m/min cutting velocity under (a) Dry, (b) HPC, and (c) RHPC	74
Fig. 4.10	:	3D response surface plots showing the interaction effects of V_c and f on R_a at 0.75 mm depth of cut under (a) Dry, (b) HPC, and (c) RHPC	75
Fig. 4.11	:	3D response surface plots showing the interaction effects of a_p and f on R_a at 24 m/min cutting velocity under (a) Dry, (b) HPC, and (c) RHPC	76
Fig. 4.12	:	Ramp graphs of optimization results with desirability value	78
Fig. 4.13	:	Simulation domain with boundary conditions of the milling process	79
Fig. 4.14	:	Variation of average cutting temperature with changing process parameters under dry milling of Ti-6Al-4V alloy	85
Fig. 4.15	:	Effect of cutting velocity on cutting temperature under different cooling conditions	86
Fig. 4.16	:	Effect of feed rate on cutting temperature under different cooling conditions	87

Fig. 4.17	:	Effect of depth of cut on cutting temperature under different cooling conditions	87
Fig. 4.18	:	Geometry of chip formation in slot milling	89
Fig. 4.19	:	Different cutting forces in (a) orthogonal, and (b) oblique cutting	92
Fig. 4.20	:	(a) Chip formation based on Oxley's theory, and (b) relationship between shear velocity and chip flow velocity with cutting velocity	95
Fig. 4.21	:	Validation of simulated results compared to its corresponding experimental results	98
Fig. 4.22	:	Comparative analysis of prediction accuracy of RSM and FEM results	98
Fig. 4.23	:	Experimental and predicted values of cutting forces	100

List of Symbols

V_c : Cutting velocity (m/min)

V_s : Shear velocity (m/min)

f : Feed rate (mm/min)

f_t : Feed/tooth (mm/tooth)

a_p : Depth of cut (mm)

a_e : Radial depth of cut (mm)

V_f : Volumetric flow rate (L/min)

P : Oil flow pressure (bar)

D : Diameter of the tool (mm)

d : Diameter of the nozzle(mm)

r_n : Nose radius of the tool (μm)

CC : Cooling condition

Env. : Environment

CHT : Conjugate heat transfer

T : Cutting temperature (℃)

F_c : Cutting force (N)

F_t : Tangential cutting force component (N)

F_r : Radial cutting force component (N)

F_a : Axial cutting force component (N)

SE : Specific energy (J/mm^3)

K_{tc} : Tangential cutting force coefficients (N/mm^2)

K_{rc} : Radial cutting force coefficients (N/mm^2)

K_{ac} : Axial cutting force coefficients (N/mm^2)

K_{te} : Tangential edge force coefficients (N/mm^2)

K_{re} : Radial edge force coefficients (N/mm^2)

K_{ae} : Axial edge force coefficients (N/mm^2)

R_a : Surface roughness (μm)

V_b : Flank wear (μm)

HSS : High-speed steel

DoE : Design of Experiments

RSM : Response surface methodology

CDA : Composite desirability approach

CCD : Central composite design

BBD : Box-Behnken design

ANOVA : Analysis of variance

∈ : Error

SS_i : Sum of square

MS_i : Mean of square

PC : Percent contribution

R^2 : Coefficient of determination

C_v : Coefficient of variation

D_i : Desirability value

T_c : Total cost ($)

C_m : Machining cost ($)

C_n : Non-machining cost ($)

C_c : Consumable cost ($)

C_E : Energy cost ($)

C_o : Operating cost ($)

C_{HPC} : HPC set up cost ($)

C_A : Rotary applicator's cost ($)

C_{CE} : Cost for operating HPC set up ($)

C_{SE} : Specific energy cost ($/slot)

C_{TC} : Tool change cost ($)

C_R : Re-use cost ($)

C_{chip} : Chip separation cost ($)

C_W : Work-piece cost ($)

C_T : Tool cost ($/piece)

C_{CF} : Cutting fluid cost ($/L)

T_p : Predicted cutting temperature by RSM (ºC)

F_{cp} : Predicted cutting force by RSM (N)

R_{ap} : Predicted surface roughness by RSM (µm)

T_n : Predicted cutting temperature by FEM (ºC)

F_{tm} : Predicted tangential cutting force by mechanistic model (N)

F_{rm} : Predicted radial cutting force by mechanistic model (N)

F_{am} : Predicted axial cutting force by mechanistic model (N)

F_{cm} : Predicted resultant cutting force by mechanistic model (N)

APE : Absolute percentage error

MAPE : Mean absolute percentage error

FEM	:	Finite Element Modelling
CFD	:	Computational Fluid Dynamics
ALE	:	Arbitrary Lagrangian Eulerian
CEL	:	Coupled Eulerian Lagrangian
J-C	:	Johnson-Cook
σ	:	Equivalent true stress
ε	:	Equivalent strain
T_m	:	Melting point temperature of work-piece
T_r	:	Room/ambient temperature of work-piece
A	:	Initial yield stress
B	:	Strain hardening parameter
c	:	Strain rate sensitivity
n	:	Temperature exponent
m	:	Strain hardening exponent
ε^f	:	Equivalent plastic strain rate
D_m	:	Damage parameter (m=1, 2, 3, 4, 5)
G_f		Fracture energy dissipation (mJ/mm^2)
E	:	Young's modulus
υ	:	Poison's ratio
η	:	Inelastic heat fraction
σ_m	:	Hydrostatic pressure
τ_s	:	Shear stress (N/m^2)
σ_s	:	Von-mises shear stress (N/m^2)
σ_f	:	Frictional stress (N/m^2)
σ_n	:	Normal stress (N/m^2)
γ_d	:	Damage initiation parameter
Re	:	Reynolds number
Nu	:	Nusselt number
Pr	:	Prandtl number
ρ	:	Density (Kg/m^3)
h	:	Heat transfer coefficient (W/m^2-°C)
G	:	Surface film coefficient
d	:	Diameter of the nozzle (mm)
V_{jet}	:	Velocity of the jet (m/min)
K_{jet}	:	Thermal conductivity of the jet (W/m-K)

P_s	:	Pressure of the jet at the stagnation point (N/m^2)
γ	:	Shear strain
C_o	:	Strain rate constant
θ	:	Rotation angle (^{o})
θ_s	:	Start angle (^{o})
θ_e	:	Exit angle (^{o})
i	:	Helix/inclination angle (^{o})
δ	:	Lag angle (^{o})
ω	:	Chip velocity angle (^{o})
θ_p	:	Pitch angle (^{o})
φ_n	:	Normal shear angle (^{o})
α_n	:	Normal rake angle (^{o})
β_n	:	Normal friction angle (^{o})
μ	:	Friction coefficient
h_c	:	Chip thickness before cut (mm)
l	:	Length of shear plane (mm)
MQL	:	Minimum quantity lubrication
MQCL	:	Minimum quantity cooling lubrication
NFMQL	:	Nanofluids based minimum quantity lubrication
LN_2	:	Liquid nitrogen
CO_2	:	Carbon-di-oxide
HPC	:	High-pressure cooling
PVD	:	Physical vapor deposition
MRR	:	Material removal rate
TCL	:	Tool-chip contact length
BUE	:	Built-up edge

Acknowledgements

First and foremost, I would like to express my heartiest gratitude to the Almighty for his kindness and blessings to do this job successfully. I'd like to thank everyone associated with the work directly or indirectly. I am eternally thankful to my supervisor Dr. Nikhil Ranjan Dhar, Professor, Department of IPE, BUET, for his constant support, insight, and patience: this thesis would have not been completed without his ongoing trust and, at times, encouragement. His extensive knowledge, thought-provoking thoughts, and excitement for scientific inquiry taught me a lot. My heartfelt sincere thanks to the evaluators of my doctoral thesis, Dr. A. K. M. Masud, Dr. Ferdous Sarwar, Dr. Shuva Ghosh, Dr. Fahmida Gulsan, and Dr. Sukhomay Pal for their insightful comments on how to improve the quality of this thesis. I would like to express my thanks to all the teachers and officers of the Department of IPE, BUET for their direct or indirect support. My grateful appreciation goes to Dr. Prianka B. Zaman, Associate Professor, Department of IPE, BUET, for her insightful recommendations and counsel, which also inspires me to do this work. I am thankful to the Director, DAERS, BUET for generous funding, which allowed me to embark on my path without financial concerns. A special thanks to all employees of the Central Machine Shop and IPE Machine Tools Lab, especially M. C. Dey, M. A. Razzak, S. C. Das, and T. G. Gomes, for their assistance with the experimental work. Additionally, I would like to thank the welding shop staff members, in particular Md. Salauddin, for helping to prepare the designed rotary liquid applicator. I am grateful to the Departments of Materials and Metallurgical Engineering (MME) and Nanomaterials and Ceramic Engineering (NCE) at BUET for their assistance with the thermal calibration and SEM, respectively.

Special thanks to Aurpon Tahsin Shams and Md. Ashab Shakur, Postgraduate students, Department of IPE, BUET for their availability and inspiration throughout the experimental work. Last but not least, I am eternally grateful to my husband Muhammad Anamul Haque and beloved daughter Mahira Sultana Wasfia for their unconditional love and dedication, which inspired and encouraged me to complete this research.

Abstract

An effective cooling approach with appropriate process parameters can enhance the machinability as well as productivity. In this regard, this study focuses on enhancing the machinability of widely used Ti-6Al-4V alloy with the use of high-pressure coolant jets compared to dry milling. A novel rotary applicator has been designed and developed to feed high-pressure coolant jets without any drastic change of solid end mill tool. In order to estimate the optimum design parameters for the proposed cooling approach, Taguchi based DoE has been integrated with CFD analysis. The optimum design parameters for the rotary applicator have been selected as 80 bar pressure, 3.0 L/min oil flow rate, and 0.50 mm nozzle dia. while keeping other factors such as inclination angle, radial distance, and jet inlet to tool distance constant. Average cutting temperature, resultant cutting force, mean surface roughness, and tool wear are all taken into account in evaluating the machinability of various speed-feed combinations. Compared to dry milling, in rotary high-pressure cooling (RHPC), cutting temperature, cutting force, and surface roughness are reduced by 37.56 %, 21.5 %, and 41.3 %, respectively that may be attributed by the cooling and better lubrication effect. Similarly, flank wear is considerably decreased with extended tool life (9 min). Regarding to multi-response optimization, 32 m/min cutting velocity, 26 mm/min table feed rate, and 0.60 mm depth of cut has been selected as the optimal process parameters. Beside this, the complicated milling process has been simulated by using ABAQUS/EXPLICIT 6.14, which took into account the process's dynamic behavior such as variable boundary conditions, Johnson-Cook plastic flow stress model and damage model, thermo-mechanical coupling, film thickness coefficients, load constraints, Coulombs' friction law with hard contact behavior for the detail analysis of temperature distribution. Finally, the simulated results are cross-checked with the real-world experimental results for the validation of the used model. A satisfactory agreement has been obtained with a margin of error of 14.8%. Predicting cutting forces is essential in such machining process since it affects significantly to better surface integrity as well as longer tool life. To assess cutting forces during milling Ti-6Al-4V alloy, an integrated analytical model based on Armarego-Oxley's predictive machining theory and modified Johnson-Cook's material law is proposed incorporating the cooling effect of HPC. The proposed model's viability is confirmed by the real experiment data in milling Ti-6Al-4V alloy. Experimental studies have demonstrated strong agreement. Lastly, a cost analysis is conducted to determine whether the suggested cooling method is economically viable.

Chapter-1

Introduction

Titanium alloys have stimulated attention in a variety of industries (aerospace, automotive, military components, high-pressure cryogenic containers, and chemical industries) and biomedical sectors in the contemporary period due to its certain intrinsic properties. Ti-6Al-4V alloy is one of more than ten distinct types of titanium alloy, and it belongs to the $\alpha+\beta$ alloy group, which accounts for around half of total titanium alloy production [Rashid et al. 2011]. The lightweight, increased toughness, high strength, and corrosion resistance of this unique alloy make it ideal for aircraft applications. Ti-6Al-4V alloy's biocompatibility expands its clinical applications [Lepicka and Gradzka-Hahlke 2016]. This alloy is used in the chemical industry because it has a greater corrosion resistance [Lepicka and Gradzka-Hahlke 2016]. Because of its greater strength-to-weight ratio and improved corrosion resistance at extreme temperatures, Ti-6Al-4V alloy is currently employed more in industrial sectors than other metals such as aluminum and steel.

Despite those advantages, Ti-6Al-4V alloy is more expensive than typical steels and aluminum (the ninth richest element found in the earth's outer layer and the fourth richest metal utilized for structural construction), therefore improved machinability is required [Donachie 2000]. But this super alloy has been classed as a hard to cut alloy because of its poor machinability such as elevated heat generation, high cutting pressures, quick tool wear, increased chatter, and vibration with lower MRR [Sun and Guo 2009]. The growing number of applications for Ti-6Al-4V alloy has prompted scientists and manufacturers throughout the world to look for ways to improve the machinability of this super alloy. Machinability may be improved by using the proper cutting fluids and application procedures, as well as the appropriate cutting tool and the right process parameters [Ezugwu and Wang 1997]. This research project aims to design and develop an applicator for supplying cutting fluids in milling that will greatly improve the machinability of Ti-6Al-4V alloy, allowing for a wider range of applications for this super alloy.

1.1 Dry Machining of Ti-6Al-4V Alloy

Dry machining has achieved more attention in recent years for its higher sustainability since it does not pollute the air or water, and there is no expense associated with cutting fluid disposal. Lower thermal conductivity (7.3 w/m-k) of Ti-6Al-4V alloy is responsible for accumulating more heat on the cutting zone rather than dissipating it, ultimately raising the cutting temperature and reducing tool life [Hong et al. 1993]. Specifically in milling, the tool is subjected to the fluctuation of excessive loading and unloading so the aforementioned difficulties are noted severely [Jawaid et al. 2000]. Surface roughness, dimensional deviation, cutting forces, tool wear, and chip morphology all suffer as a result of entrapped elevated temperature at the cutting zone [Ghani et al. 2013]. At high temperatures (more than 500°C), the Ti-6Al-4V alloy's chemical reactivity increases, resulting in chip welding, galling, and smearing along the tool's cutting edges [Lepicka and Gradzka-Hahlke 2016]. The lower elastic modulus (110 GPa) of Ti-6Al-4V alloy causes more deflection (twice that of steel), posing additional manufacturing challenges. Ti-6Al-4V alloy springs away from the cutting tool at higher pressures, resulting in rubbing rather than cutting, increasing friction, and rising the temperature at the cutting region [Hong et al. 2001]. Rubbing has a detrimental effect on the quality of the surface [Maier et al. 2020].

Due to thermal plastic instability, the formation of saw tooth serrated chips increases the micro fatigue stress on the cutting edges, resulting in severe tool flank wear. Cutting force increases as chip load increases at greater feed rates [Sen et al. 2019]. The cyclic nature of cutting force caused by serrated chip formation, along with the work material's lower elastic modulus, causes significant chatter vibration in the cutting tool, exaggerating cutting force, temperature, and tool wear [Komanduri & Hou 2002]. Caggiano et al. [2017] described dry turning of Ti-6Al-4V alloy as a difficult machining method due to quick tool wear, greater vibrations, and chattering, all of which result in higher cutting forces. Higher cutting temperatures can make machining easier due to thermal softening, but also increase tool wear rate [Kumar et al. 2018]. Recently, advanced tool materials or coated cutting tools (almost 85% of carbide tools are coated) with superior tooling have already been employed to improve machinability. Researchers reported that coated tools perform better than uncoated tools due to three reasons- increased hardness, minimum exposure of tool material, and reduced friction [Debnath et al. 2019]. However, the selection of proper coated tool materials is very crucial because coating material has a relative impact on machinability. In machining Ti64 alloy, Kustas et al. [1997] compared multi-layer coated HSS drills with uncoated drill tools in terms of torque and found that coated drill tools performed better (33% torque reduction). In another investigation, triple-coated carbide tools (TiN/TiCN/TiC) were used to turn titanium alloy and showed improved tool life with less abrasion and diffusion [Nabhani 2001]. The coating materials provide a protective barrier between the tool and the workpiece, preventing tool wear to a higher extent. In spite of those benefits, costs of such coated tool material are higher that restricts its use at a certain range. Moreover, fire risks exist in dry machining of Ti-alloy with coated tool materials, so alternative solution is needed to search out [Taylor et al. 2018].

1.2 Effects of High Cutting Temperature

Due to the conversion of the majority of mechanical energy into thermal energy during machining of Ti-6Al-4V alloy at greater speeds, tremendous amounts of heat are formed, raising the temperature at the chip-tool and tool-work interfaces closer to the cutting zone [Patil et al. 2016]. In real scenario of machining, the temperature at the rake face or tool-chip contacts is the highest, and it generates crater wear due to the secondary heat source [Kumar et al. 2015]. The heat distribution among the chip, tool and workpieces is 80:10:10, respectively. The surface roughness of the machined item, as well as the cutting temperature and forces, are all affected by rubbing in the tertiary heat zone. Excessive tool wear and poor surface integrity are two major problems of higher cutting temperature [Patil et al. 2016]. Abrasive wear exists in all surfaces because of the thermal softening of the work material [Wright and Bagchi 1981]. Due to abrasion or rubbing action of the tool on the work-piece, flank wear occurs mostly at the clearance face of the cutting tool [Childs et al. 2000]. The adherence of workpiece metal on the tool flank face generates a built-up edge (BUE) during high-speed machining of Ti-6Al-4V alloy that increases tool wear at elevated cutting temperature [Ingle 1993]. For high cutting temperatures in high-speed machining with cemented carbide tools, attrition wear may be noticed between tool flank face and work-piece material [Wright and Bagchi 1981]. Excessive pressure and temperature load usually cause crater wear on the rake face of the tool. Diffusion of chip material onto the rake face of the tool happens often at higher pressures and temperatures [Childs et al. 2000]. Chipping is formed by thermal shocking. Fracture wear is the resultant effect of a greater cutting force at a higher temperature under difficult cutting conditions [Wright and Bagchi 1981]. Excessive tool damage on both the flank and rake faces causes notching, which accelerates the failure of worn-out tools [Turkes et al. 2011]. In a word it can be concluded that, severe tool wear may be seen because of the entrapped heat at the cutting zone [Joshi et al. 2014].

In the phenomena of subsurface deformation, cutting temperature plays a crucial role. When thermal softening occurs at a high temperature, the deformation depth under the machined surface increases [Edkins et al. 2014]. Furthermore, cutting temperature hurts the morphology of Ti -6Al-4V alloy chips. In respect of chip formation in Ti-alloy machining, macroscopically long curling chips are observed at high cutting speeds owing to longer tool chip contact length, while shorter or discontinuous chips are observed at low or moderate cutting speeds due to shorter chip tool contact length. Ke et al. [2017] also manifests that temperature has a significant impact on titanium alloy chip deformation. Furthermore, as cutting speed rises, the chip height ratio and serrated pitch rise as well. This is because of titanium alloy's strain and strain rate strengthening properties, as well as its poor heat conductivity [Zhao et al. 2018]. In the metal cutting process, higher cutting temperatures result in a large rise in chip height ratio and serrated pitch. This means that cutting titanium alloy at a lower temperature reduces the contact length between tool and chip, which helps to reduce tool wear and extend tool life. Because the tool-chip contact length is minimized, the frictional heat is also reduced, resulting in less tool wear. This discovery is consistent with previous findings [Bermingham and Kirsch et al. 2011]. Under dry cutting conditions, the morphology of the cross-section of the chip is serrated with adiabatic shear bands. The grains of the shear zone are elongated and fibrous as compared to the surrounding tissues because of shear localization in a very narrower region and thermal softening by the entrapped heat that was also revealed by Aramcharoen [2016]. When the thermal softening effect is dominant, the material experiences shear instability, resulting in the formation of an adiabatic shear band. Cutting temperature is not only responsible for tool life reduction but also degrades the surface quality of machined parts, as evidenced by the reviewed data. This phenomenon is particularly prone to intermittent milling cutting because of the frequent dynamic loading and unloading of the tool. So, choosing the right process parameters could be the solution to get rid of such problematic issues.

1.3 Literature Review

It is already mentioned that machinability of titanium alloys is poor because of its relatively higher hardness and tensile strength, lower modulus of elasticity (50% lower than that of steel), and poor thermal conductivity (approximately 80% lower than that of steel) [Zhang et al. 2018]. The greater 'spring back' and deflection effect of the workpiece is the resultant effect of the lower modulus of elasticity. So, rigid set-ups and enough clearances for tools are required. In the tool contact zones, high pressures and temperatures occur (the tool-to-work piece interface) due to minimum tool-chip contact length. Moreover, during machining, only 25% amount of the heat is carried away by laminar chips and approximately the rest 75% is removed via the tool [Mouritz 2012]. For this, titanium alloys can be machined at lower cutting speeds that affects productivity.

1.3.1 Controlling Cutting Temperature in Machining

Researchers have recently attempted to control cutting temperature by using different approaches of cooling such as conventional flood cooling, minimum quantity lubrication (MQL), minimum quantity cooling lubrication (MQCL), Nanofluids based minimum quantity lubrication (NFMQL), cryogenic cooling (using LN_2 or supercritical CO_2), high-pressure cooling (HPC), and hybrid cooling/lubrication. During machining of Ti-6Al-4V alloy, a massive heat is concentrated at the cutting zone due to the lower conductivity of the workpiece. The entrapped heat increases the local temperature on the machined surface and occurs surface/subsurface damage. Moreover, this higher heat accelerates the tool wear faster and more severely. In another way, this rapid wear is responsible for lower tool life, dimensional inaccuracy, and higher chattering [List et al. 2005]. Based on a statistical report, it was noticed that the machining cost index of titanium alloys is 5.1 while this index value for aluminum is only 0.4 [Mouritz 2012]. In this severe situation of Ti-6Al-4V alloy machining, the use of cutting fluids is one of the possible ways to dissipate extensive heat generation in the cutting zone. Cutting fluids exert three effects-lubrication effects through which it reduces the heat generation, cooling effect through which it carries away heat by convection heat transfer, and cleaning effect by which it flushes away the chips from the machined surface. The cooling and lubrication capability depends on the thermal and mechanical properties of cutting fluids. Cutting fluids with a high specific heat capacity can easily absorb heat and its proper viscosity ensures the oil flow capacity with oil film formation. Conventional cutting fluids can be classified into four categories-straight cutting oil, soluble oil or water emulsions, semi-synthetic and synthetic oil, as shown in Fig. 1.1.

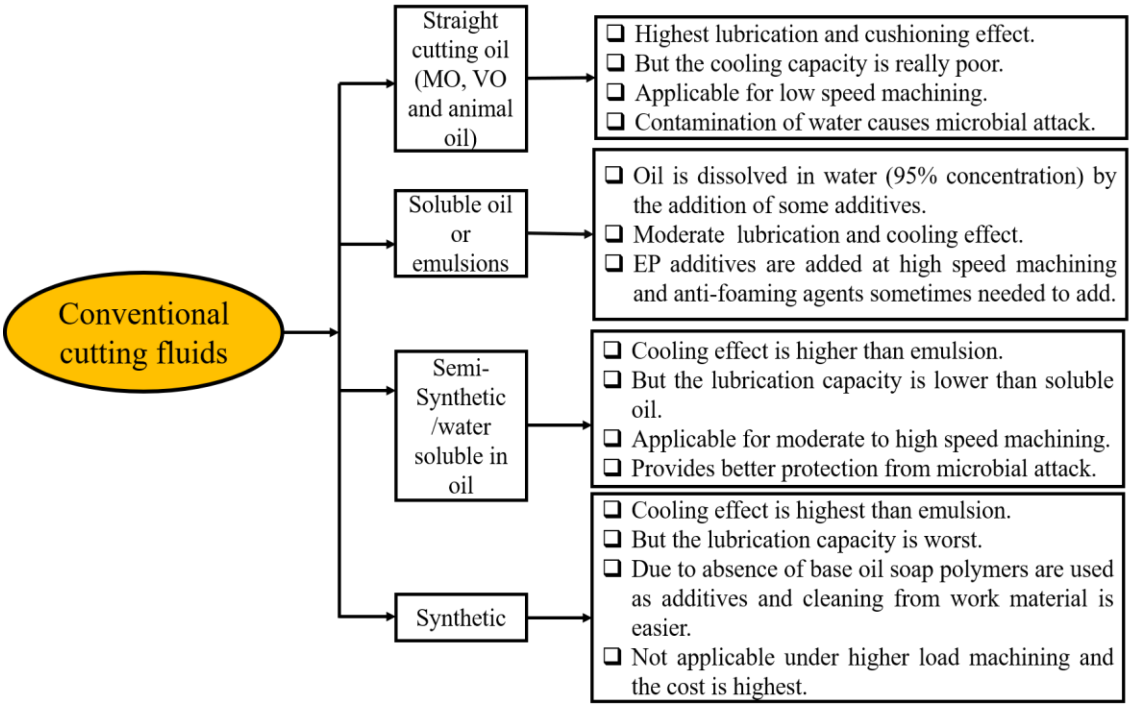

Fig. 1.1 Types of conventional cutting fluids with their corresponding characteristics

Generous or flood application of cutting fluids is the most common idea of coolant application. But this cooling technique is associated with various negative effects (wetting and dirtiness of the working area, frequent corrosion, inhalation problem, biological hazards, water pollution, and soil contamination) related to economy, environment, and health issues [Sultana et al. 2019]. Klocke and Eisenblätter [1997] reported that almost 15% of production costs is due to the application of cutting fluids during machining while the tooling cost is only 4%. In high-speed machining, minimum quantity lubrication (MQL), cryogenic cooling, and high-pressure cooling (HPC) may be possible alternatives. In recent decades, the performance of MQL has been examined by many researchers as a sustainable green cooling technique. Chetan et al. [2016] checked out the effect of sunflower oil as MQL coolant in machining Ti-6Al-4V alloy and observed nose wear in tools. Zaman and Dhar [2020] suggested double jet MQL for machining of Ti-6Al-4V alloy in respect of reducing the cutting temperature, cutting forces, and surface roughness. In another research, MQL has been suggested as a sustainable cooling technique for reducing tool wear, cutting forces, and surface roughness in turning titanium alloy [Shastri et al. 2021]. Garcia and Rebeiro [2015] carried out end milling of Ti-6Al-4V alloy using MQL with compressed air as a cooling technique and vegetable oil as coolant (60 ml/h) by PVD TiCN coated cutting tools. The authors concluded that this green technique provided better lubrication by the formation of thick lubrication film at the cutting interface. Pervaiz et al. [2013] performed a comparative analysis between emulsion-based flood cooling and MQL in turning Ti-6Al-4V alloy by using both coated and uncoated tools. Flood cooling is observed comparatively better cooling strategy than MQL. But, MQL losses its superiority during machining at high cutting speed because the minute amount of mist is easily evaporated before reaching the heated cutting zone with the formation of a temperature blanket [Ezugwu et al. 2005].

For the enhancement of MQL performance in machining, nanofluids are used as a coolant in very recent years. Nanofluids are a liquid suspension of nanoparticles (size 1-100 nm) and base fluids (oil, water, emulsion, or alcohol) [Sultana et al. 2020a]. The superior characteristics of nanoparticles including higher thermal conductivity, better viscosity, better lubricating property with higher rolling, mending, and polishing effects are tried to incorporate with conventional cutting oils. Gupta and Sood [2017] evaluated the effect of different nanoparticles (Al_2O_3, MoS_2 and GO) on surface roughness in machining sticky titanium (grade 2) alloy and found minimum surface roughness for graphene oxide (GO) because of its lower viscosity which ensures better penetration between tool-work interfaces and better settlement of micro-holes into work surfaces. Hegab et al. [2018] recommended the use of multi-walled carbon nanotube (MWCNT) as an additive into vegetable oil for the enhancement of tool life and reduction of power consumption in turning titanium alloy (Grade 5) due to its high heat-carrying capacity. Another researcher, Musavi et al. [2019] observed better surface quality with higher tool life using copper oxide (CuO) and silicon-di-oxide (SiO_2) nanofluids with surfactants in MQL. The surfactant acts as a reinforcement media of nanofluids which helps to retain its better thermophysical properties for a longer time. In turning Ti-6Al-4V alloy, hybrid Al_2O_3 and MWCNT nanofluids reduced surface roughness by 8.72%, cutting forces by 11.8%, and enhanced 23% tool life more than cryogenic cooling. Li et al. [2019] evaluated the effect of 0.01% wt. graphene nanoplatelet into LB 2000 vegetable oil on surface integrity of TC21 alloy during end milling and compared with dry, air cooling, and pure MQL. They reported that the oil films formed by nanofluid provided the highest load-bearing capacity which contributed minimum surface roughness (0.528μm) and lowest micro-hardness (382.73 HV). In sum, it can be said that enhanced thermal property and protective film formation capacity of single or hybrid nanofluids improved machinability more than pure MQL. But the higher cost of nanoparticles and complex synthesis process of nanoparticles as dry powder form limits its industrial use. Minimum quantity cooling lubrication (MQCL) is another way of utilizing a minute supply of coolants into the cutting zone. Emulsion mist is used in MQCL instead of oil mist (MQL). Martinez et al. [2019] noted MQCL as a better option than conventional MQL because of the positive synergistic effects of MQL and supplemental coolant. MQCL can effectively reduce cutting temperature and coefficient of friction between interfaces through its special cooling agent. An investigation was carried out by Pejryd et al. [2010] on the performance of MQCL using ester and fatty alcohol-based oils and air in machining different superalloys. After investigations, MQCL was found a better option for enhancing tool life. Pervaiz et al. [2015] carried out turning of Ti-6Al-4V using MQCL under both external and internal supply systems in respect of surface roughness, cutting force, and tool life. The experimental results revealed that internal MQCL is a better cooling option than external application at high cutting speed. Despite those mentioned benefits of MQCL, the application of a mixture of air and soluble oil creates a mist in the environment with problems of bad odor, bacterial and fungal infections.

The application of non-oil-based cooling media such as liquid nitrogen (LN_2) and carbon dioxide (CO_2) to the cutting zone is popularly known as cryogenic cooling. Acceptability of this cooling technique has been increased due to its better cooling performance and cleanliness [Sultana et al. 2020b]. At normal atmospheric pressure, the boiling temperatures of LN_2 and CO_2 are -196˚C and -78˚C respectively. The comparative benefits of cryogenic cooling over other oil-based cooling techniques are its cleanliness, colorless, odorless, tasteless, non-toxic, non-combustible, and non-corrosive characteristics [Aramcharoen 2016]. After spraying LN_2 into the cutting zone, it is easily evaporated to the atmosphere without any harmful residue and contamination on the environment. Moreover, coolant disposal and post-process cleaning due to contamination is not needed and the process is environmentally friendly compared to conventional cooling fluids [Sultana and Dhar 2021]. Wang and Wang [2019] studied the oxidation wear effect in cryogenic cooling during milling Ti-6Al-4V alloy and compared it with flood cooling. They observed a better cooling effect at 180K temperature and a significant reduction rate of oxidation. Stampfer et al. [2020] applied liquid nitrogen through the rake face of the tool in the orthogonal turning of Ti-6Al-4V alloy for avoiding the quick evaporation of cryogen before proper cooling. Even though cryogenic cooling had shown better performance, still there is a major drawback of using this particular method. Due to the excessively low-temperature coolant, the workpiece hardness increased and hence produces a higher cutting force. Shokrani et al. [2013] observed an increase of hardness from 32 HRC to 42 HRC during machining titanium alloy (Ti-6Al-4V) under cryogenic cooling (LN_2). Some other researchers also faced the same problems while machining titanium alloy under cryogenic cooling [Ahmed et al. 2016]. Moreover, the cost of liquid nitrogen is higher and its maintenance is a complex process. Air cooling is not suitable because of its lower convective heat transfer capacity [Boswell and Chandratilleke 2009].

Application of hybrid cooling such as the combination of MQL and cryogenic cooling has been introduced for the enhancement of machinability of difficult-to-cut metals and alloys. Park et al. [2017] also tried to utilize the synergistic effect of MQL and cryogenic cooling in milling titanium alloy but observed excessive hardening of work surface, higher tool wear, and higher cutting forces. The control of temperature and pressure of cryogen along with the maintenance of oil flow rate in MQL is undoubtedly a complex task that hinders its exposure of use in practical applications. After reviewing the limitations of different progressive cooling techniques in critical machining such as turning and milling, it is clear that the growing demand of MRR necessitated much-increased cutting speed which eventually requires the higher efficiency of cooling methods to cope with the elevated temperature at the cutting zone. On the other hand, because of environmental issues, there is a limit to the use of cutting fluids. Recently, the promising high-pressure cooling (HPC) has been thoroughly examined by various researchers as an alternative to conventional flood cooling [Zaman et al. 2020].

1.3.2 Effects of HPC in Machining Ti-6Al-4V Alloy

High-pressure cooling (HPC) is one of the better options for cooling/lubricating the tool-chip interface during machining [Fratila 2013]. In this technique, high-pressurized water or cutting oil are injected directly to cutting zones in the range of 80 to thousand bar pressure through a nozzle with a small hole (0.15~1 mm) [Courbon et al. 2009]. Compared to conventional cooling, the consumption of cutting fluid is small and due to high pressure, the coolant jets can penetrate tool rake face and chip effectively. Generally, external nozzles are designed to supply these high-pressurized coolant jets for pin-point impingement of cutting fluids. The use of high-pressure coolant jets was introduced in the USA for washing out valuable materials such as gold in mining applications at the beginning 1900s. But the use of HPC jets disclosed its identity as a coolant by Pigott [1953]. The researcher injected the cutting fluid at 2.76 MPa directed towards the clearance face of the tool in high-speed machining of steels and observed temperature reduction by 24ºC with eight times better tool life than low pressurized coolant jets with high flow rate.

The initial goal of HPC was to increase the MRR of advanced materials such as hardened steels, superalloys such as Ni-based alloys, and Ti-based alloys in different industries including gas turbines processing, Cr-Co alloy-based prosthesis, and aerospace industry [Dahlman and Escursell 2004]. Besides the superior cooling effect, this technique provides better control of friction between tool-chip and tool-work interfaces. After the development of the first hydraulic intensifier pump (pressure ≤400MPa) in 1970, the application of HPC jets increased in chronological order. In any machining such as turning, milling, or drilling high cutting temperature hinders the machinability of different metals and alloys. The necessity of HPC jets is unavoidable in high-speed machining of different super alloys such as titanium or nickel-based alloys because of complexities in dry machining with high heat generation [Outeiro et al. 2008]. In continuous machining such as turning, this conventional high-pressure cooling (HPC) technique is to be found more effective in reducing the temperature, minimizing seizure effect, and washing away chips from the cutting zone with good lubrication [Kamruzzaman and Dhar 2009]. Moreover, high pressure coolant jets can easily break continuous chips into smaller ones and reduce the radius of curvature of chips by its wedge action [Podder and Paul 2012]. Naves et al. [2013] proved the efficiency of high-pressure cooling in reducing tool wear by minimizing temperature between tool-chip and tool-workpiece interfaces using cemented coated tools in turning steels. Machining with high-pressure coolant jets is also an alternative to flood cooling in respect of increasing metal removal rate and improving chip control in the manufacturing industry [Mia and Dhar 2018]. Before this, Mia and Dhar [2017] evaluated the positive effects of high-pressure cooling in turning different types of hardened steels (40, 48, and 56 HRC) in terms of cutting temperature and surface roughness. Like hardened steels, high-pressure cooling (HPC) can be considered as a feasible alternative for suppressing cutting temperature and improving productivity in machining Ti-6Al-4V alloy. The high-pressure coolant jets penetrate critical cutting zones and directly extract heat that helps to minimize tool wear effectively. Nandy et al. [2009] studied the effect of high-pressure cooling in turning titanium alloy (Grade 5) in respect of surface roughness, temperature, tool life, cutting forces, and coefficient of friction. The authors concluded that the penetration of high-pressure coolant jets improves the frictional, mechanical, and thermal behavior between tool-chip interfaces effectively. Bermingham et al. [2012] conducted turning of Ti-6Al-4V alloy under high-pressure water emulsion cooling and cryogenic cooling. After experimentation, the authors recommended high-pressure cooling as a better promising technique of extending tool life rather than cryogenic cooling. Slodki et al. [2019] carried out turning of Ti-6Al-4V alloy with the delivery of 70 bar pressurized coolants using coated carbide tools and found better chip formation with process stability.

The above-mentioned research works are conducted in turning steels and titanium alloys under high-pressure cooling. All the research results reported high-pressure cooling as a better option for drastic temperature reduction along with longer tool life and better surface quality. But very limited research works are found on the application of HPC in milling. Bermingham et al. [2014] observed reduced tool wear and higher productivity using HPC over flood cooling in deep pocket milling of Ti-6Al-4V alloy with 20% increased cutting speed. In another research work, the effect of HPC through spindle on surface roughness and tool wear in milling of Ti-6Al-4V alloy has been investigated [Palanisamy et al. 2009]. At higher cutting speed and feed, HPC can enhance 35% machinability through the significant improvement of chip breakability, reduced cutting forces, and better tool life [Courbon et al. 2009]. Senthilkumar et al. [2002] performed milling of Ti-6Al-4V alloy under high-pressure cooling and observed lower surface roughness (< 1μm, better than grinding), cutting forces, and tool wear with shorter chips. Mia et al. [2017a] conducted turning of Ti-6Al-4V alloy using high-pressure cooling and concluded that proper impingement of coolant jets at both rake and flank faces enhances the machinability in terms of reduction cutting forces and surface roughness. High-pressure cooling using specially designed duplex jets can reduce built-up edge (BUE) formation, adhesion, rubbing of chips, tool wear by proper cooling and effective lubrication [Mia et al. 2017b]. In another research, Mia and Dhar [2018] employed twin jets high-pressure cooling in turning Ti-6Al-4V alloy in which one jet was applied into tool-work interface and the other jet was projected to a tool-chip interface for higher heat dissipation from the cutting zones. Due to the high pressure of coolant jets into critical cutting zones, the heat is effectively removed by coolant. Some potential benefits of HPC in machining are:

- The application of HPC jet into the cutting zone appropriately avoids bulk cooling of work surfaces and maintains consistency of machining process.

- HPC jets break out chips effectively and prevent built-up-edge formation. Moreover, the coolant jets wash away chips on the work surface and adhered chips on the tool faces.
- Better heat removal by HPC jets positively affects the surface quality and tool life that have a direct effect on manufacturing economics.

By using HPC, the coolant costs can be reduced, environmental effects can be minimized and machining efficiency can be maximized. By applying HPC at reduced flow rates, the friction and the heat-induced in a tool-chip interface can be reduced. Machining of hard-to-cut alloys at traditional cutting speeds can be performed by using low-cost cutting tools such as high-speed steel (HSS), uncoated or coated carbide tools.

1.3.3 Modelling of Machining Responses

In respect of productivity and expense, machining remains the most important industrial process. So, accurate models for predicting machining outcomes are required. Modelling of machining responses can help to improve the performance and efficiency of the process. Three different approaches - Empirical, numerical, mechanistic, or hybrid methodologies can all be used to predict the machining process [Arrazola et al. 2013]. A well-designed experiment can ensure improved process outputs, reduce development time, and overall cost. The traditional approach of experimental design is empirical. Empirical models express the relationship between inputs and outputs mathematically in the easiest way. Taylor [1967] produced the first empirical model in the field of machining, demonstrating the link between tool life and cutting velocity. Empirical models are frequently utilized by researchers for controlling the machining responses systematically in place of the trial-and-error method. The random selection of input parameters is not always fruitful for a particular process environment. In that case, the design of experiments (DoE) provides a better solution. This term is generally associated with experiments in which the design introduces conditions that directly affect the variation, but may also refer to the design of quasi-experiments, in which natural conditions that influence the variation are selected for observation. In its simplest form, an experiment focuses on predicting the outcome by introducing a change of the pre-conditions, which is represented by one or more independent variables, also referred to as input variables or predictor variables. The change in one or more independent variables is generally hypothesized to result in a change in one or more dependent variables. The experimental design may also identify control variables that must be held constant to prevent external factors from affecting the results. Experimental design involves not only the selection of suitable independent, dependent, and control variables but planning the delivery of the experiment under optimal conditions given the constraints of available resources. One Variable-at-a-time experiment often is unreliable, inefficient, time-consuming, and may yield false optimum conditions for the process. The use of factorial experiments instead of the one-factor-at-a-time method is efficient at evaluating the effects and possible interactions of several factors (independent variables). Analysis of experiment design is built on the foundation of the analysis of variance, a collection of models that partition the observed variance into components, according to what factors the experiment must estimate or test. Statistical thinking and statistical methods play an important role in planning, conducting, analyzing, and interpreting data from engineering experiments. There are many methods of DOE like multi-vari chart, variable search, full factorials, Taguchi methods, response surface methodology (RSM), etc.

Taguchi's method is fractional factorial DoE that requires less time and less complexity without loss of information within the range of interest compared to conventional DoE techniques [Zaman and Dhar 2020]. This method is simple and systematic containing two parts of calculation in respect of optimization- orthogonal array (OA) for designing experiments and signal to noise (S/N) ratios for optimizing the process parameters [Shanmughasundaram and Subramanian 2013]. Mia et al. [2018] employed Taguchi S/N-based optimization in hard turning for finding out the optimum process parameters in minimizing surface roughness, tool wear, and maximizing MRR independently. Zerti et al. [2017] used Taguchi-based optimization in machining AISI D3 steel for minimizing surface roughness, cutting force, and power requirements. Similarly, many researchers used this method for availing the benefit in respect of minimum wastage of time and resources [Sultana et al. 202℃]. RSM is a widely used statistical modelling and optimization technique. RSM is a collection of statistical and mathematical methods for mapping single or multiple responses which are dependent on different input factors within the boundary of interest. Hashmi et al. [2016] determined the optimum combination of input factors for lowering surface roughness during machining of titanium alloy (Ti-6Al-4V) at high speed by using RSM. Vardhan et al. [2017] attempted to find out the optimal value of cutting speed, feed, and depth of cut in milling P20 steel using both Taguchi and RSM methods. Hazir and Ozcan [2019] carried out RSM for modelling surface roughness with the change of speed, feed rate, nose radius, and depth of cut. They observed that spindle speed has the highest influence (28.02%) on surface roughness. Mokhtar and Razak [2021] carried out modelling and optimization of cutting parameters in end milling of Ti–6Al–4V alloy in respect of lowering surface roughness using RSM and concluded that table feed is the most influential factor for changing roughness. Asilturk et al. (2016) examined the effect of speed, feed, depth of cut, and tooltip radius on roughness in turning Co28Cr6Mo using Taguchi-based DoE and response surface methodology (RSM). In that case, 318 rpm speed, 0.1mm/rev feed, 0.7mm depth of cut, and 0.8mm tool tip radius were achieved as the optimum values for minimum surface roughness. So, it can be concluded that RSM is effective in predicting and optimizing responses individually while machining various metals and alloys. In multi-response optimization, the desirability function has already exhibited its usefulness in different machining operations. Gupta et al. [2016] optimized chip tool contact length, cutting force, surface roughness, and tool wear in turning Ti–6Al–4V alloy using RSM-based desirability function. In another research, Nam et al. [2018] carried out drilling of Ti–6Al–4V alloy and optimized drill diameter, speed, feed, and nanofluid concentration in respect of enhancing drilling performances using RSM and desirability function. From the literature review, it is apparent that many researchers conducted the Taguchi method [Ramana and Aditya 2017], RSM [Mello and Pai 2018] and desirability function [Singh et al. 2019] for optimizing cutting speed, feed, depth of cut in turning Ti–6Al–4V alloy rather than milling. Although those empirical models provide satisfactory solutions in some analyses, the use of those specific methods is limited due to constraints involved, assumptions made, and shortcomings of the modelling technique [Dureja et al. 2014].

Statistical modelling only provides the inter-relationships between inputs and outputs linearly, quadratically, and exponentially within a range. Such models are beneficial to define the cause-and-effect relationship, but not to analyze. During machining, plastic deformation of work material and intense friction between tool-work are frequently observed which generates a huge amount of heat among tool-work-chip areas and it impacts the workpiece material behavior along with the quality of the final surface, and the cutting tool's wear directly [Kanellos et al. 2019]. The temperature in the contact between the cutting tool and the workpiece should be kept low to prolong tool life. There is a scientific interest in predicting the temperature of the cutting process considering the process's dynamic behavior. Because of the poor approximation of the realistic metal cutting process resulting in inadequate quality and accuracy of the employed input data, the efficacy of those statistical empirical models to anticipate machining performance has been questioned [Zhang et al. 2015]. In such a situation, the thermo-mechanical behavior of the work material might be regarded as significant input data. Unlike forming, in the metal cutting process, the fracture of excess metal from the machined part as chips forms. Such fracture mechanisms can be explained more accurately using numerical models. The physics-based numerical methods (Finite element modelling (FEM), computational fluid dynamics (CFD) developed at a rapid rate during the last four decades provide a strong foundation for quantitative modelling of various aspects of machining processes. Astakhov and Shvets [2004] provided proper numerical modelling of material flow stress under similar conditions as those observed in machining as well as to model the fracture adequately. Due to advancements in computational methodologies such as adaptive meshing and automated re-meshing, numerical hurdles in solution convergence for severe mesh distortions have been mostly overcome [Arrazola et al. 2013]. However, because of the high computing needs, numerical approaches did not become a valuable and practical tool until the late 1990s.

The Lagrangian technique is extensively used in FEM to characterize the motion specification inside the cutting model [Arizmendi et al. 2008]. However, this method causes model mesh deformation, which may be prevented by using the Eulerian and Arbitrary Lagrangian-Eulerian (ALE) methods. When compared to the Lagrangian model, the latter can be used at the expense of a non-real chip and computation time. The mesh is fixed in space and material flows across the element faces in the coupled Eulerian Lagrangian (CEL) technique comprises of Eulerian workpiece and Lagrangian tool, allowing enormous stresses without mesh distortion concerns [Attanasio et al. 2008]. Until now, most of the researchers worked out with 2D FEM because of its simplicity and less time-consuming nature. Deng et al. [2009] proposed Normalized Cockroft– Latham damage criterion for 2D FEM in respect of analyzing burr formation at the exit of the tool during continuous cutting. Mohammadpour et al. [2010] developed a 2D FEM for showing the stress distribution in turning AISI 1045 steel using Lagrangian mesh formation. Zhang et al. [2015] investigated the Johnson-Cook elastic and fracture model for a variety of values and mesh forms, including Lagrangian, arbitrary Lagrangian, and coupled Eulerian Lagrangian, to determine the best numerical model for analyzing cutting force and chip formation. Setia and Chauhan [2021] used the Johnson-Cook elastic and fracture model in the ABAQUS coupled temperature displacement module to construct a 2D FEM for forecasting cutting temperature in dry turning of composite material. Zang et al. [2018] analyzed serrated chip formation in turning Ti-6Al-4V alloy using 2D FEM by ABAQUS/Explicit.

Milling is more complex than turning and some researchers have also paid their interest to analyze the critical aspects of this. Wu and Zhang [2015] tried to define the differences of the mechanisms intended for dry up milling and down milling forces under a variety of cutting conditions using 2D FEM. As previously stated, it is vital to describe the temperature distribution in the cutting zone under various cutting situations to maintain longer tool life and higher production with improved surface quality. Eltaggaz et al. [2020] developed an integrated 2D numerical model (FEM and CFD) for mapping temperature distribution in turning austempered ductile iron. The mechanism of temperature distribution is more critical in milling due to its complex tool geometry and its intermittent cutting nature with varying chip thickness. Yang and Zhu [2014] developed a 2D temperature model in dry milling of Ti-6Al-4V alloy and observed that temperature at rake face is higher than flank face. A higher temperature was observed at the tool-chip interface that is needed to control. In milling, it is difficult to see the penetration of cutting fluids at the cutting zone, and numerical modelling might help to comprehend such complicated behavior. Karas et al. [2013] constructed a temperature model that took into account the effects of three major heat zones but the cooling process was not taken into account in the developed models. Some researchers are also interested to explain machining processes using 3D FEM. Wu and Zhang [2014] studied cutting temperature, cutting forces, and stress formation in milling titanium alloy using 3D FEM considering thermo-mechanical coupling, damage criterion, elastic and plastic deformation. In another study, Ucun et al. [2017] investigated the effects of cutting process parameters on tool stress, cutting temperature, cutting forces, and chip formations in micro-milling Ti-6Al-4V alloy using 3D FEM. Kanellos et al. [2019] studied the cooling effect on tool life and cutting temperature in turning Ti-6Al-4V alloy using coupled FEM-CFD analysis. Kim et al. [2019] explored the effect of spray angle (0^o,45^o, and 90^o) on the penetration ability of spray cooling in milling titanium alloy using 3D FEM and mentioned that 90^o spray cooling is not suitable for milling. In this study, it is tried to develop a more realistic 3D FEM for measuring the tool-chip interface temperature under three distinct cutting conditions. The 3D tool form, the Johnson-Cook plastic flow model, and the material damage model are all included in the model. This research is unique in that it visualizes the impacts of milling process factors such as speeds, feeds, and depth of cuts, as well as cooling condition, on cutting temperature in milling Ti-6Al-4V alloy. Furthermore, detailed experimental tests were used to confirm the simulation results.

Not being satisfied with such statistical and numerical models which are derived from the experimental data itself, few researchers are also tried to explain the machining processes qualitatively such as mechanistic model to predict cutting force from basic principles considering mechanical properties of materials based on their knowledge. The development of a mechanistic model is important to analyze the cutting process and get a clear understanding of the mechanism involved. Mechanistic models consider physical behaviors related to machining and fitting the outcomes as a function of different inputs [Aristimuno et al. 2018]. These mechanistic models are more accurate and less time-consuming than both empirical and numerical models but complex. In end milling, prediction of cutting force and its coefficients is very important because it provides the relevant information related to vibration, chattering, process stability, tool life, and tool failure which are vital to know for higher productivity with better surface quality. Until now, the very common way of modelling cutting forces in milling is to build up a relationship between a chip and cutting forces as well as to predict cutting force coefficients accurately. Earlier research [Lee and Altintas 1996] manifests that, calibration of cutting force coefficients can be done using two common methods –the transformation method (orthogonal to oblique cutting) and the direct calibration method. In the transformation method, for measuring the cutting force coefficients orthogonal cutting test results related to stress, shear angle, friction angle, and chip thickness were used [Sonawane and Joshi 2010]. This approach was also used in ball-end milling by some researchers [Yang and Park 1991, Budak et al. 2009]. Many researchers also followed the direct calibration method for determining cutting force coefficients [Cheng et al. 1997, Bayoumi 1994, Shin and Waters 1997, Azeem et al. 2004, Ko and Cho 2005]. This approach was firstly introduced by Kline et al. [1982] to set up a mechanistic cutting force model for peripheral end milling. In this approach, the cutting force coefficients were kept constants by assuming the cutting forces directly proportional to the uncut chip thickness. Sutherland and DeVor [1986] extended the application of this model by considering cutter runout and cutter/workpiece flexibility. In the direct calibration method, two ways of modelling are followed-exponential force model or average chip thickness-dependent model and the linear force model or average chip thickness independent model. In the exponential force model, shearing and plowing mechanisms are presented by a single specific force coefficient which is complex to calculate. Altintas and Spence [1991] formulated cutting force coefficients as exponential functions of the average uncut chip thickness which reflect the size effect in metal cutting. Here, the main limitation lies that predicted cutting forces always deviate from measured ones at the peak and valley positions, where the average chip thickness is much different from the instantaneous ones. Wan et al. [2007] and Azeem et al. [2004] enhanced the applicability of this modelling approach by substituting the average chip thickness with the instantaneous ones.

A systematic procedure was finally proposed to determine the instantaneous cutting force coefficients and the cutter run-out parameters for peripheral end milling and ball end milling, respectively. It was found that this substitution made the cutting force model more accurate and efficient. On the other hand, in the linear force model shearing and plowing mechanism are presented by separate cutting and edge force coefficients which is easier to apply in different milling processes such as general end milling [Gradisek et al. 2004], flat end milling, ball-end milling [Narita 2013], bull end milling [Gao et al. 2013]. Later, Zheng et al. [1998] developed a mechanistic model of cutting forces in end milling and face milling involving multi-flute end mill cutter without considering any tool run out. Generally, two types of tools run out are observed- axial run out and radial run-out. Axial run-out has a very negligible effect on the variation of cutting forces so this component is avoided by most researchers but radial run-out has a great significance on the process. Campatelli and Scippa [2012] experimentally validated that the main cutting coefficient for down milling is not only influenced by instantaneous chip thickness but also by cutting speed and feed/tooth considering radial run out. Wan et al. [2010] proposed an efficient way of modelling cutting force in cylindrical end milling considering instantaneous chip thickness, size effect, and tool run out. Gonzalo et al. [2010] proposed a new reverse method of determining specific cutting force coefficients using both instantaneous force values and average force values in flat end milling where the helix angle of the tool was 0º. Wu et al. [2013] deduced a cutting force model for circular end milling considering the effects of tool path curvature, entry and exit angles with a variable and constant radial depth of cut. But, the effect of chatter, vibration, and tool deflections was considered very negligible. Based on the mechanistic model [Lee and Altintas 1996], a force model for ball-end milling was developed by Dikshit et al. [2014] considering both shearing effects due to the chip formation on the rake face and plowing effect on the flank face of the tool. Some researchers developed mechanistic models of cutting force in the micro-end milling process [Joshi and Melkote 2004, Li et al. 2007, Lai et al. 2008, Rao and Shunmugam 2012]. Wang et al. [2014] developed a novel mechanistic model of cutting forces in flat end milling for predicting the shearing and ploughing force efficient as a function of average cutting forces with the variation of feed/tooth at a constant speed, axial and radial immersion. However, those results cannot be directly applied in the macro-end milling process due to the size effect. Deng et al. [2009] proposed a mechanistic force model considering cutting forces at the flank face and bottom face of three flute flat end mill cutter as an exponent function of instantaneous uncut chip thickness in dry end milling. The main drawback of this method is that a larger number of experimental trials are required. However, based on the current state of mechanistic modelling of milling forces, it appears that the majority of studies were simplified without taking into account the cooling effect. There is very few research on modelling cutting forces that take cooling effects into account. Prediction of cutting forces in milling Inconel alloy with wavy edged bull-nose end mill cutters incorporating emulsion cooling strategy was conducted by Okafor & Sultan [2016]. In another study, force models for various shaped wavy edged end mill cutters were developed while using minimum quantity lubrication as a cooling strategy [Sultan & Okafor 2016]. To address the aforementioned gap, another goal of this research is to develop a mechanistic model of cutting force using the average cutting force method in relation to feed/tooth, uncut chip thickness, helix angle, rotation angle, and cooling effect. To incorporate the cooling effect in cutting force modelling, Johnson Cook-Oxley's predictive machining theory [Oxley & Welsh 1963] is integrated with the basic force model provided by Armarego [1985].

1.3.4 Summary of the Review

After reviewing, it can be clearly understood that the prime concern of milling Ti-6Al-4V alloy is to control higher cutting temperature and its detrimental effects. There is a link between cutting temperature and other quality responses including cutting forces, tool wear, tool life, and surface roughness. All these responses are very crucial in assessing the overall performance of the process. At the elevated temperature, plastic deformation and rapid tool wear by adhesive, abrasive, chemical and diffusion wear at the flanks and the crater is found on the cutting tools as the resultant effect. The surface quality of the final shape also deteriorates due to high temperatures. Application of conventional cutting fluids is not effective in high-speed machining, particularly for hard-to-cut alloys. Additionally, flood cooling is not environmentally friendly. Disposal of huge amount cutting fluids occurs soil contamination and water pollution. Recycling and reuse of used cutting fluids are further problems. Application of different progressive ways of MQL is also a better option for lubrication but it has some limits to reach critical zones during interrupt cutting processes such as milling. Excessive work hardening for bulk cooling and complex control of temperature and pressure of cryogen limits the use of cryogenic cooling. In such a situation, high-pressure cooling (HPC) is a promising technique in high production machining that can penetrate into the critical zones more effectively than lower pressure cooling jets. In HPC, the energy consumption is higher which is compensated by higher MRR and lower tool wear with better surface quality. Considering the potential benefits, HPC is considered a sustainable cooling approach. The performance of HPC is influenced by workpiece and tool material, tool geometry, oil pressure and flow rate, nozzle position, cutting velocity, feed, and depth of cut. Unfortunately, no research work has been carried out yet regarding the effect of the HPC process parameters on milling performances. Detail analysis about the influence of HPC on milling performance is badly needed. This research has been motivated to explore the applicability of HPC using newly designed rotary liquid applicator in end milling of Ti-6Al-4V alloy and to compare its performance with dry and conventional HPC. Moreover, modelling of machining responses and multi-response optimization have been carried out.

1.4 Scope of the Thesis

The main focus of this study is to explore the effect of high-pressure coolant jets by using a newly designed rotary applicator on the machinability of Ti-6Al-4V alloy in surface milling by end mill cutter under different cutting conditions. Beside this, modelling and optimization of quantitative measures of milling performance such as cutting temperature, cutting force, and surface roughness have been carried out. **Chapter 1** begins with the introduction followed by literature review regarding the details of problems regarding dry machining of Ti-6Al-4V alloy, effects and controlling of high cutting temperature in machining Ti-6Al-4V alloy, the possible benefits of high-pressure cooling, and modelling of machining responses. The objectives of the current research, and a full overview of the methodology, are also discussed in this section.

Chapter 2 presents the details of the experimental investigations. The design and fabrication of the external rotary liquid applicator are also discussed in this chapter. Finally, graphical presentation of the experimental data for the variables of chip morphology, cutting temperature, cutting forces, tool wear, and surface roughness are provided.

In particular, **Chapter 3** discusses the reasons for the change of responses with changing process parameters based on the experimental results. In comparison to dry and HPC, the effects of RHPC on those responses are also explained.

Chapter 4 demonstrates the empirical modelling of machining responses such as cutting temperature, cutting force and surface roughness. Numerical evaluation of cutting temperature by FEM and mechanistic modelling of cutting forces are also presented. Finally, a comparative validation test is provided to show the accuracy of different modelling techniques in this specific analysis within a boundary of machining conditions.

Chapter 5 contains a summary of conclusions of the current study and recommendations for future scope of this research. References and a list of publications are provided at the end.

1.5 Objectives of the Present Work

After analyzing the aforementioned literature review, it can be revealed clearly that precision milling of the extensively used Ti-6Al-4V alloy without a coolant is challenging. In this context, the adoption of a more intelligent cooling system based on rotating high-pressure coolant jets has been prioritized. The objectives of the present work are as follows:

(a) Design and fabrication of a suitable external rotary liquid applicator for impinging high-pressure coolant jet along the flute length of the end mill tool effectively.

(b) Experimental investigation on the effects of high-pressure coolant jets using rotary liquid applicator in end milling of Ti-6Al-4V alloy in respect of:

- i) Chips morphology
- ii) Cutting temperature
- iii) Cutting forces
- iv) Surface roughness
- v) Tool wear and tool life

(c) Development of mathematical models for predicting the quantitative responses (cutting temperature, cutting force, and surface roughness) and determining the significance of process parameters on the mentioned responses.

(d) Development of a numerical model for predicting cutting temperature in end milling of Ti-6Al-4V alloy under three different cutting environments using ABAQUS-ANSYS analysis.

(e) Development of an analytical mechanistic model for principal cutting force from the characterization of physical processes taking place during end milling and its validation.

1.6 Methodology

Experimental investigations and modelling of responses in milling of Ti-6Al-4V alloy with different cutting conditions are the main focus of this study. To fulfill this objective a systematic approach has been followed which is outlined below:

(i) An external rotary liquid applicator with an embedded nozzle has been designed and fabricated for proper impingement of a high-pressure coolant jet along the flute length. For selecting the design parameters of the proposed applicator, CFD with Taguchi based Design of Experiment (DoE) has been followed.

(ii) The systematic experimental study has been conducted to find out the effects of designed rotary applicator and process parameters (cutting speed, table feed, and axial depth of cut) on performance (cutting temperature, cutting force, tool wear, and surface roughness) of end milling Ti-6Al-4V alloy by four flute HSS end mill tools.

(iii) Chips morphology has been analyzed by using Scanning Electron Microscopy (SEM) for finding out the nature of chips under different cooling conditions.

(iv) The growth of tool flank wear has been observed with machining time using a metallurgical microscope. SEM has also been carried out to see the actual effects of cutting environment on end mill tool.

(v) RSM has been used to predict milling performance by using Design Expert v. 12.0. Finally, the Validation of the developed models is verified by comparing the predicted results with the real experimental results. Additionally, the desirability approach has been followed for multi-response optimization.

(vi) Numerical analysis of cutting temperature with different cutting conditions has been performed by using ABAQUS. Prediction of cutting forces in milling has been done by using mechanistic model incorporating the cooling effect of high-pressure coolant jets.

Chapter-2

Experimental Investigations

Application of cutting fluids to avoid poor machinability of Ti-6Al-4V alloy is recommended by many researchers [Mia and Dhar 2015]. Due to several appealing intrinsic qualities, high-pressure cooling (HPC) is considered as a superior technique of providing cutting fluids at the cutting zone during machining [Kamruzzaman et al. 2017]. However, when using HPC in machining, the following considerations must be kept in mind.

- Effective and uniform cooling along with the avoidance of bulk cooling to control any unfavorable metallurgical changes of the tool and workpiece.
- Controlling the oil flow rate and pressure to the required levels.
- Effective reuse of cutting fluids for preventing its excess consumption.

The comparative performance evaluation of the designed applicator in respect of enhancing machinability is performed in this chapter in brief.

2.1 Experimental Procedures and Conditions

Ti-6Al-4V alloy (Grade 5, hardness 37HRC) has been selected as the workpiece material in this investigation due to its reduced density and superior strength-to-weight ratio when compared to conventional steels and Aluminum. The chemical composition of the used Ti-6Al-4V alloy can be specified as follows: 6.14% Al, 4.44% V, 0.40% Fe, 1.19%O, 0.012% N, 4.13% C, and 83.71% Ti which are collected from EDX analysis as shown in Fig. 2.1. Table 2.1 mentioned the thermos-physical properties of the Ti-6Al-4V alloy used in this investigation which are gathered from a prior study conducted by Mia et al. [2017b]. Milling experiments have been conducted on a vertical knee and column milling machine (7.5hp, Sunlike, China). High-speed steel (HSS-E-PM) end mill tool (Brand name: DORMER; Type: Finishing, No. of flutes: 4) with hardness 65 HRC has been chosen due to its cost effectiveness. It is very well known that the productivity and performance of carbide tools are better than HSS tools at higher cutting speed but the performance of these HSS-E-

PM tools is acceptable within the range of 30~50 m/min speed [Zeman et al. 2017]. In this study, the maximum cutting speed is kept 32 m/min, so it is considered more economical to use the HSS-E-PM end mill. The geometry of the used tool can be specified as follows: actual cutting length 27 mm, total length 83 mm, tool dia. 12 mm, no. of flutes 4, helix angle 30º, radial rake angle 5º, clearance angle 15º, and square shaped end face.

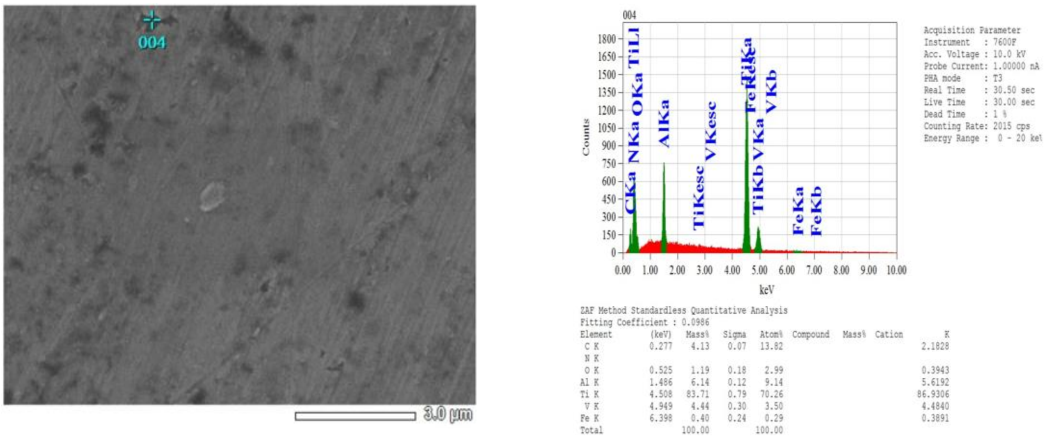

Fig. 2.1 EDX results of the used Ti-6Al-4V alloy

Table 2.1 Thermo-physical properties of Ti-6Al-4V alloy (Grade 5)

Melting point (ºC)	Specific density (g/cm^3)	Thermal conductivity (W/m-k)	Specific heat (J/g-ºC)	Ultimate tensile strength (MPa)	Young's Modulus (N/m^2)	Yield strength (MPa)	Hardness (HRC)
1604	4.43	6.7	0.5263	1050	110	950	37

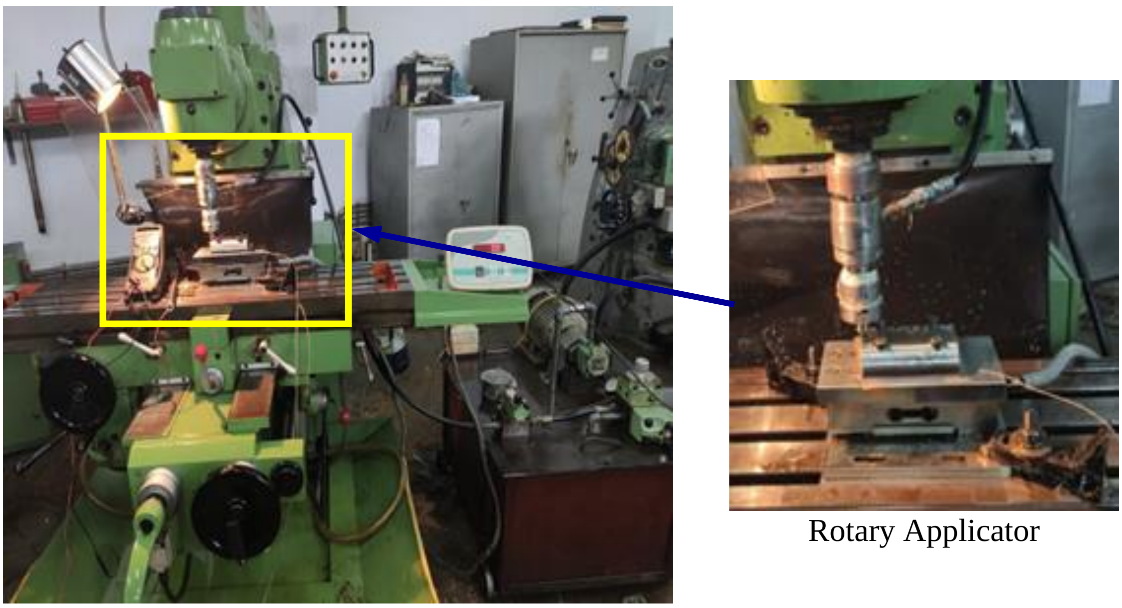

Fig. 2.2 Photographic view of experimental set up with embedded nozzles

Because the employed tool material is HSS, the cutting velocity (V_c) has been set to the lower range 16~32 m/min. Similarly, for avoiding the productivity loss the feed rate (f) is kept higher 22~68 mm/min as well as the axial depth of cut (a_p) lies between 0.50~1.00 mm but radial depth of cut (a_e) has been kept constant. Milling has been performed under three distinct cutting conditions: dry, conventional high-pressure cooling (HPC), and rotary high-pressure cooling (RHPC). The supremacy of HPC over flood cooling has already been discussed. Two major functions were tried to fulfill by using the fabricated HPC set up: creating high pressure and supplying uninterrupted flow of high-pressurized coolant jets in an economic way. For continuous supply of cutting fluids in HPC, 30^o inclined nozzle with 2.0 mm dia. has been used with maintaining constant flow rate of 2.0 L/min and oil pressure of 80 bar positioning 20 mm away from the stagnant point of sprayed jets. To avoid the formation of mist, severe bacterial and allergic infection caused by the frequent use of water-based emulsions, biodegradable, environmentally friendly, and fire-resistant VG-68 ISO grade hydraulic oil has been used as a high-pressure cutting fluid.

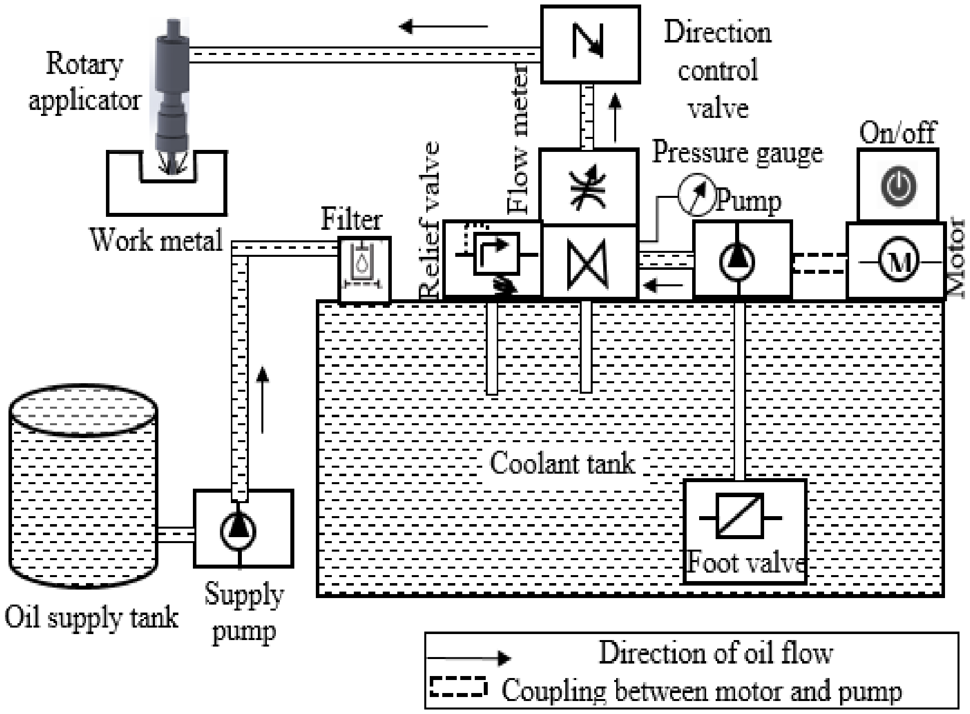

Fig. 2.3 Schematic diagram of experimental set up with embedded nozzles

VG-68 ISO grade hydraulic oil is a mixture of vegetable oil and additives that boost resistance to oxidation and metal passivation. The specific characteristics of this used cutting fluid are: density 932 Kg/m^3 at 20°C, Viscosity index 68 at 40°C, flash point 300°C [Mia and Dhar 2019]. Furthermore, some researchers have already used this cutting oil as coolant jets in milling [Mia et al. 2017c] and turning [Saha et al. 2022] of difficult to cut alloys at lower cutting speed. The efficiency of using cutting fluids depend on two factors- sufficient supply and proper positioning [Astakhov & Godlevskiy 2012]. Without satisfying those aspects, any cutting fluid cannot perform satisfactorily. Beside this, proper cutting fluid penetration at the secondary shear zone is a challenge in intermittent milling due to the complex tool geometry and critical chip creation. In this situation, a unique cooling method RHPC with an external rotary applicator has been used. Figs. 2.2 and 2.3 depict a photographic and schematic view of the used RHPC setup. The experimental investigations are designed to determine the machinability of Ti-6Al-4V alloy in respect of cutting temperature, cutting force, surface roughness, and tool wear. Table 2.2 lists the experimental details of conducted milling tests. After each trial of experiment, chips are collected and analyzed.

Table 2.2 Experimental conditions

Machine tool	**:**	Vertical knee and column type milling machine
Work-material	**:**	Ti-6Al-4V alloy (Grade 5), Dimension: 100×50×25 mm
Tool type	**:**	HSS end mill tool (Dia. 12 mm)
Cutting fluid type	**:**	Cutting oil (VG-68)
Cutting conditions	**:**	Dry, HPC, and RHPC
Process parameters		
Cutting velocity (V_c)	:	16, 24, 32 m/min
Feed rate (f)	:	22, 44, 68 mm/min
Depth of cut (a_p)	:	0.50, 0.75, 1.00 mm
HPC parameters		
Oil flow rate	:	2.0 L/min
Nozzle type	:	External
No. of nozzles	:	1
Nozzle dia.	:	2.00 mm
Nozzle position	:	20 mm away from stagnant point
RHPC parameters		
Oil flow rate	:	2.0 L/min
Nozzle type	:	Embedded and external
No. of nozzles	:	4
Nozzle dia.	:	0.50 mm
Nozzle position	:	20 mm away from stagnant point
Responses	:	Chips morphology, cutting temperature (T), cutting force (F_c), tool wear and tool life, surface roughness (R_a).

Cutting temperature (T) has been measured by using the tool-work thermocouple method under all cutting conditions, utilizing Ti-6Al-4V alloy and HSS end mill tool as dissimilar metals followed by one of the published research projects [Yashiro et al. 2013].

This approach is straightforward but accurate for monitoring the cutting temperature across the full contact region within a large temperature range. The specific tool-work thermocouple loop for measuring the generated electromotive force is shown in Fig. 2.4. Two wires are utilized to connect the tool and the work. One end of the thermocouple wire has been attached to the sliding rod of high-speed steel (the same material as the tool) in contact with the tool (acting as the hot junction), and the other end has been linked to the multi-meter (Rish multi 15S, India). Similarly, the other thermocouple wire has been linked to the work-piece (acting as the cold junction), and the other end of that wire has similarly been connected to the multi-meter. Both the Ti-6Al-4V alloy and the HSS end mill tool are properly insulated. Mica-sheet has been placed slightly beneath the workpiece to insulate it from the milling table, and the shank of the end mill tool has been coated with insulated cloth to insulate it from the spindle. Due to the temperature difference between the tool and the work, a finite voltage is formed throughout the cutting action. During cutting, the tool acts like a heat sink and maximum temperature is located at the tool tip. Due to the complex cutting mechanism of milling, it is not possible to hold the HSS rod at the closest location of tool tip so this approach is unable to measure the highest cutting temperature, same phenomena was also noticed in another research [Yashiro et al. 2013]. The measured temperature is always lower than the maximum temperature which is the main drawback of this measuring approach.

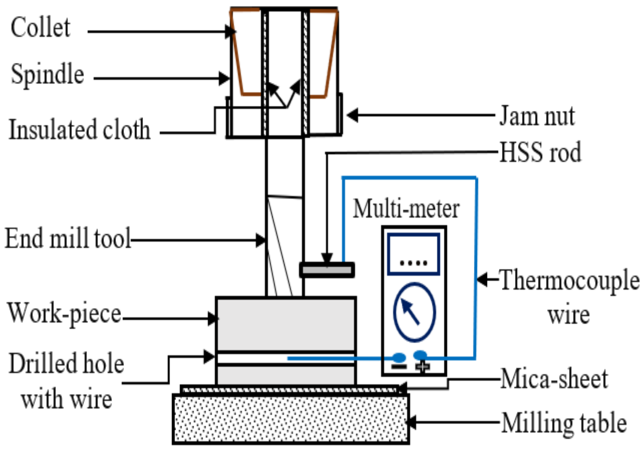

(a) Schematic view

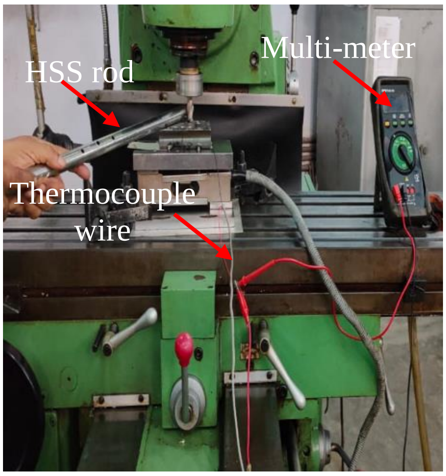

(b) Photographic view

Fig. 2.4 Tool-work thermocouple set up

Because the thermocouple connection between Ti-6Al-4V alloy and HSS tool is not standard so calibration is required to define the relationship between voltage generation and real temperature for the tool-work combination being employed. To facilitate calibration, a long length of chip and a segment of the HSS tool have been brazed together at one end, rather than the actual work material and end mill tool. A graphite block is placed on the porcelain of an electrically powered radiant heater to act as a heat sink. In the graphite block, the brazed junctions of the tool-work thermocouple and the standard thermocouple (K-TYPE) are kept adjacent to one another. The chip and HSS tool segment's other ends are connected via the digital multi-meter. The porcelain and graphite blocks are then electrically heated, and the brazed connection acted as the thermocouple's hot junction. The multi-meter has been used to record the thermoelectric voltage created, as well as the direct temperature (°C) of the heated graphite block using a digital thermometer (Eurotherm, UK). Finally, the calibration curve is shown in Fig 2.5 with the observed voltage and temperature. Figs. 2.5(a) and 2.5(b) depict the photographic perspective of the setup for tool-work thermocouple and calibration curve, respectively. A nearly linear relationship between temperature and voltage has been established with a coefficient of determination of 98.74 percent. To calculate the temperature of the chip-tool interface from the thermocouple voltage the following Eqn. (2.1) has been used. Cutting force (F_c) was measured as the resultant force of this three: feed force (F_t), radial force (F_r), and axial force (F_a) by using a 3D KISTLER dynamometer equipped with a load cell and charge amplifier. To calculate F_c, Eqn. (2.2) has been used:

$$\text{Temperature } (^0\text{C}) = 6.59 + 80.13 \text{ voltage (mV)} \quad (2.1)$$

$$F_c = \sqrt{F_t^2 + F_r^2 + F_a^2} \quad (2.2)$$

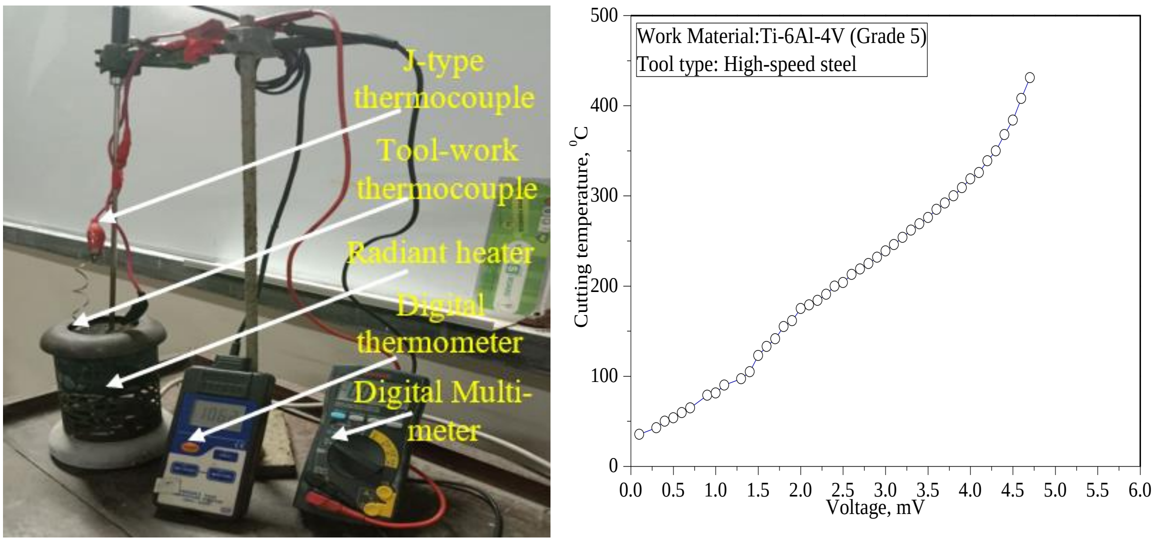

(a) Tool-work thermocouple (b) Calibration curve

Fig. 2.5 Temperature measurement using tool-work thermocouple method

Surface roughness has been measured for each slot using a portable Talysurf roughness checker (Surtronic 3+, Rank Hobbs, UK), with a sampling length of 0.80 mm. The rise of flank wear with machining time at constant velocity-feed-depth of cut has been monitored by using a metallurgical microscope (Carl Zeiss, Germany) equipped with a micro-meter with a resolution of 1 μm for the purpose of determining tool life under three separate cutting scenarios where the pattern and severity of tool wear was detected by using a high-resolution scanning electron microscope (JEOL-JSM-7600F).

2.2 Design and Fabrication of External Rotary Liquid Applicator

Earlier research studies reveal that, although HPC is an excellent cooling approach in chips management, reducing residual stress, and minimizing tool wear but in some cases, the cooling capability of HPC is limited by the inaccurate design parameters [Habak and Lebrun 2011, Li et al. 2018, Diniz and Micaroni 2007]. Beside this, in milling it is more critical to supply coolant jets effectively at the cutting zone because of the complex helical shaped end mill tool. In such situation, RHPC is proposed keeping mind the following facts:

- To achieve the proper penetration of cutting fluids focusing the multiple cutting edges with the use of identical number of outlets/embedded nozzles.
- To avoid the destructive impacts of internal cooling in respect of tool's strength.
- To reduce the hassles of positioning separate nozzles.

To achieve the mentioned goals, the detail analysis regarding coolant jets delivery through nozzle with suitable parameters is badly needed. Researchers suggested computational fluid dynamics (CFD) as a more economic and time-efficient method of analyzing such fluid flow mechanical problems [Zhang and Coddet 2016]. Following that, in this study, CFD analysis has been carried out to analyze the cooling effect of HPC and RHPC on a rotating end mill cutter with a diameter of 12.0 mm by using ANSYS Fluent 19.0. Moreover, the effect of design parameters such as nozzle diameter, volumetric flow rate, and oil flow pressure are also analyzed while the inclination angle, stand-off distance, radial distance is kept constant at 30º, 20 mm, and 14 mm, respectively. Many researchers have already suggested to find out the appropriate level of oil flow pressure because insufficient pressure hinders proper penetration of cutting fluids at the cutting zone [Obikawa and Yamaguchi 2013]. Along with this, it is needed to optimize oil flow rate without compromising the machinability because massive oil consumption is non-economic, unhygienic, and hazardous. Nozzle size is another key influential factor affecting the fluid flow. It has been observed that the velocity of the cutting fluids may vary with the change of nozzle diameter while flow rate is kept fixed [Courbon et al. 2011]. In a word, it can be agreed that it is mandatory to optimize the oil flow pressure, flow rate, and nozzle dia. for achieving proper cooling in a systematic way.

For reducing computational time, the rotational speed of the cutter has been fixed at 850 RPM. The design of the external rotary liquid applicator is shown in Fig. 2.6 with marking the zone for CFD analysis. But, prior to this, it is mandatory to plan 'how to conduct the simulation tests' with the variation of boundary conditions. Taguchi based design of experiment (DoE) is a popular structured approach of process designing, and analyzing experiments with minimum wastage of money and time for getting a valid and reliable conclusion. For the current research work, Taguchi-based DoE has been employed to conduct experiments as well as to analyze the impacts of the selected design parameters on the given response based on the CFD results. Total eight simulation runs have been planned to carry out for RHPC as per the design of Taguchi based DoE. Cooling efficiency has been quantified by the simulation results in respect of temperature. Table 2.3 summarizes the simulation trials with the variation of selected input parameters.

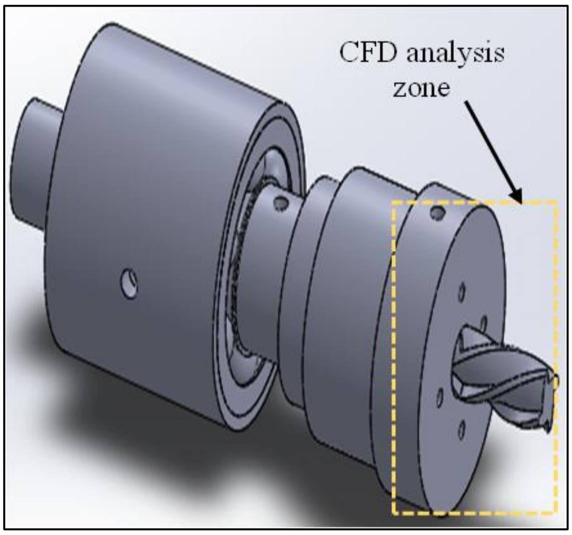

(a) Isometric view

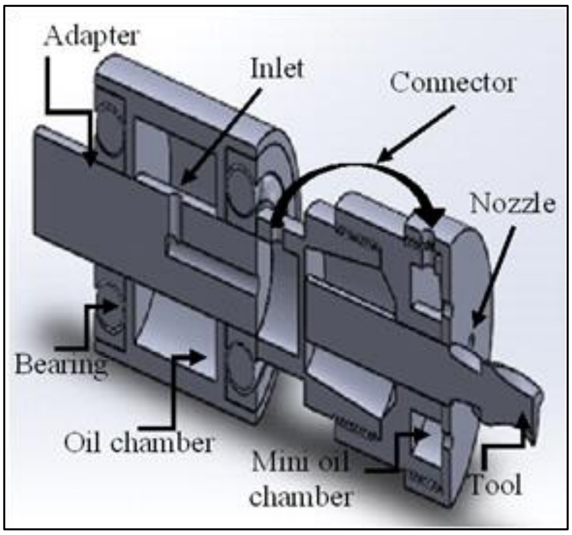

(b) Sectional view

Fig. 2.6 CAD drawing of the designed rotary liquid applicator

After that, the CFD simulation has been conducted to evaluate the effects of RHPC design parameters as well as to compare the performance of HPC and RHPC based on thermal analysis. To simulate the temperature encountered during machining, a uniform constant heat flux of 68 W/mm^2 has been created at the hot tool body. During modelling, it is assumed that the cutter's thermal conductivity is uniform and does not change with temperature. Table 2.4 lists 10 different cooling configuration for CFD analysis. Initially, a CAD model of the multi-point cutter with the specified geometry has been drawn by using Solidworks software. Then, the generated CAD model is imported in design modeler of ANSYS FLUENT for further CFD analysis. In the next step, different cooling nozzle profiles have been added in the generated fluid domain targeting the cutter. The size of the cylindrical fluid domain is: radius 15 mm and height 20 mm.

Table 2.3 L8 orthogonal array of fluid flow parameters

Trial runs	Oil flow pressure (P), bar	Volumetric flow rate (V_f), L/min	Nozzle dia. (d), mm
1	70	2.0	0.50
2	70	2.0	0.75
3	70	3.0	0.50
4	70	3.0	0.75
5	80	2.0	0.50
6	80	2.0	0.75
7	80	3.0	0.50
8	80	3.0	0.75

The proposed numerical model has the same dimensions as those of experimental tests except the total length of the tool. In the current analysis, the length of the end mill cutter has been taken smaller (5.0 mm) than the real value because the actual working depth of cut in our study was only 1.0 mm.

Table 2.4 Different cooling configurations for CFD

Case 01	:	HPC with d=2.00 mm, V_f= 2.0 L/min, P= 80 bar
Case 02	:	HPC with d=2.00 mm, V_f= 3.0 L/min, P= 80 bar
Case 03	:	RHPC with d=0.50 mm, V_f= 2.0 L/min, P= 70 bar
Case 04	:	RHPC with d=0.75 mm, V_f= 2.0 L/min, P= 70 bar
Case 05	:	RHPC with d=0.50 mm, V_f= 3.0 L/min, P= 70 bar
Case 06	:	RHPC with d=0.75 mm, V_f= 3.0 L/min, P= 70 bar
Case 07	:	RHPC with d=0.50 mm, V_f= 2.0 L/min, P= 80 bar
Case 08	:	RHPC with d=0.75 mm, V_f= 2.0 L/min, P= 80 bar
Case 09	:	RHPC with d=0.50 mm, V_f= 3.0 L/min, P= 80 bar
Case 10	:	RHPC with d=0.75 mm, V_f= 3.0 L/min, P= 80 bar

The specific design parameters of HPC and RHPC are listed in Table 2.5. To assess the fluid flow characteristics and temperature distributions of solid cutter, the fluid-solid coupling method has been selected. Two different cooling profiles for HPC and RHPC are shown in Fig. 2.7. Meshing is an important aspect of simulation since it determines the accuracy of the model. Fig. 2.8 shows the unstructured tetrahedral meshing of the cooling system with an average element size of 2.26 mm for the total meshes. Densification of the mesh has been done near the oil inlets. The mesh aspect ratio of 1.08~3.56 confirms the degree of conformity of a mesh element to the regular element of its type. Following mesh formation, pressure-based solver (PBS) has been chosen to define the characteristics of steady ($\frac{\partial \rho}{\partial t} = 0$) incompressible (ρ is constant) flow. All the used boundary conditions are summarized in Table 2.5.

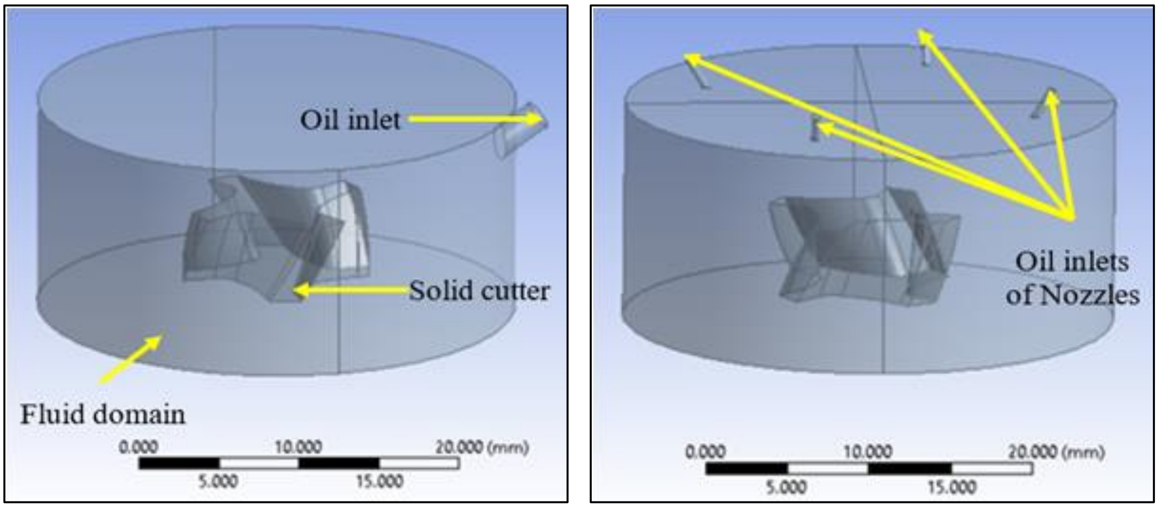

(a) HPC (b) RHPC

Fig. 2.7 Physical model of (a) single nozzle, and (b) multiple embedded nozzles

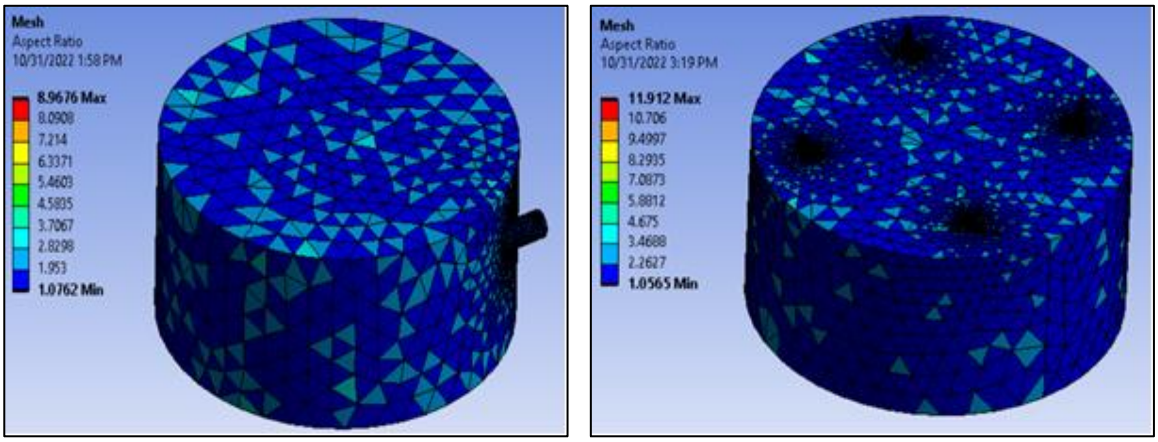

(a) HPC (b) RHPC

Fig. 2.8 Mesh model of (a) single nozzle, and (b) multiple embedded nozzles

At the inlet of the cooling channels velocity inlet has been chosen as the boundary condition while atmospheric pressure (1 atm) is set as outlet boundary condition, as shown in Fig. 2.9. ISO VG-68 cutting oil has been chosen as a working fluid with ambient temperature (25℃). The velocity inlet boundary represents an inlet where velocity and initial gauge pressure are known. No-slip (zero velocity) stationary wall with 'via system coupling' thermal condition has been considered as wall boundary conditions. For better heat transfer between cutting fluids and solid walls fluid-solid interface (FSI) has been considered as a coupled system. One of the most critical parts in CFD analysis is the selection of appropriate viscosity model for simulating the specific type fluid flow. Turbulent model is applicable for free stream jet flow through nozzle over any solid domain because flow area at open surface is infinite [Perri et al. 2016, Ishak et al. 2019]. Following that, in this current study, the shear stress transport (SST) k-ω turbulence model has been used to obtain a detailed visual flow field structure of the high-pressure coolant jets [Zachert et al. 2021].

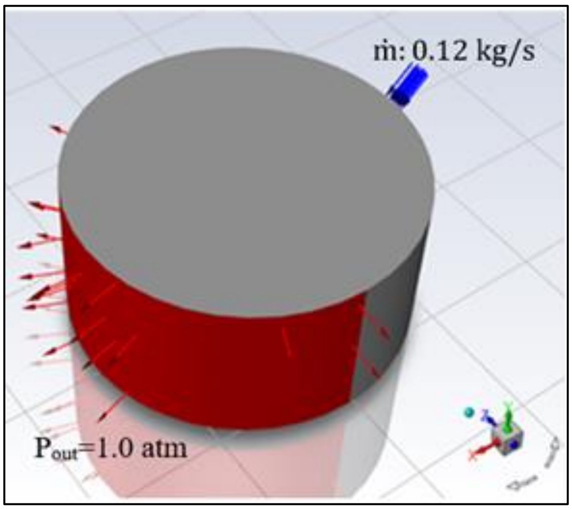

(a) HPC

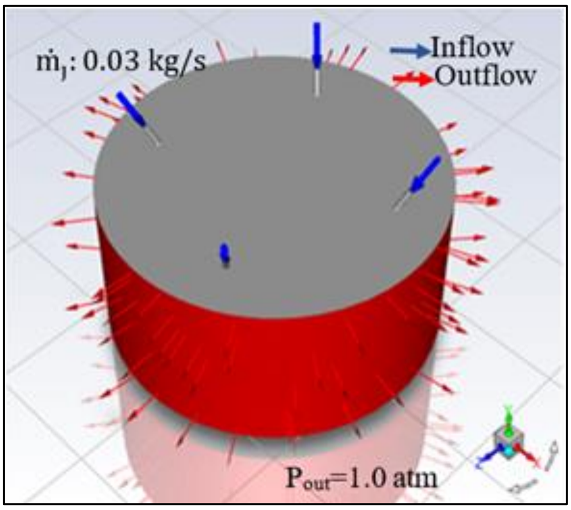

(b)RHPC

Fig. 2.9 Mesh model with boundary conditions of (a) single nozzle (HPC), and (b) multiple embedded nozzles (RHPC)

This model is quite different from the standard k–ω model with an additional feature of SST that switches k-ω behavior to a k−Ɛ behavior in the free-stream, that reduces the sensitivity of standard k-ω in respect of the inlet free-stream turbulence properties. This model provides a better prediction of flow separation than most of the Reynolds average Navier-Strokes (RANS) models. This model also performs better in adverse pressure gradients. It has the ability to account for the transport of the principal shear stress in adverse pressure gradient boundary layers. It is the most commonly used model in the industry. Coupled model was used as the solution method with the 2nd order upwind scheme of pressure, momentum, turbulent kinetic energy (TKE) and turbulent dissipation rate (TDR) with spatial discretization in x, y, and z directions for more accuracy.

Table 2.5 Numerical set up parameters for HPC and RHPC

Specific design parameters for HPC	
Inlet dia. (mm)	: 2.00 mm
Inclination angle from horizontal plane (^{o})	: 30
Stand-off distance (mm)	: 20
Radial distance (mm)	: 14
Specific design parameters for RHPC	
Inlet dia. (mm)	: 0.50, 0.75 mm for each nozzle
Angular distance between two consecutive nozzles (^{0})	: 90
Inclination angle from horizontal plane (^{o})	: 30
Stand-off distance (mm)	: 20
Radial distance (mm)	: 14
Type of solver	**:** 3D pressure-based solver (PBS), Double precision
Flow type	**:** Steady state incompressible turbulent flow
Types of the models	**:** Energy model, SST k-ω turbulence model
Fluid type	**:** VG-68 oil
Solid type	**:** High-speed steel (HSS)
Cell zone condition for solid	**:** Rotational frame motion
Boundary conditions for HPC	
Volumetric flow rate, V_f (L/min)	2.0, 3.0
Mass flow rate, $\dot{m}$ (Kg/s)	: 0.03
Flow velocity through inlet (m/s)	: 11.06, 15.92
Ambient temperature for inlet (K)	: 298
Flow pressure at inlet (Pa-s)	: 80,0000
Boundary conditions for RHPC	
Volumetric flow rate, V_f (L/min)	: 2.0, 3.0
Mass flow rate, $\dot{m}_{j=1,2,3,4}$ (Kg/s)	: 0.0072, 0.011for each inlet
Flow velocity through inlet (m/s)	: 18.94, 28.94, 42.46, 63.70
Ambient temperature for inlet (K)	: 298
Flow pressure at inlet (Pa-s)	: 70,0000; 80,0000
Model type for inlet and outlet	: Velocity inlet and pressure outlet
Heat transfer method between interfaces	: Via system coupling
Gradient method	: Green-Gauss cell based
Solution method	: Coupled
Discretization method	: Spatial discretization
Time stepping method	: Pseudo time method
Pressure, momentum, energy, turbulent kinetic energy and turbulent dissipation rate calculation method	: Second order upwind scheme
Fluid type	: ISO VG 68 oil (Density: 932 Kg/m^3, specific heat:1670 J/Kg-K, thermal conductivity: 0.161 W/m-K, Viscosity: 0.061Pa-s

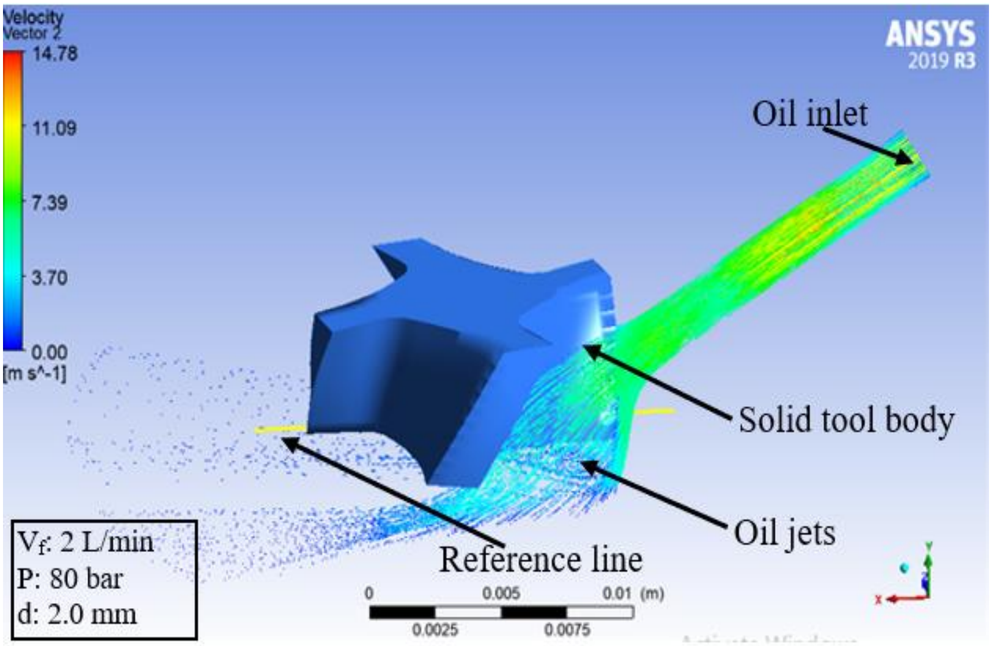

(a) HPC

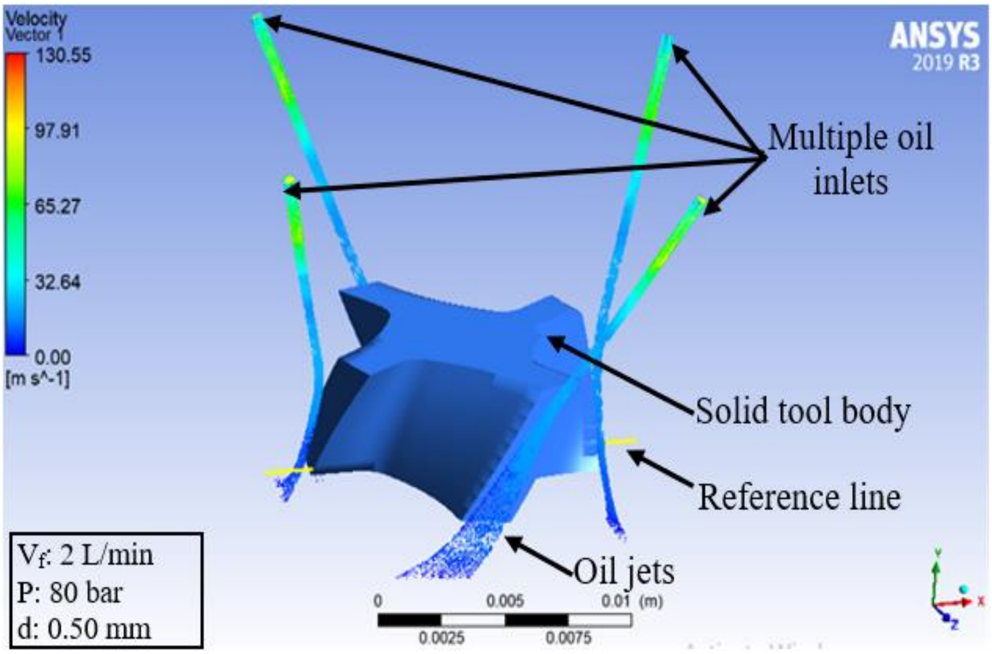

(b) RHPC

Fig. 2.10 Velocity contours of (a) HPC and (b) RHPC

Because of unstructured meshing, Green Gauss cell-based gradient has been chosen [Syrakos et al. 2017]. All the residuals are required to be below than 1e-06. The CFD model-based CHT analysis for the end mill cutter has been developed in the current study. The results are produced by the CFD model using the variation of the mentioned input parameters at ambient temperature 25 °C. Fig. 2.10 shows the velocity contour plots of HPC and RHPC with a reference line across the solid tool, constructed in the post-processing environment to take respective temperature measurements. From the velocity contour, it can be revealed that the velocity of oil flow through inlet over the solid tool is much higher in RHPC (42.46 m/s) rather than HPC (11.09 m/s) that helps the oil jets to penetrate properly into cutting zone with quicker rate of heat exchanging between the hot zone to cutting fluid during milling. It has also been noticed that the velocity of sprayed oil jets reduced to zero at the surface of the solid tool that satisfies the principle of stagnation velocity and also validates the accuracy of nozzle positioning. Fig. 2.11 shows the temperature contour plot for both HPC and RHPC with 2.0 L/min oil flow rate, and 80 bar oil pressure. It has been noticed from the contour plot that temperature drops from 783K to 640K in RHPC compared to HPC which signifies 22.3% enhancement of convective cooling rate in the proposed method. Uniform cooling rate of end mill cutter in RHPC can be clearly visualized in Figs. 2.11 and 2.12 that also affects the tool life positively.

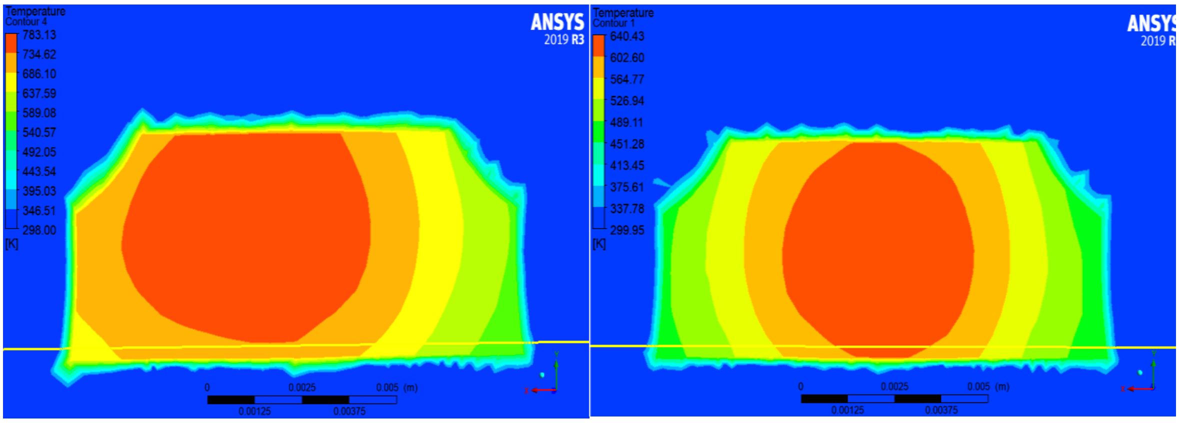

(a) HPC (b) RHPC

Fig. 2.11 Temperature contour plot under (a) HPC, and (b) RHPC

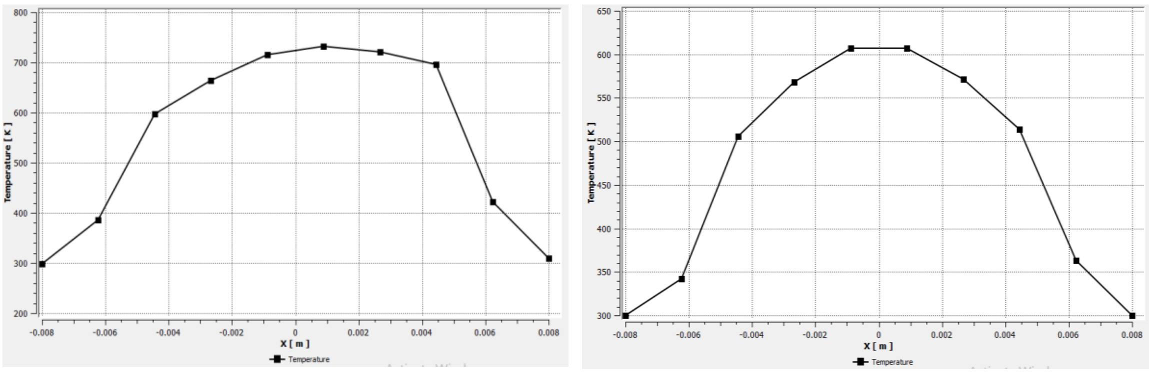

(a) HPC (b) RHPC

Fig. 2.12 Temperature distribution along the path of a reference line (shown in Fig. 2.11) under (a) HPC, and (b) RHPC

Fig. 2.13 shows the effect of oil flow pressure on the cooling rate when the other two design parameters for RHPC are kept constant. It has been observed that the temperature drops from 610 K to 605 K for increasing pressure from 70 bar to 80 bar.

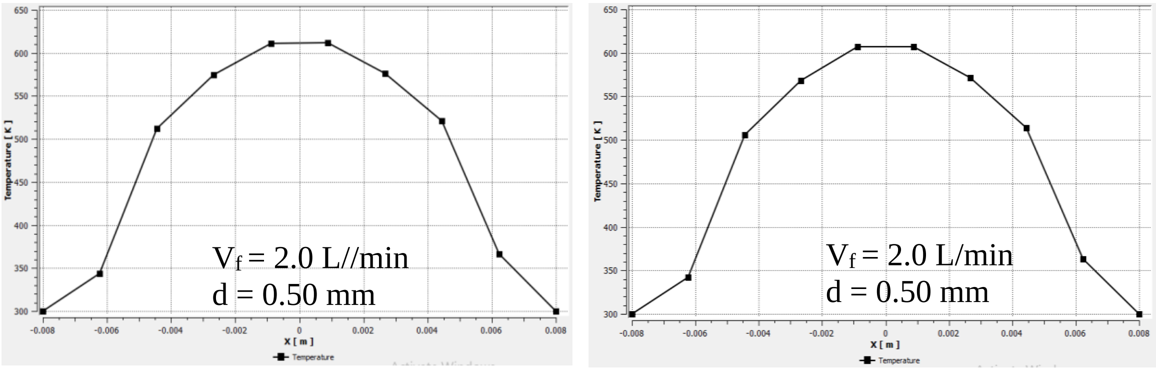

(a) Pressure at 70 bar (b) Pressure at 80 bar

Fig. 2.13 Influence of oil flow pressure on T in RHPC along the path of a reference a line

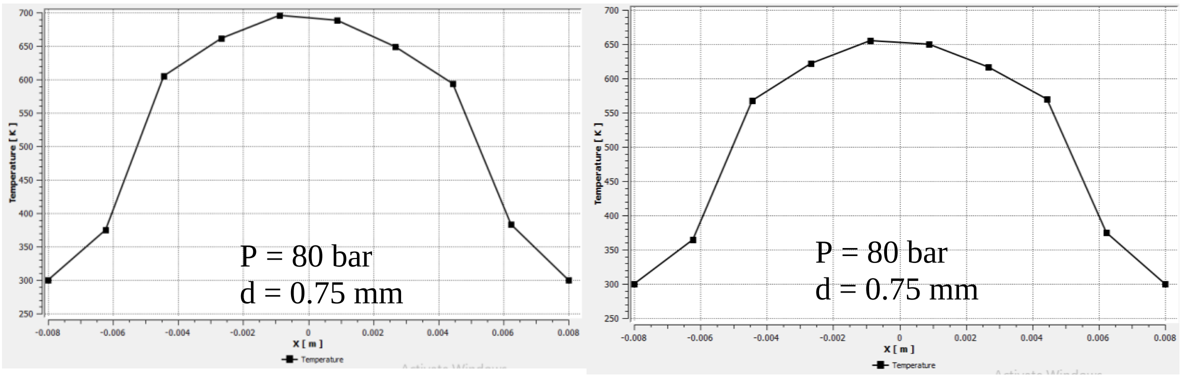

(a) Flow rate 2.0 L/min (b) Flow rate 3.0 L/min

Fig. 2.14 Influence of the flow rate on T in RHPC along the path of a reference line

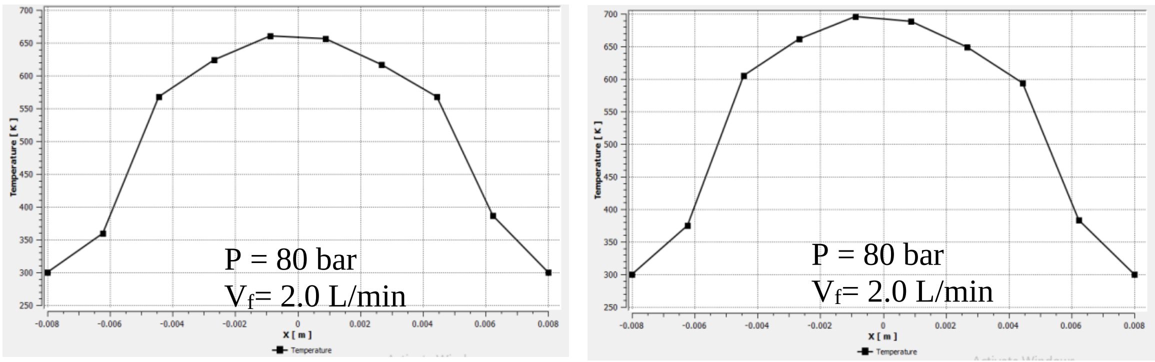

(a) Nozzle dia. 0.50 mm (b) Nozzle dia. 0.75 mm

Fig. 2.15 Influence of nozzle dia. on T in RHPC along the path of a reference line

Fig. 2.14 manifests that increased mass flow rate at constant pressure by using a specific sized nozzle reduces temperature that may be the resultant effect of bulk cooling. In this study, the maximum temperature drops from 660 K to 625 K has been noticed for 3.0

L/min volumetric flow rate with 0.75 mm dia. nozzle. Table 2.15 reveals that cooling rate is significantly affected by nozzle dia. The graphical results depict that for small diameter nozzles, oil mist penetration is effective, and as a result, with a diameter of 0.50 mm, cutting temperature is minimum, and temperature increases with larger diameter owing to inappropriate penetration. Fig. 2.16 shows the cooling rate of 10 different cooling conditions by showing the average temperature through the reference line considering 10 sample points counts. Bar 1 and 2 represent the cooling rate of HPC with 2.0 L/min and 3.0 L/min flow rate. Due to bulk cooling in HPC with 3.0 L/min, temperature drops from 610 K to 534 K. But this cooling is not recommended because of greater fluid consumption rate with higher coolant costs.

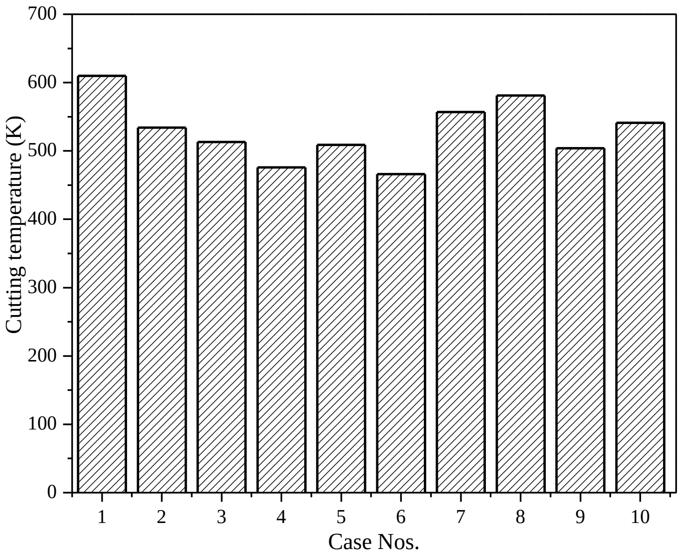

Fig. 2.16 CFD results of cutting temperature under different cooling configurations

Generally, the main focus of Taguchi signal to noise (S/N) ratio-based optimization is to reduce the variability. Signal is the value of expected target and noise is the uncontrollable factor [Sultana et al. 2021]. So, S/N ratio can be expressed as the reflection of the positive effect of signal to unexpected noise. This analysis varies with the objective function such as -maximization, target the value, and minimization. In the current study, minimization of temperature is required. Based on the principle of the Taguchi optimization (as summarized in Table 2.6), the level with the highest value of the S/N ratios, the final parameters of the rotary liquid applicator are selected. The accepted optimum parameters are oil flow pressure at 80 bar, volumetric flow rate at 3.0 L/min, and nozzle diameter of 0.50 mm. The effects of those parameters on temperature are graphically presented in Fig. 2.17. The oil flow rate has been noticed as the highest influential input parameter followed by the nozzle dia. and lastly, by oil flow pressure depending on their delta value. After the finalization of process parameters using CFD, the proposed external rotary applicator has been fabricated. The developed rotary applicator's key components include an adapter, an oil chamber, heatproof bearings and Teflon seals, a particularly designed jam nut, a tiny oil chamber with four embedded nozzles (for each outlet, dia. 0.50 mm), and a connector.

Table 2.6 Ranking of process parameters based on Taguchi S/N ratio

Level	Oil flow pressure (bar)	Volumetric flow rate (L/min)	Nozzle dia. (mm)
1	-54.92	-55.18	-54.55
2	-54.73	-54.47	-55.09
Delta	0.19	0.71	0.54
Rank	3	1	2

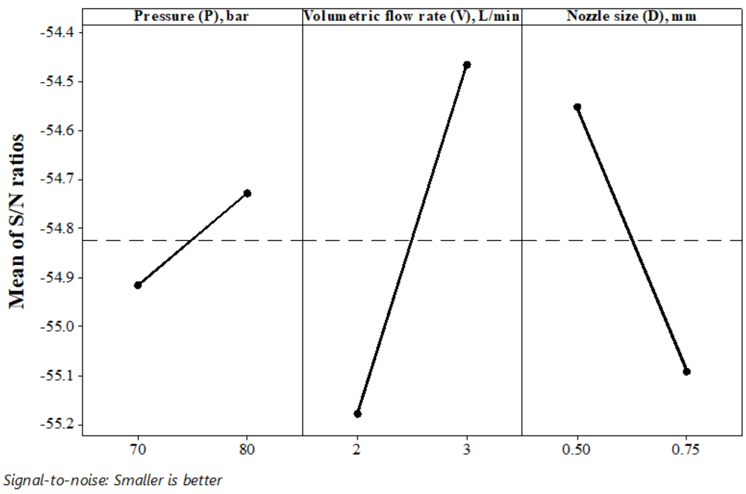

Fig. 2.17 Main effect plot for S/N ratios of temperature with changing input variables

Smooth bar of mild steel has been used to make the structural parts such as adapter, oil chamber and mini oil chamber for reducing the pressure drop of oil flow due to friction. The designed external rotary union has been mounted on a spindle tightly to hold the end mill tool. The design of adapter allows it to securely hold the other components coupled with a spindle via a collet and jam nut. The high-pressure coolant jets are provided from the flexible hose to the oil chamber via a small hole (dia. 4.0 mm) and then, to flow from the oil chamber to the adapter and finally, to the mini oil chamber via a channel. Following that, coolant jets are sprayed from four angularly positioned nozzles targeting the cutting edges.

2.3 Experimental results

A systematic analysis has been conducted to assess the machinability of milling titanium (Ti-6Al-4V) alloy with HSS end mill tool under dry, HPC, and RHPC cutting conditions regarding chips morphology, cutting temperature, cutting force, tool wear, tool life, and surface roughness at varied cutting velocities, feeds and depth of cuts. Finally, a comparative economic analysis among the used cooling conditions is presented.

2.3.1 Chips Morphology

Chip formation is partial fracturing of deformed material (a piece of metal debris removing from the raw material) due to internal cracking by the higher strain rate under compressive stresses within or near the primary shear zone around the cutting edge [Kovac and Sidjanin 1997]. Chip formation analysis is regarded as an essential machinability measure in end milling because it has a substantial impact on cutting forces, tool life, and surface quality. It is obvious that the hardness of the tool, properties of work material, cutting parameters such as velocity, feed rate, depth of cut, and cooling conditions affect the chip formation mechanism highly [Li et al. 2012]. In general, saw tooth serrated chips are produced in Ti-6Al-4V alloy machining as a result of periodic fracture propagation caused by high-stress creation on the free surface of the chips or thermal softening caused by high heat generation in the major shear zones of cutting [Pradhan et al. 2018]. In this study, an experimental examination of chip formation in end milling of Ti-6Al-4V alloy has been carried out for varied cooling conditions at cutting velocity 24 m/min, table feed 44 mm/min, and depth of cut 0.75 mm.

(a) Dry (b) HPC (c) RHPC

Fig. 2.18 Photographic views of chips under (a) Dry, (b) HPC, and (c) RHPC conditions in milling at V_c=24 m/min, f=44 mm/min and a_p=0.75 mm

After collecting the chips, SEM analysis has been conducted to examine the morphology of the collected chips in detail, as shown in Figs 2.18~2.21, sequentially.

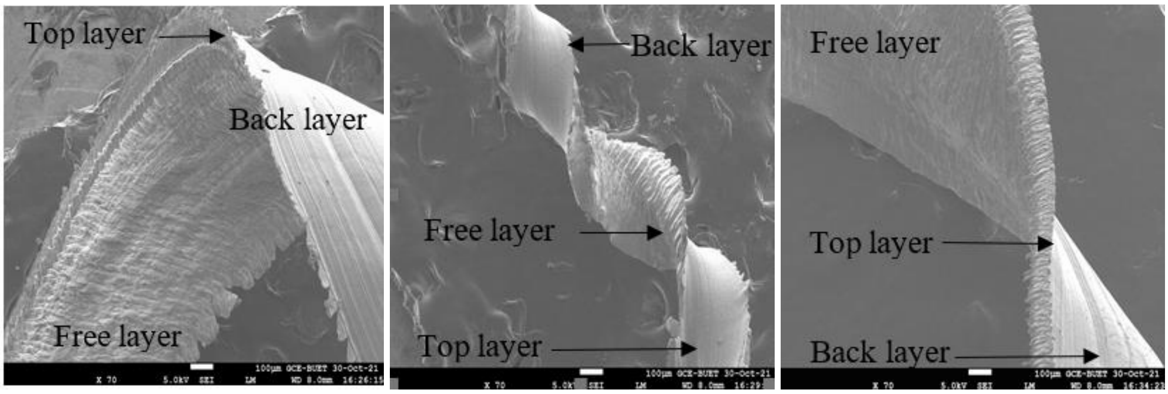

(a) Dry (b) HPC (c) RHPC

Fig. 2.19 SEM views of chips under (a) Dry, (b) HPC, and (c) RHPC conditions in milling at V_c=24 m/min, f=44 mm/min and a_p=0.75 mm

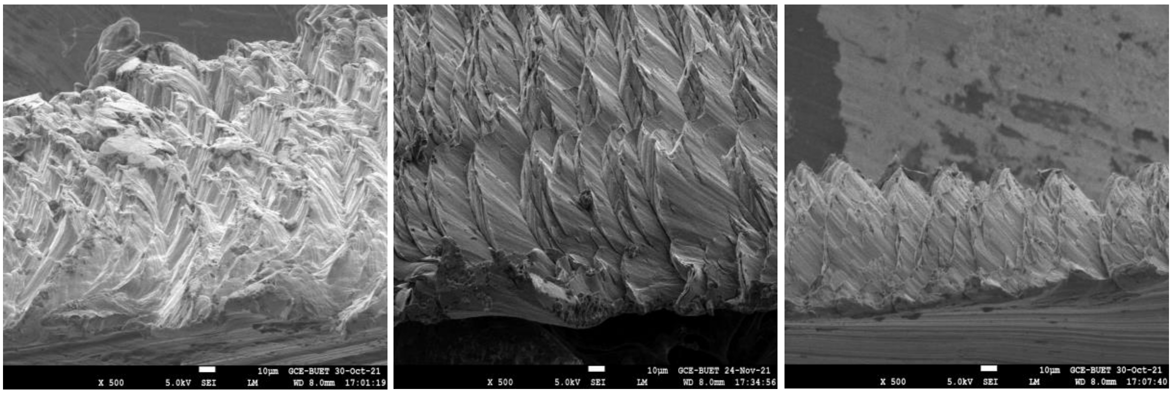

(a) Dry (b) HPC (c) RHPC

Fig. 2.20 Cross sectional views of chips under (a) Dry, (b) HPC, and (c) RHPC conditions in milling at V_c=24 m/min, f=44 mm/min and a_p=0.75 mm

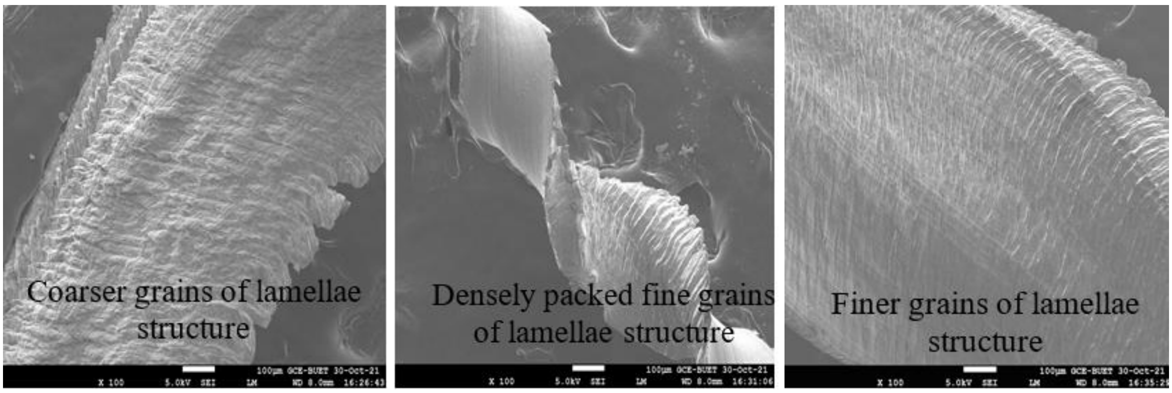

(a) Dry (b) HPC (c) RHPC

Fig. 2.21 Free layer of chips under (a) Dry, (b) HPC, and (c) RHPC conditions in milling at V_c=24 m/min, f=44 mm/min and a_p=0.75 mm

2.3.2 Cutting Temperature

In end milling, power is mostly converted into heat energy which generates higher temperature at the critical interfaces of a chip-tool, and work-tool. Tools cannot retain their strength at a higher cutting temperature that propagates tool softening, adhesion of work metal into tool surface, tool wear, and tool breakage at a shorter period of machining [Sivasakthivel and Sudhakaran 2013]. In some cases, the poor surface may be observed due to the formation of a hardened layer on the work metal surface at a moderate cutting temperature [Lazoglu and Altintas 2002]. The variation of cutting temperature at different cutting velocities, feed rate, and depth of cut under different cooling conditions is depicted in Fig. 2.22.

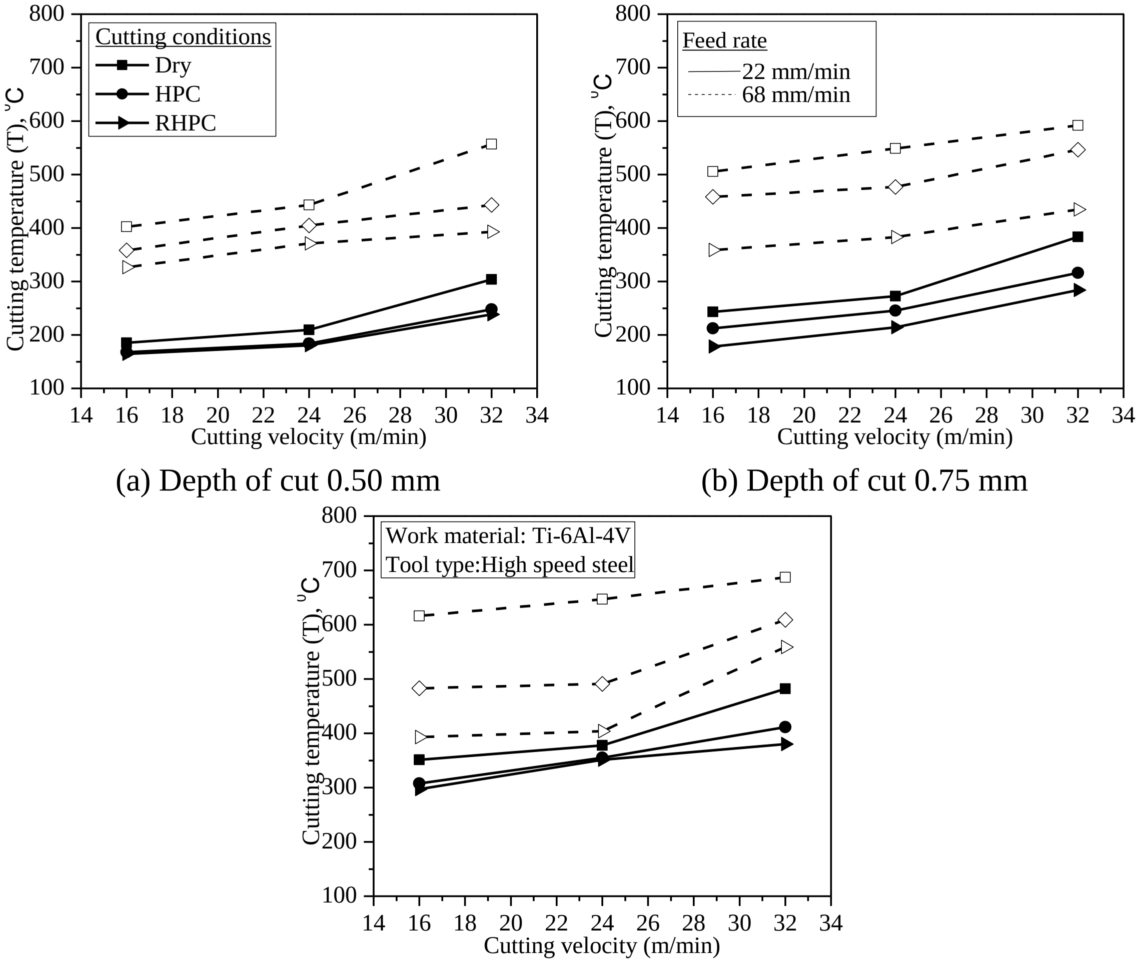

(a) Depth of cut 0.50 mm

(b) Depth of cut 0.75 mm

(c) Depth of cut 1.00 mm

Fig. 2.22 Variation of cutting temperature with cutting velocity at different feed rates and depth of cuts under various machining conditions

2.3.3 Cutting Force

Tool wear, chatter, vibrations, and tool work deflections greatly affect the performance of end milling. Cutting force (F_c) is considered as one of the fundamental sources of such process disturbances [Dikshit et al. 2017]. Cutting force is a representative index of process stability (power and energy, tool vibration, and chattering) that is strongly influenced by tool-work material, process variables (V_c, f, a_p), coolant types, and machining methods [Jamil et al. 2019]. Increased cutting force is detrimental to tool life and surface quality. The variation in F_c as a function of process factors such as cutting velocity, feed rate, and depth of cut under three different cutting conditions are shown graphically in Fig. 2.23.

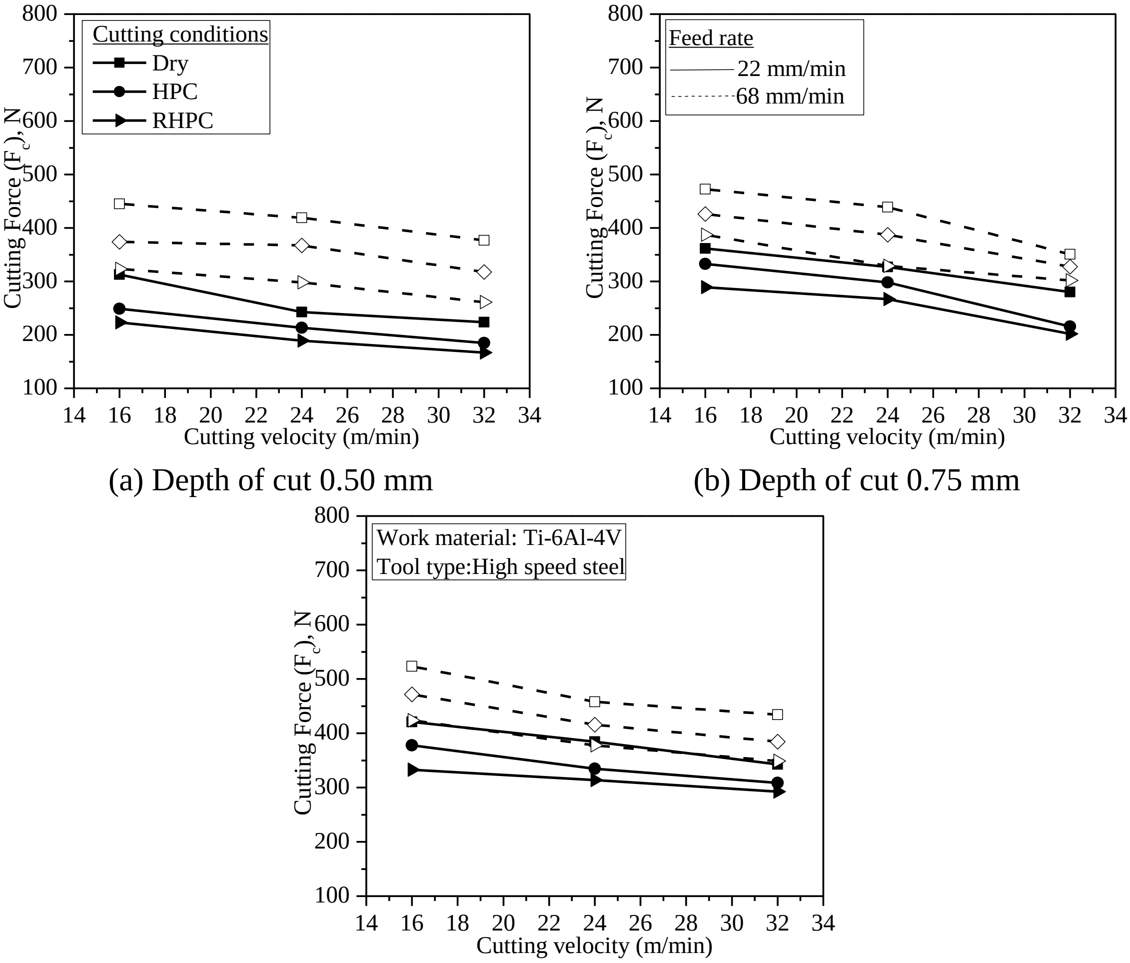

(a) Depth of cut 0.50 mm

(b) Depth of cut 0.75 mm

(c) Depth of cut 1.00 mm

Fig. 2.23 Variation of cutting force with cutting velocity at different feed rates and depth of cuts under various machining conditions

2.3.4 Surface Roughness

Surface roughness is a quantifiable product quality indicator that has a significant impact on machining costs and critical in boosting the machined part's quality and service life [Zhang et al. 2007]. Grinding is generally used to get the ultimate finish on any turned or milled product. Although grinding is necessary for highly finished items, it will save time and money if it can make pieces close to their final shape with the least amount of roughness. Frequent feed marks, built-up edges, unstable machining conditions with increased vibration and chattering, a weak machine-fixtures-tool-work system, increased tool wear, increased work material hardness, and improper machining condition selection is considered to be the primary causes of increased surface roughness [Mia et al. 2017b].

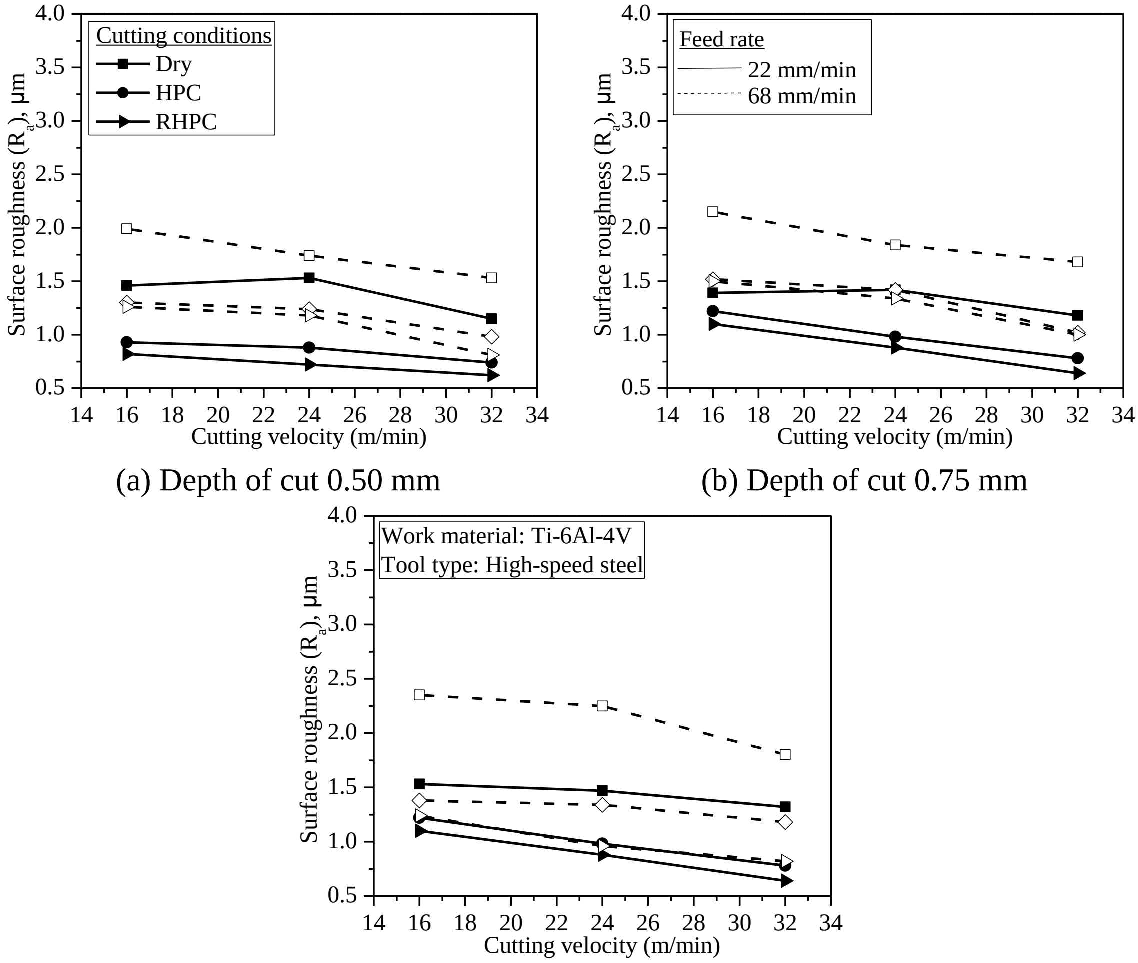

(a) Depth of cut 0.50 mm (b) Depth of cut 0.75 mm

(c) Depth of cut 1.00 mm

Fig. 2.24 Variation of surface roughness with cutting velocity at different feed rates and depth of cuts under various machining conditions

The nature of surface roughness is quite dynamic with the changing machining environment, (work material, tool material, machining time, type of coolants, cutting speed, feed, and depth of cut). To get information on the shape and magnitude of irregularities existing in the machined surface, surface roughness must be measured. Several variables influence surface roughness, including tool-work material, tool life, cutting environment, speed, feed, and depth of cut. Fig. 2.24 illustrates the changing behavior of average surface roughness (R_a) as a function of cutting velocity, feed rate, and depth of cut under three different cutting conditions.

2.3.5 Tool wear and Tool Life

The tool's longevity during machining is determined by its wear resistance, toughness, and intense hardness to the work metal since the tool's life is continuously reduced by wear development. Thus, tool life can be defined as the effective length of cutting time required to achieve the specified surface quality. Tool wear is significantly influenced by the cutting temperature, vibration magnitude, and nature of tool-work interactions, as well as the machining circumstances. On the other hand, the pattern and geometry of tool wear have a substantial effect on the finished surface finish of the machined object [Sultana et al. 2021]. During milling operation, higher cutting temperature, high cutting force, interfacial friction between the tool and work metal reduces the tool sharpness along with premature failure. During surface milling, the end mill tool fails mainly by abrasion, adhesion, diffusion, chemical erosion, etc. and the tool wear rate depends upon the selection of tool-work materials and cutting conditions.

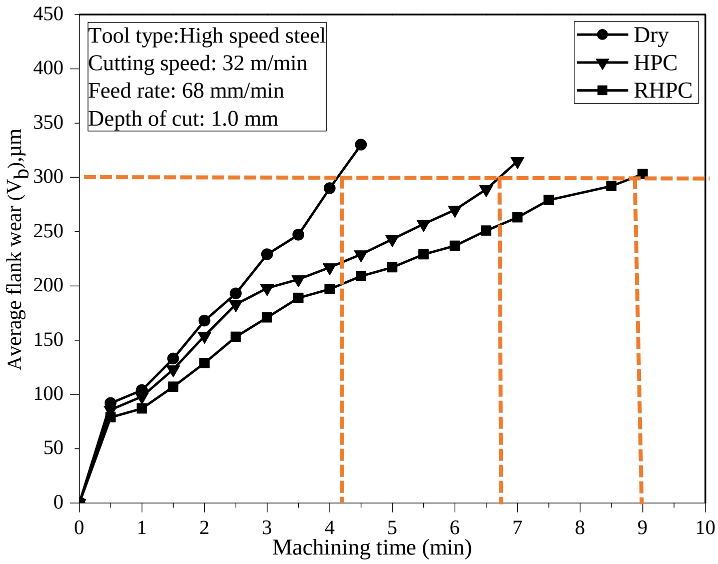

Fig. 2.25 Growth of average flank wear with machining time while machining Ti-6Al-4V alloy under different cooling conditions

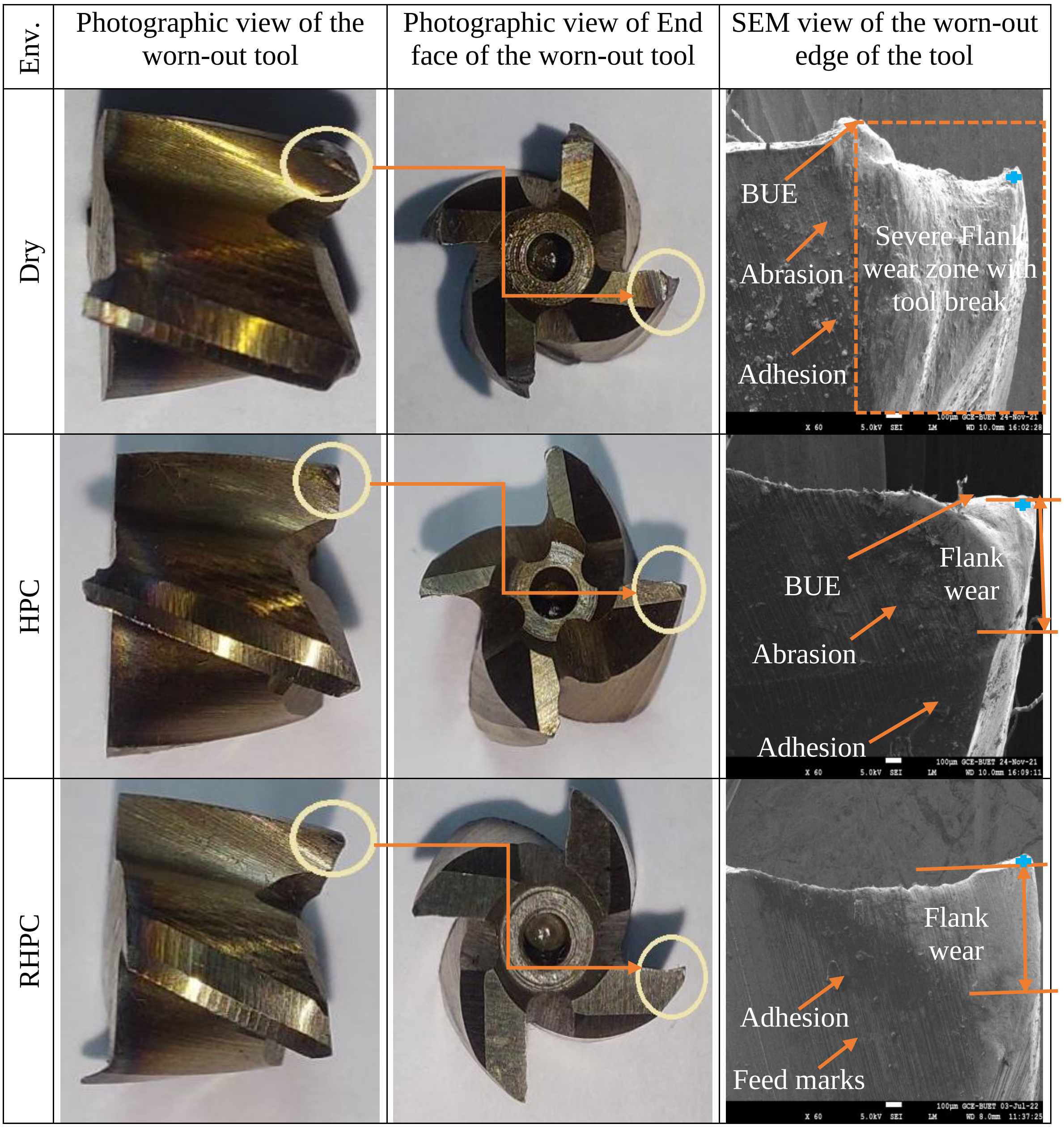

Fig. 2.26 Photographic view and SEM image of tool wear under different cooling conditions at V_c=32 m/min, f=68 mm/min, and a_p= 1.0 mm

A faster rate of tool wear has adverse effects on machinability and in the present research, gradual tool wear has been observed which is measured at preset regular intervals of milling operation at a specific cutting speed and table feed combination under dry, conventional HPC, and RHPC. The growth rate of wear at varying machining times with a specific cutting speed, table feed, and depth of cut are presented in Fig. 2.25. Catastrophic and premature failure may occur due to higher plastic deformation under dynamic loading/unloading or at excessive pressure and temperature. At the beginning of machining, the growth of tool wear rate is generally higher because of micro-chipping at the cutting edges. This phenomenon is commonly known as break-in-wear. Moreover, the tool life fails by gradual flank wear (V_b) that provokes cutting temperature, cutting forces, surface roughness, vibrations, and chattering. Fig. 2.26 shows the details of a worn-out face, as well as the corresponding scanning electron microscope image for one cutting edge. Moreover, the EDX results of the marked point at the analyzed cutting edge is shown in Fig. 2.27.

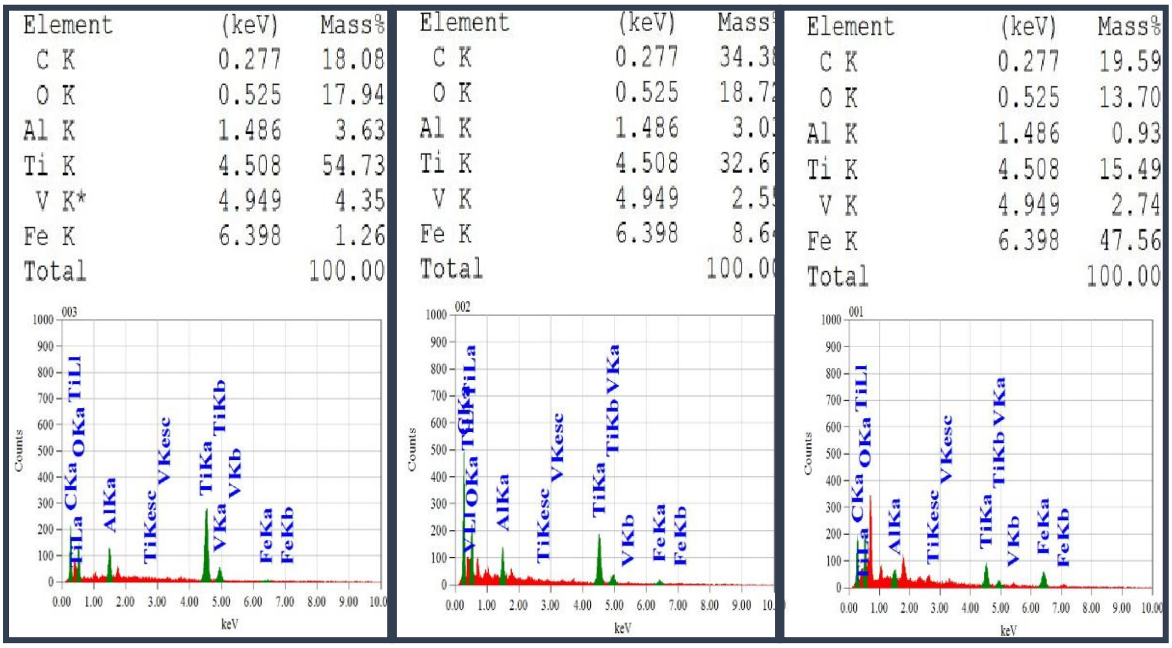

(a) Dry (b) HPC (c) RHPC

Fig. 2.27 EDX analysis of the worn tools under different cooling conditions

2.4 Costs Analysis

Despite the fact that RHPC has been found to improve machinability in milling Ti-6Al-4V alloy by reducing cutting temperature, cutting force, tool wear, and increasing product quality, another indicator of RHPC's applicability is its cost effectiveness. The considered assumptions for costs analysis are presented below:

- Total cost (T_c) to produce each slot comprises of machining cost (C_m), non-machining cost (C_n) and consumable cost (C_c) that can be mathematically expressed as Eqn. (2.3). Machining cost (C_m) comprises of two costs such as operating cost (C_o) and energy cost (C_E). All costs are measured as a function of time. Because the same vertical milling machine was utilized in this study for three distinct cutting circumstances, the initial cost has been assumed to be the same ($ 10,000). Rather than, HPC set up cost (C_{HPC}) and rotary applicator's cost (C_A) are included. The cost of an in-house built-in HPC setup and the cost of the used rotary applicator are considered as $1000, and $37.50, respectively, both of which are factored into the overall cost of cutting fluids for RHPC calculations. The cost of the designed conventional HPC nozzle is only $5. Then, operating cost has been assumed $100/h (including labor cost and depreciation cost of machine). The energy cost (C_E) is divided into two parts: one comprises the energy cost for operating the HPC setup (C_{CE}) and the other was the cost of specific energy requirements for producing each slot (C_{SE}). Eqns. (2.4) and (2.5) can be used to calculate the value of C_{SE}.

- The unit cost of energy is assumed to be $ 0.101/KW-h. Only the power required during machining has been considered in this study with no energy consumption during milling machine considering self-contained mode. During machining, the power consumption of the machine tool and the HPC setup are 5.22 and 0.372 KW, respectively.

- The total cost of energy consumption has been calculated using this information: non-machining cost (C_n) includes tool change cost (C_{TC}), oil collection cost for re-use (C_R) and chip preparation cost (C_{chip}). Tool change, chip removal, and oil collection are estimated to take 3, 2, and 3 minutes, respectively. Finally, consumable cost (C_c) incorporates tooling cost (C_T), work-piece cost (C_W), and coolant cost (C_{CF}). Work-part cost is considered equal for three machining conditions so it is discarded. The estimated cost for a single end mill tool is $22.50 per unit. Tool life has been found 4.2, 6.8 and 9 minutes for dry, HPC, and RHPC, respectively, according to the description. As a result, tooling costs for HPC and RHPC are lowered by approximately 35.7 percent and 50 percent, respectively, when compared to dry milling. Because cutting fluids are collected for re-use in this study, it is estimated that 1% of sprayed coolant jets (2 L/min) are actually consumed, based on earlier research [Mia and Dhar 2018]. The unit cost of used VG-68 cutting oil in the local market is $4.38/L, and the cost of consumed cutting fluids has been estimated using this pricing rate.

$$T_c = C_m + C_n + C_c \tag{2.3}$$

$$\text{Specific energy, SE} = \frac{F_c}{f \times a_p}\ (\text{J/mm}^3) \tag{2.4}$$

$$C_{SE} = \text{SE} \times \text{unit cost} \tag{2.5}$$

Based on the costs analysis in Table 2.7, initially, it can be stated that RHPC aided milling requires higher cost than dry milling. Now, consider how RHPC saves resources by lowering downtime, power consumption, and improving machinability on one hand.

Table 2.7 Costs analysis of milling Ti-6Al-4V alloy with HSS end mill tool under three different cooling conditions

Cost	Description	Dry	HPC	RHPC	Remarks
Machining cost	Initial set up cost of milling machine, $ (a)	10,000	10,000	10,000	Total machining cost of HPC and RHPC is comparable but much higher than dry milling.
	HPC set up cost, $ (b)	0	1005	1037.50	
	Specific energy required for a single slot, KW/mm³	106.5	94.17	85.33	
	Energy consumption costs for each slot, $ (c)	0.134	0.119	0.108	
	Energy consumption costs for high-pressure coolant supply, $ (d)	0	0.0374	0.0374	
	Total cost of energy consumption, $ (e = c + d)	0.1340	0.1564	0.1454	
	Total machining cost, $ (C_m = b + e)	0.1340	1005.15	1037.65	
Non-machining cost	Total Tool changing time for making 24 slots, min	12	9	6	Downtime cost for RHPC is 21.4% lower than both HPC and dry milling.
	Chip removal, oil collection for re-use and its preparation time, min	2	5	5	
	Total downtime, min	14	14	11	
Consumable cost	Tool life, min	4.5	7	9	Compared to HPC and dry milling, consumable cost of RHPC is reduced by 33.3% and 50%, respectively.
	No. of slots within tool life	6	9	12	
	No. of tools required for making 24 slots	4	3	2	
	Total tooling cost, $ (f)	90	67.5	45	
	Coolant cost, $/min (g)	0	0.175	0.175	
	Total consumable component cost (C_c = f + g)	90	67.675	45.175	

Tool cost is generally acknowledged to be a major factor in any machining [Söderberg & Hogmark 1986], which must be minimized. RHPC lowered tool costs by nearly 50% while simultaneously lowering power consumption by 21.4%. It is believed that such cost savings combined with improved machinability will reduce machining costs. From all of the research, it is reasonable to conclude that RHPC-assisted milling of Ti-6Al-4V alloy is more advantageous in terms of machining and cost. A comparative analysis of the achieved results with the published literatures has been listed in Table 2.8.

Table 2.8 Comparative analysis of enhanced machinability with RHPC in milling Ti-6Al-4V alloy with the published literature

Machining characteristics	Published results from existing literature	Comparative novelty/strength of RHPC aided milling
Cutting temperature	Liu et al [2011] proposed MQL with 10 mL/h supply of oil with 0.6 MPa pressure in milling Ti-alloy.	RHPC reduced cutting temperature by a factor of two, which is superior to HPC.
Cutting force	Bermingham et al. [2014] claimed that HPC enhanced machinability of Ti-6Al-4V alloy by lowering cutting force 15%, increasing tool life with 15~64% reduction of machining costs. However, the perspective of cutting temperature and surface roughness were absent.	In comparison to dry milling, 8~13.12%, and 14.05~21.4% reduced cutting force has been found in HPC and RHPC, respectively.
Surface roughness	Paschoalinoto et al. [2021] studied only the positive effect of MQL on the surface quality rather than tool wear, chips morphology and temperature.	Better surface has been achieved in RHPC with less burr formation.
Tool wear and tool life	Shokrani et al. [2019] reported that 30 times better tool life can be achieved in milling Ti-alloy with hybrid MQL-cryogenic cooling over flood cooling. But, cutting force, cutting temperature and cost analysis were not performed.	Compared to dry and conventional HPC, RHPC increased tool life by 50% and 28.5%, respectively through its better cooling and lubrication effect.
Cost	Bermingham et al. [2014] also performed cost analysis in drilling and milling of Nimonic alloy.	RHPC performs better than HPC.

Chapter-3

Discussions on Experimental Results

Many researchers suggest the use of high-pressure coolant jets as a sustainable cooling technique in comparison to flood cooling by addressing the potential benefits of HPC in machinability enhancement. Higher productivity, longer tool life, and improved chip breakability broaden its application in machining hard-to-cut alloys. Kovacevic et al. [1995] conducted a comparative study on flood cooling and HPC in milling Ti-6Al-4V alloy in respect of surface roughness, cutting force, tool wear and chip type. Based on their evaluation, it was revealed that the presence of higher shearing force at tool-chip interface during flood cooling leads in higher tool wear and larger serration of chips due to the poor penetration capabilities of low-pressure waterjets at the intimate zone between tool and chip. On the other hand, when high-pressure water jet is used via the tool rake face, friction is reduced at the tool-chip interface due to the formation of a cushion layer that precludes intimate contact at the tool-chip interface, resulting in chip bending and self-breakage. The tool-chip contact area is reduced when using a high-pressure waterjet through an external nozzle because the chip is fragmented by the impinging jet. But, cutting temperature was not considered in this study. According to Machado et al. [1998], HPC outperformed conventional flood cooling in terms of better chip fragmentation and increased 300% tool life when turning Ti-6Al-4V alloy using cemented carbide inserts with water soluble oil. But other important performance index such as cutting temperature, cutting force and surface roughness were not evaluated. In this chapter, the performance of RHPC is compared with dry and HPC in respect of chips morphology, cutting temperature, cutting forces, tool wear, tool life and surface roughness.

3.1 Chips Morphology

Discontinuous chips of various patterns were generated under all machining conditions. Dry milling created C-shaped and short tubular shaped chips, but HPC produced thinner and significantly longer washer type spiral shaped chips than RHPC, as shown in Fig. 2.18 which is matched with a prior research study conducted by Li et al. [2017]. SEM is crucial since serrations are not visible in photographic images of chips. As indicated in Fig. 2.19, chips can be separated into three segmental layers/surfaces: back layer, free layer, and top layer. The back layer refers to the first layer of machined surfaces that is cut by intense shear stress with thermal softening effects and flows across the tool's rake face. A smooth shiner back layer is formed as a result of the intense adiabatic shear stress and significant heat generation. Back layer with fewer feed marks, fractures, and holes indicates a superior machined component surface. However, dry milling produced more feed marks of chips because of the increased sliding friction generated by the lack of a coolant/lubricant. Reduced contact area using high-pressure coolant jets is the resultant effect of its suitable wedge effects that is agreed with another research results conducted by Alagan et al. [2021]. Fig. 2.20 shows the cross-sectional views of serrations, and it has been noticed that dry milling creates chips with sharply edged serrations, whilst HPC and RHPC make oval shaped dull edged serrations that are less deleterious to tool wear and machined surfaces. Free layer is just opposite to back layer containing rough and fibrous surface since this surface is out of machining. In RHPC, chips have a free layer with a more regular shaped dense lamellae structure was formed rather than dry and HPC, as shown in Fig. 2.21. This lamellae structure is extended to the top layer, indicating the frequency of segmentation. Proper cooling decreases the equivalent chip thickness by preventing sticking on tool faces those results increasing frequency of segmentation with the frequent breaking of thinner chips, that is necessary for greater machinability, as agreed by previous research work [Sahoo and Datta 2020]. In conclusion, RHPC surpasses dry and HPC in respect of chip formation by effective cooling and lubrication.

3.2 Cutting Temperature

Cutting temperature is a critical factor in determining machinability. Despite its beneficial impacts on machining, it is the primary cause of inefficient machining processes [Torii and Yang 1995]. Higher cutting temperatures have a noticeable effect on tool life, power consumption, and surface finish. Fig. 2.22 shows the trend of varying cutting temperature with cutting velocity, feed rate, and depth of cut regardless of cooling conditions, which is consistent with prior research findings [Sultana et al. 2021, Jamil et al. 2019]. Fast chip formation combined with severe tool wear at high cutting velocity leads to an increase in the cutting temperature at the secondary shear zone. Similarly, the increased cutting temperature associated with high feed rates is attributable to the increased tool-chip contact zone with higher friction and rubbing [Zaman et al. 2020]. Because of greater chip loads at higher depth of cut, cutting temperature increased significantly. These catastrophic effects are successfully mitigated in this research work by utilizing high-pressure cooling (HPC). The higher thermal conductivity of the used cutting fluid enables the removal of more heat via convection rather than conduction into the surfaces of a tool and work material [Nandy et al. 2009]. This cooling rate of high-pressure coolant jets is contingent upon their successful penetration into the cutting zone via chip removal through the wedge effect.

Table 3.1 Percentage reduction of cutting temperature, cutting force, and surface roughness under HPC and RHPC over dry milling

Trial No.	a_p (mm)	f (mm/min)	V_c (m/min)	Percentage Reduction of T (°C)		Percentage Reduction of F_c (N)		Percentage Reduction of R_a (μm)	
				HPC	RHPC	HPC	RHPC	HPC	RHPC
1	1.00	22	16	12.34	15.38	10.27	20.97	9.80	18.95
2			24	6.04	13.89	12.88	18.39	8.84	34.69
3			32	14.63	21.16	10.06	14.63	10.61	37.88
4		44	16	13.96	25.83	9.50	21.53	11.66	20.25
5			24	12.43	27.27	10.54	19.56	14.84	21.29
6			32	16.05	20.88	11.56	18.27	6.06	24.24
7		68	16	21.59	36.20	9.85	19.07	26.81	39.57
8			24	24.11	37.56	9.20	17.51	29.33	41.33
9			32	11.35	18.63	11.52	19.69	26.67	40.00

Table 3.1 manifests that RHPC offers superior cooling to conventional HPC. HPC results in a temperature decrease of 6.04~24.11%, while RHPC results in a temperature reduction of 13.89~37.56%. In RHPC, the increased penetration of high-pressure coolant jets along the tool-chip interfaces increased wettability and accelerate temperature reduction rate. Additionally, it decreases friction area, which enables rapid heat dissipation. At 32 m/min cutting velocity, 68 mm/min feed rate and 1.0 mm depth of cut the average temperature for dry and HPC was determined to be roughly 687℃ and 609℃ HPC, which is closer to the earlier study results given by [Ezugwu and Bonney 2004] for end milling with minimal lubrication. However, in RHPC, this cutting temperature was observed to be 559℃, implying that RHPC has a better cooling efficiency than HPC. The percentage reduction of cutting temperature in HPC and RHPC over dry milling is plotted in Fig. 3.1.

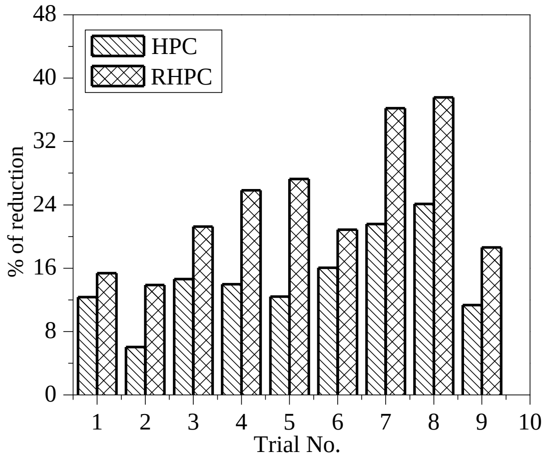

(a) Cutting temperature

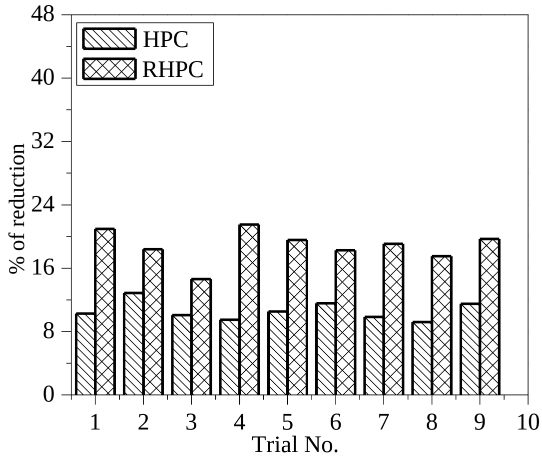

(b) Cutting force

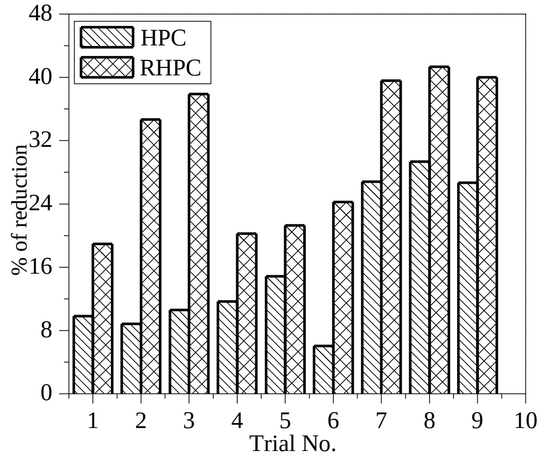

(c) Surface roughness

Fig. 3.1 Percentage reduction of (a) cutting temperature, (b) cutting force, and (c) surface roughness under HPC and RHPC over dry milling

3.3 Cutting Force

Fig. 2.23 shows the variation of cutting force with changing process parameters under different cutting environments. It has been noticed that cutting force decreases as cutting velocity increases, but increases with higher feed rates and depth of cuts, irrespective to cooling conditions. At higher cutting velocity, cutting force is negatively affected by thermal softening before plastic deformation, whereas the increase in cutting force at a higher feed rate is attributed to strain hardening with increased chip load, which is consistent with previous research results [Mia and Dhar 2018, Liu et al. 2011]. On the other hand, cutting force rises with increased depth of cut because of increased friction and chattering associated with rapid tool wear development. Apart from cutting velocity, feed rate, and depth of cut, cooling has a considerable effect on cutting force reduction. The maximum cutting force (523.21 N) was found during dry milling at cutting velocity 16 m/min, feed rate 68 mm/min, and depth of cut 1.0 mm, which is the result of high heat formation combined with rapid plastic deformation, that suppresses thermal softening via strain hardening, more consistent with earlier studies [Mia and Dhar 2018]. Additionally, high heat accelerates tool wear progression significantly, which increases the tool's rubbing and friction behavior, as well as process instability during dry milling, that can also be noted for the enhancement of cutting force. By the wedge effect and lubricity, high-pressure coolant jets reduce cutting force by reducing the seizure area and friction coefficients. Additionally, the increased tool life achieved through the use of high-pressure coolant jets has a beneficial influence on cutting force reduction. Table 3.1 depicts that HPC and RHPC reduced cutting forces by 11.52% and 19.69%, respectively at 32 m/min cutting velocity, 68 mm/min feed rate, and 1.0 mm depth of cut compared to dry milling. The percentage reduction rate of cutting forces is also graphically shown in Fig. 3.1.

3.4 Surface Roughness

Fig. 2.24 demonstrates that the average surface roughness gradually reduces as the cutting velocity increases. This can be related to the work material's local thermal softening (a less thermally conductive Ti-6Al-4V alloy confines heat for an extended period) at a specific temperature, as shown in another research finding [Braham-Bouchnak et al. 2015]. Additionally, less BUE generation with a smaller contact area and less chattering at a faster cutting velocity [Mia et al. 2017b] decrease surface roughness. However, under all cutting conditions, the changing trend is reciprocal with the feed rate, which is consistent with the established inverse relationship between these twos [Mia and Dhar. 2017]. Additionally, this can be explained mechanically, as a faster feed rate results in frequent feed markings and increased vibration as a result of the increased chip load [Zaman et al. 2021]. The effect of cutting circumstances on the average roughness of the surface is also noteworthy. In dry milling, greater surface roughness was noticed, which is the result of increased rubbing between tool and chip, as well as increased friction between tool and work due to frequent chattering. Dry milling of Ti-6Al-4V alloy at higher cutting velocities create an imbalanced hardness due to plastic deformation at high temperatures. Furthermore, the adhesion of chips to work surface results in increased roughness [Islam et al. 2017]. Increased surface roughness is also caused by the faster evolution of tool wear in the absence of coolant/lubricant [Mia and Dhar 2017]. High-pressure coolant jets reduce friction between interfaces [Mia and Dhar 2017], prevent burr formation by breaking chips [Dhar and

Kamruzzaman 2007], and reduce adhesion on the job surface by washing away chips [Kamruzzaman and Dhar 2009], all of which result in reduced surface roughness for both types of HPC, though the rate of reduction is greater for RHPC. Table 3.1 shows, RHPC performs massively better than HPC in terms of minimizing surface roughness. In comparison to both dry and HPC, RHPC enforcement reduces surface roughness from 1.81 µm and 1.32 µm to 0.82 µm at a cutting velocity of 32 m/min, feed rate of 68 mm/min and 1.0 mm depth of cut, respectively. The percentage reduction of surface roughness attained by HPC and RHPC over dry milling for various cutting velocities and feed rates at constant depth of cut (1.0 mm) have also been plotted in Table 3.1 The reduction rate of surface roughness in HPC and RHPC over dry milling were 6.06~29.63% and 18.95~41.04%, respectively. As previously indicated, the delivery of high-pressure coolant jets through a rotating liquid applicator ensures excellent lubrication at frictional surfaces by quick penetration into the cutting region. Properly directed high-pressure cutting fluids improve the tribological properties of the work material [Kaminski and Alvelid 2000], and thus the fluid jets from the rotary applicator through the embedded nozzles improve the surface quality by improving the work material's tribological characteristics and effectively removing unwanted chips from the machined surface. This indicates that better quality with higher productivity at higher value of cutting velocity can be achieved in RHPC.

3.5 Tool Wear and Tool Life

The average flank wear (V_b) is widely used to measure tool life due to its significant implications on machinability. Following ISO 8688-2, the tool rejection criteria were fixed as 300 µm [Courbon et al. 2011]. Fig. 2.25 shows the trend of average flank wear with machining time at a certain cutting velocity (32 m/min), feed rate (68 mm/min) and depth of cut (1.0 mm) under different cooling conditions. Due to high entrapped heat at the tool-work interface, rapid growth of wear or break-in-wear was observed until 1.5 min for all cooling conditions, as shown in Fig. 2.25. Following that, due to insufficient heat convection rate by surrounding air and lack of lubrication, severe flank wear was observed during dry milling. A great amount of heat is stored at the cutting zone due to the lack of cutting fluid, which burns out the cutting edges and causes catastrophic failure, as shown in Fig. 2.26. Furthermore, the majority of heat is absorbed by the tool attributable to the Ti-6Al-4V alloy's low thermal conductivity, which accelerates tool wear. The rapid expansion of flank wear combined with greater nose wear greatly reduces tool life during dry milling, as seen in Fig.

2.26. Following that, as the process progressed from dry milling to HPC and RHPC, slower mechanical wear was observed because the presence of high-pressure coolant jets reduced friction between tool and workpiece and minimized temperature, ultimately slowing down the wear progress. It can be evident that use of neat oil as high-pressure coolant jet enhances longer tool life, which is also reported by another researchers [Jebaraj et al. 2019]. Although the growth pattern of flank wear is comparable in HPC and RHPC, the rate of flank wear is faster in HPC due to insufficient penetration of cutting fluids [Koné et al. 2013]. Reduced tool wear in milling under RHPC is allegedly the consequence of the synergistic impact of superior temperature management and friction reduction via the effective wedge effect of high-pressure coolant jets. Additionally, in RHPC, correct impingement of coolant jets through the flute length enables a greater reduction in tool wear by producing a more effective oil lubricating layer around the cutting edges. This lubricating layer considerably minimizes rubbing and friction between tool/work contacts. Tool life was observed to 4.2 mins for dry milling using the tool rejection criteria, which is increased to 6.8 mins and 9.0 mins for traditional HPC and RHPC, respectively. Finally, it can be inferred that RHPC can increase tool life by nearly 53% and 24% in milling Ti-6Al-4V alloy over dry and HPC, respectively, due to its superior cooling and lubrication.

Moreover, Fig. 2.26 shows SEM images of flank face of worn-out end mill tools used in dry, HPC, and RHPC aided milling of Ti-6Al-4V alloy. Edge chipping, mild and severe adhesion, abrasion, and gradual flank wear are the most common HSS tool wear patterns [Braghini and Diniz 2009]. Severe built-up edge (BUE) formation, excessive abrasion with feed marks, adhesion, edge chipping, and premature tool break were all seen in dry milling, all of which were signified by dot lines in Fig. 2.26. Higher thermal stress, cyclic stress, increased friction, rubbing, and chemical affinity all contribute to the severity of tool wear in dry milling. Due to trapping heat at the cutting zone, BUE development is exacerbated by increased chemical affinity of foreign materials to adhere onto the tool's flank face. Lack of lubrication at tool-work interfaces causes frequent feed marks. Moreover, due to a lack of flushing away chips from the cutting zone, some chips weld on the tool's surface, resulting in severe edge chipping. This creates abrasion on the tool surface and chemically damages the cutting tool, potentially resulting in cutting tool failure. Flank wear at the nose was also noticed as another dominant form of tool wear, which occurs at the depth of cutline due to rubbing action between tool-workpiece. Finally, the tool failure owing to plastic deformation caused by increased cyclic stress in intermittent cutting with sudden impact load by chips at elevated temperature.

It can be revealed from Fig. 2.26, the development of BUE was minimized when milling was done with HPC, which reflects the lower chemical affinity of the work material at the tool tip due to the lower temperature. Jebaraj et al. [2019] discovered similar type adhesion when milling 15-5PH stainless steel with only a small amount of neat oil. On the flank face, there were numerous feed marks, which were caused by the inappropriate lubricating action of high-pressure coolant jets at the tool-work interface. Adhesion was also observed over the entire flank face, though in lesser amounts than with dry milling. Milling with RHPC produced the best tool surface. Fig. 2.26 also shows little abrasion, or adhesion with no BUE in RHPC that is the resultant effect of its better cooling/lubrication properties. Higher heat transfer with improved penetration offered better cooling and lubrication with less friction at the tool-work interfaces, resulting in a better surface of flank face with no significant feed marks. Because tool life was longer in this environment than in dry and HPC, plastic deformation at the nose area may be attributed by the tool particle damage owing to mechanical fatigue. The tool particles were removed due to cyclic stress and mechanical fatigue, i.e., the tool chipping was induced by a significant number of interactions between the tool and the workpiece. Fig. 2.27 (a, b, c) shows the results of an EDX analysis of tool wear under three different cutting conditions, including dry, HPC, and RHPC. The highest amount of titanium (54.73%), aluminium (3.63%), and vanadium (4.35%) in the chemical composition of dry tool wear implies the greatest adhesion of work material to the tool's face. To some extent, HPC resists adhesion, whereas RHPC has the least amount of adherence. This is due to RHPC's higher reduction in cutting temperature and better lubrication when compared to HPC.

Chapter-4

Modelling of Machining Responses

The key problem for today's manufacturers is determining the process parameters that will achieve great surface quality while keeping production costs reasonable. As a result, the optimal combination of input parameters must be chosen in order to provide the intended answers. The output variables can be defined using a variety of modelling approaches. Using BBD based design matrix of RSM, the experimental data of different responses were collected. After that, three popular modelling approaches were followed to predict those to build a link between the specified milling parameters, cutting velocity, feed, depth of cut and cutting conditions to each of the output responses – cutting temperature, cutting forces and surface roughness. While a single combination of process parameters may be appropriate for one quality characteristic, the same settings may be unfavorable to other quality characteristics. In such cases, multi-response optimization may be the best option for optimizing distinct response at the same time. In this study, composite desirability approach (CDA) has been utilized to improve key performance metrics.

4.1 Empirical Modelling of Temperature, Force, and Roughness

The first step in determining the appropriate process input selection is to generate mathematical models of the process to establish a link between the process's inputs and outputs. RSM is a popular statistical approach for establishing a specific relationship between a set of influential input factors and a set of performance indicators [Ikhlas et al. 2018]. The input elements are referred to as independent variables, whereas each performance measure is referred to as a response or dependent variable [Mia et al. 2017d]. RSM models are often categorized as either central composite design (CCD) or Box-Behnken design (BBD). Based on previous research conducted by Zaman et al. [2020], BBD based RSM models are employed in this work to show the mathematical relationships between the specified response (cutting temperature, cutting force, and surface roughness) and a set of independent factors (cutting velocity, feed rate, depth of cut, and cutting conditions). In general, a first-order polynomial is appropriate for determining the main effects of individual input variables with a relatively small region of the independent variable space (low response curvature), whereas a second-order model can be used to determine the interaction effects of variables on output quality [Mia et al. 2017d]. Mathematical expressions for both first-order and second-order models are written symbolically in Eqns. (4.1 and 4.2), respectively.

$$Y = \alpha_0 + \alpha_1 x_1 + \alpha_2 x_2 + \cdots + \alpha_n x_n \tag{4.1}$$

$$Y = \alpha_0 + \sum_{i=1}^{n} \alpha_i x_i + \sum_{i=1}^{n} \alpha_{ii} x_i^2 + \sum_{i,j}^{n} \alpha_{ij} x_i\, x_j + \epsilon \tag{4.2}$$

The regression coefficients of the linear, quadratic, and interaction terms are represented by the variables α_i, α_{ii} and α_{ij} , respectively whereas α_0 is a free or constant term. The input variables relating to cutting velocity (V_c), feed rate (f), and depth of cut (a_p) are represented by x_i. Since the input variable cooling approach (CC) is a categorical variable, three different forms of Eqn. are produced for dry, HPC, and RHPC milling. 'Y' represents the individual response terms such as cutting temperature (T), cutting force (F_c), and surface roughness (R_a). A random experimental error is represented by the symbol ϵ. Table 4.1 summarizes the final selection of process parameters and their associated threshold values for this. A total of 39 experimental trial runs are designed based on BBD to measure the responses. Table 4.2 lists the experimental design and the relevant responses to the design. To further investigate the relationship between input components and selected responses, analysis of variance (ANOVA) has been carried out at a 5% significance level (alpha =0.05) [Mia et al. 2017d]. ANOVA table contains the sum of squares (SS_i) and the mean of squares (MS_i), as well as the p-value, F-value, and the % contribution (PC). SS is the standard deviation of the derived result from the mean, p-value defines the significant parameters by providing a condition that falls within the defined 95% confidence interval, F-statistics is the ratio of calculated MS for each factor to calculated MS for error, and PC represents the percentage contribution of each significant factor to the derived result (as shown in Eqn. 4.3). Generally, mathematical modelling represents the relationship between process parameters and responses a more concise and clear way [Ikhlas et al. 2018].

Table 4.1 Input variables and their corresponding levels

Sl. No.	Factors	Symbols	Unit	Lower level	Upper level	
1	Cutting velocity	V_c	m/min	16	32	
2	Table feed	f	mm/min	22	68	
3	Depth of cut	a_p	mm	0.5	1.0	
4	Cooling condition	CC	-	Dry	HPC	RHPC

$$\mathrm{PC} = \frac{\text{sum of the square of each input source/factor}(\mathrm{SS_i})}{\text{The total sum of squares } (SS_\mathrm{T})} \quad (4.3)$$

Table 4.2 BBD based design matrix with corresponding responses

Run order	V_c (m/min)	f(mm/min)	a_p (mm)	CC	T (ºC)	F_c (N)	R_a (µm)
1	24	45	0.75	RHPC	367	292	0.84
2	32	22	0.75	HPC	316	216	0.78
3	24	68	1.00	RHPC	404	378	1.32
4	16	68	0.75	HPC	458	426	1.52
5	24	68	0.50	RHPC	371	298	1.18
6	24	45	0.75	HPC	425	301	1.24
7	24	68	1.00	HPC	491	416	1.59
8	32	22	0.75	RHPC	284	202	0.64
9	16	45	1.00	Dry	480	481	1.63
10	32	22	0.75	Dry	383	280	1.18
11	32	45	1.00	Dry	617	377	1.32
12	24	68	0.50	Dry	443	419	1.74
13	24	45	0.75	Dry	477	342	1.41
14	24	22	1.00	RHPC	351	314	0.96
15	32	68	0.75	HPC	546	328	1.02
16	16	68	0.75	RHPC	359	387	1.50
17	16	22	0.75	RHPC	178	289	1.10
18	32	45	0.50	RHPC	299	213	0.74
19	24	22	1.00	Dry	378	384	1.47
20	16	22	0.75	HPC	213	333	1.22
21	16	45	0.50	RHPC	249	283	0.98
22	32	45	1.00	RHPC	488	308	1.00
23	24	22	0.50	RHPC	180	189	0.72
24	24	68	1.00	Dry	647	458	2.25
25	32	68	0.75	Dry	593	351	1.68
26	32	45	0.50	Dry	484	289	1.35
27	24	22	0.50	HPC	184	213	0.88
28	16	45	1.00	HPC	413	435	1.44
29	32	45	1.00	HPC	518	333	1.24
30	16	45	1.00	RHPC	356	377	1.30
31	16	68	0.75	Dry	506	473	2.15
32	32	45	0.50	HPC	320	270	0.84
33	24	22	0.50	Dry	209	243	1.53
34	16	45	0.50	HPC	259	316	1.14

35	24	22	1.00	HPC	355	335	1.34
36	24	68	0.50	HPC	405	368	1.24
37	16	45	0.50	Dry	323	363	1.58
38	16	22	0.75	Dry	243	362	1.39
39	32	68	0.75	RHPC	435	302	1.00

Table 4.3 shows the suggested mathematical models for T, F_c and R_a. Based on the highest value of predicted R^2, quadratic models are chosen for all responses.

Table 4.3 Selection of appropriate models for cutting temperature, cutting force, and surface roughness based on model summary

Response	Source	Std. Dev.	R^2	Adjusted R^2	Predicted R^2	PRESS	Suggestion
T	Linear	37.63	0.9169	0.9043	0.8842	65146.71	
	2-Factor interaction	34.07	0.9505	0.9216	0.8712	72419.92	
	Quadratic	27.87	0.9710	0.9475	0.8978	57501.00	Suggested
	Cubic	28.13	0.9916	0.9465		*	Aliased
F_c	Linear	18.20	0.9487	0.9409	0.9292	15090.50	
	2-Factor interaction	15.01	0.9746	0.9598	0.9405	12673.00	
	Quadratic	13.22	0.9828	0.9688	0.9410	12566.57	Suggested
	Cubic	11.42	0.9963	0.9767		*	Aliased
R_a	Linear	0.1369	0.8752	0.8563	0.8263	0.8601	
	2-Factor interaction	0.1364	0.9098	0.8572	0.7641	1.17	
	Quadratic	0.1183	0.9407	0.8927	0.7968	1.01	Suggested
	Cubic	0.0829	0.9917	0.9473		*	Aliased

Cubic models are found aliased for all responses, demonstrating the inadequacy of RSM-based analysis in terms of determining the interaction effects of cubic factors. Eqns. (4.4~4.12) express the individual mathematical models for T, F_c and R_a for three different cooling conditions. The proposed mathematical models can predict the selected response for given levels of each element.

Dry: $$T = -276.4 + 6.49V_c + 10.89f + 295a_p + 0.062f^2 \quad (4.4)$$

HPC: $$T = -309.4 + 6.49V_c + 10.11f + 295a_p + 0.062f^2 \quad (4.5)$$

RHPC: $$T = -290.8 + 6.49V_c + 8.71f + 295a_p + 0.062f^2 \quad (4.6)$$

Dry: $$F_c = 173.96 - 2.84V_c + 4.66f + 172.2a_p - 3.54(V_c \times a_p) - 3.20(f \times a_p) + 163.73a_p^2 \quad (4.7)$$

HPC: $$F_c = 133.04 - 2.84V_c + 4.66f + 172.2a_p - 3.54(V_c \times a_p) - 3.20(f \times a_p) + 163.73a_p^2 \quad (4.8)$$

RHPC: $$F_c = 97.8 - 2.84V_c + 4.66f + 172.2a_p - 3.54(V_c \times a_p) - 3.20(f \times a_p) + 163.73a_p^2 \quad (4.9)$$

Dry: $$R_a = 1.67 - 0.022V_c - 0.009f - 0.49a_p + 0.0002f^2 + 1.22a_p^2 \quad (4.10)$$

HPC: $$R_a = 1.28 - 0.022V_c - 0.009f - 0.49a_p + 0.0002f^2 + 1.22a_p^2 \quad (4.11)$$

RHPC: $$R_a = 1.10 - 0.022V_c - 0.009f - 0.49a_p + 0.0002f^2 + 1.22a_p^2 \quad (4.12)$$

As shown in Table 4.4, R^2 values of 0.97, 0.98, and 0.94 are reported for T, F_c and R_a, respectively, indicating that the proposed models are better predictive. Additionally, the Predicted R^2 values of 0.90, 0.94, and 0.81 are consistent with the Adjusted R^2 values of 0.95, 0.97, and 0.90 for T, F_c and R_a, respectively; the variation is less than 0.2. The signal-to-noise ratio is measured by adequate (Adeq.) precision and this ratio greater than 4 is ideal; for T, F_c and R_a which are 31.80, 45.72 and 25.09, respectively, suggest a sufficient signal, and the produced models can be utilized to navigate the design space. Another crucial factor, coefficient of variation, denoted by C_v in the Table 4.4, denotes the degree to which experimental results for any specified response are close to their mean [Pusavec et al. 2014].

Table 4.4 Statistical fit values for cutting temperature, cutting force, and surface roughness

Statistical terms	T	F_c	R_a
Standard deviation	29.72	13.28	0.13
Mean	384.29	331.90	1.27
R^2	0.97	0.98	0.94
Adj. R^2	0.95	0.97	0.90
Predicted R^2	0.90	0.94	0.81
Adeq. Precision	31.80	45.72	25.09
C_V	7.72	4.00	10.02

It has been observed that C_v values of 7.72%, 4.00% and 10.02%, respectively for T, F_c and R_a. The lower value of C_v for F_c in contrast to both T and R_a indicates that the experimental data and mean of F_c have the least fluctuation. The normality of residuals (absolute difference between actual and predicted values) has been checked and graphically plotted in Fig. 4.1. One can easily visualize that the residuals draw a straight line which verifies the normality, as explained by Ikhlas et al. [2018]. The correlation between real experimental results and RSM predicted values are also graphically depicted in Fig. 4.2, indicating that they are in good agreement, as in a prior study [Gupta et al. 2020]. As previously stated, ANOVA has been used to determine the relevance of process characteristics that affect output. Insignificant terms from the statistical analysis are omitted using the backward elimination approach to improve the model's accuracy to a 95% confidence level. Table 4.5 summarizes the ANOVA results for all responses and the percentage contribution of each component to the selected responses. In respect of T, it can be depicted from ANOVA table that feed rate (42.17%) has the highest effect followed by depth of cut (23.31%), cooling condition (14.81%), and lastly, by cutting velocity (11.51%). In terms of F_c, linear terms, table feed has the greatest effect (30.27%), followed by the depth of cut (25.06%) cutting velocity (21.81%), and cooling condition (17.73%).

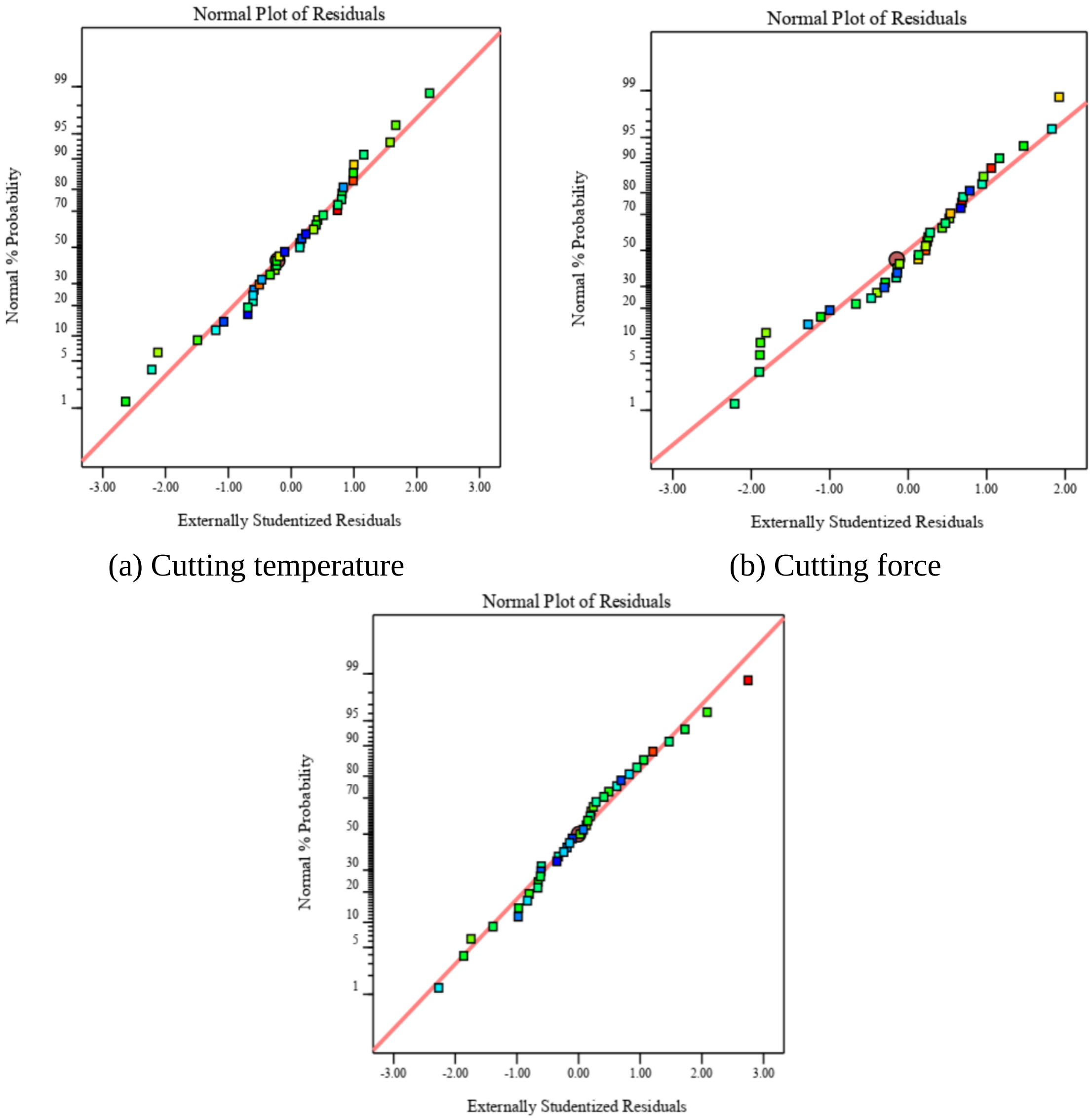

(a) Cutting temperature

(b) Cutting force

(c) Surface roughness

Fig. 4.1 Normal probability plots for (a) cutting temperature, (b) cutting force, and (c) surface roughness

Similarly for R_a, it is visible that linear terms are much more significant than quadratic terms. The cooling condition is found as the highest dominant input factor with 44.85% contribution. Actually, in dry milling, the drastic progression rate of tool wear hampers the surface quality greatly which was successfully reduced by proper cooling and lubrication. Feed rate is numbered in the second position (20.81% contribution) followed by the cutting velocity (14.57%) and lastly by the depth of cut (7.27%). Figs. 4.3~4.5 show graphically the changing trend of responses (T, F_c and R_a) at 24 m/min cutting velocity, 45 mm/min table feed and 0.75 mm depth of cut in different cutting conditions.

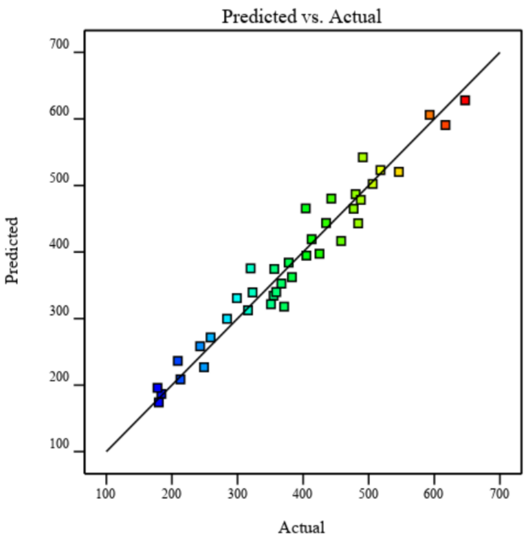

(a) Cutting temperature

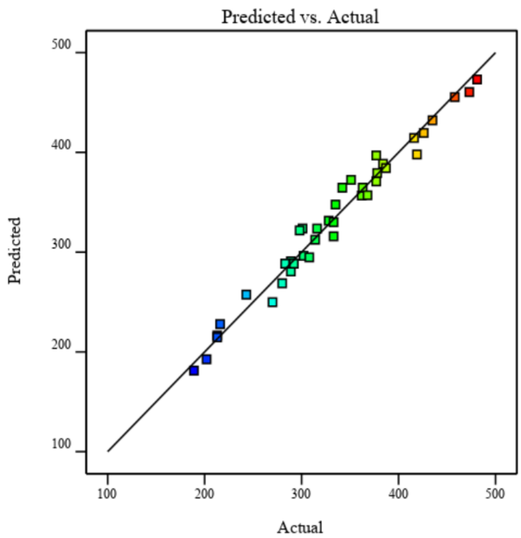

(b) Cutting force

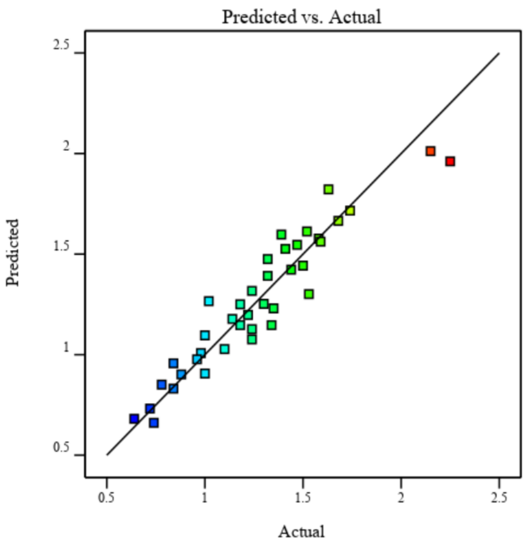

(c) Surface roughness

Fig. 4.2 Residual plots for (a) cutting temperature, (b) cutting force, and (c) surface roughness

Table 4.5 ANOVA for Reduced Quadratic model of cutting temperature, cutting force, and surface roughness

Response	Sources	SS	DF	MS	F-value	P-value	Comment	PC
T	Model	5.36E05	8	66959.1	75.68	< 0.0001	Significant	-
	V_c	64697.5	1	64697.5	73.12	< 0.0001		11.51
	f	2.37E05	1	2.37E05	267.72	< 0.0001		42.17
	a_p	1.31E05	1	1.31E05	147.622	< 0.0001		23.31
	CC	83240.1	2	83240.1	47.04	< 0.0001		14.81
	$f \times CC$	10296.4	2	10296.4	5.82	0.0073		1.83
	a_p^2	9958.25	1	9958.25	11.26	0.0022		1.77
	$\in$	26543.2	30	884.77				4.60
	Total	5.62E05	38					100.00
F_c	Model	2.02E05	5	40354	87.53	<0.0001	Significant	-
	V_c	46464	1	46464	263	<0.0001		21.81
	f	64480	1	64480	365	<0.0001		30.27
	a_p	53392	1	53392	302	<0.0001		25.06
	CC	37766	2	18883	107	<0.0001		17.73
	$V_c \times a_p$	602	1	602	3.41	0.0746		0.28
	$f \times a_p$	4070	1	4070	23.07	<0.0001		1.91
	a_p^2	967	1	967	5.48	<0.0001		0.45
	$\in$	5293	30	176.4				2.48
	Total	213034	38					100.00
R_a	Model	4.44	6	0.7394	45.81	<0.0001	Significant	-
	V_c	0.7211	1	0.7211	45.81	<0.0001		14.57
	f	1.03	1	1.03	44.67	<0.0001		20.81
	a_p	0.3601	1	0.3601	64.02	<0.0001		7.27
	CC	2.22	2	1.11	22.31	<0.0001		44.85
	f^2	0.1018	1	0.1018	68.77	<0.0001		2.06
	$\in$	0.5165	32	0.0161	6.31	0.0173		10.44
	Total	4.95	38					100.00

The sharpness of slope relative to reference point indicates the dominancy of any factor in changing response [Mia and Dhar. 2018]. Irrespective of the cooling approach, T is varied sharply with a_p and f, followed by V_c, on the other hand, F_c is quickly changed with f and a_p while the least reverse effect has been noticed for V_c. similarly, for R_a, f is identified as the most dominant factor followed by V_c, and lastly by a_p. Graphical presentation with a 3D surface plot is an excellent method for showing the effects of two process parameters on a single response simultaneously. Figs. 4.6 and 4.7 depict that cutting temperature increases with increasing V_c, f, and a_p. Because at higher RPM with greater chip loads requires more specific energy to cut metal and the maximum proportion of this specific energy is generally converted into heat results higher temperature at the cutting zone. From the graphical plots of Fig. 4.8, the continual increase of F_c with rising f was noticed, however, the reverse interaction between V_c, and F_c has also been detected, which is consistent with prior study results by Gunay et al. [2011]. The first observation may be described as follows: when f grows, the chip load at the tooltip increases, resulting in significantly reduced tool life, extreme tool wear, and tool bluntness; as a result, larger cutting forces are required. The second point may be attributed to the fact that a faster cutting velocity causes more strain, which raises the temperature of the work zone.

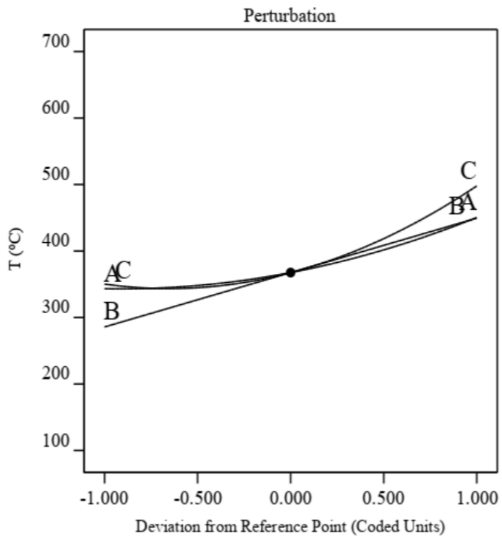

(a) Dry

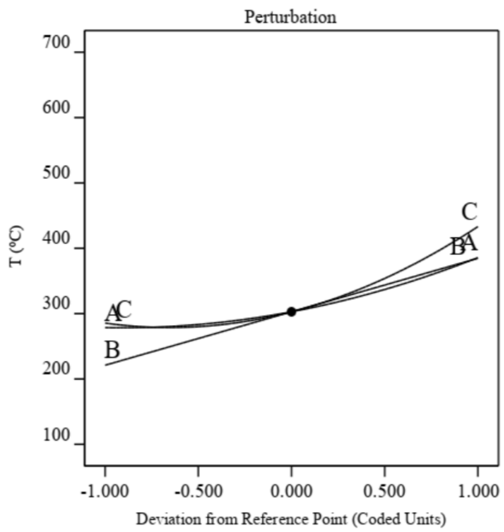

(b) HPC

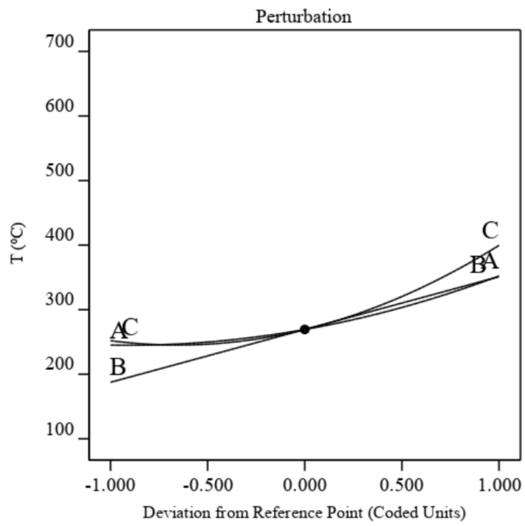

(c) RHPC

Fig. 4.3 Perturbation plots for cutting temperature under (a) Dry, (b) HPC and (c) RHPC conditions [A: cutting velocity, B: table feed, C: depth of cut]

As the temperature rises, the material softens and the yield strength of the work material decreases, resulting in a reduction in cutting forces. Fig. 4.9 also shows a progressive rise in F_c with increasing f and a_p. This issue can be described in the following way: based on the relationship among productivity($MRR = f \times a_p \times a_e$), with increasing f and a_p, it can be claimed that as productivity grows, the contact area between tool-chip increases, resulting in increased tool wear and cutting forces.

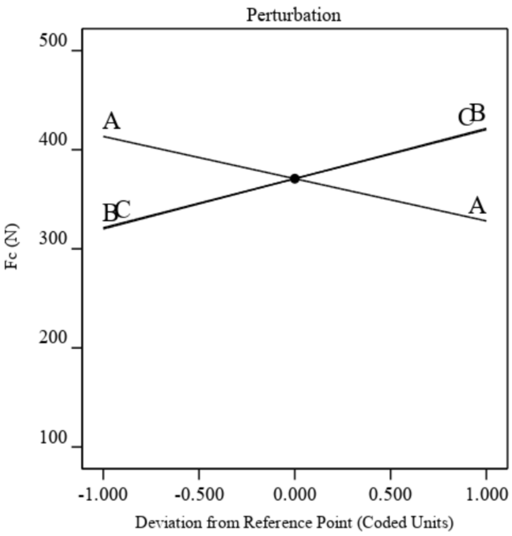

(a) Dry

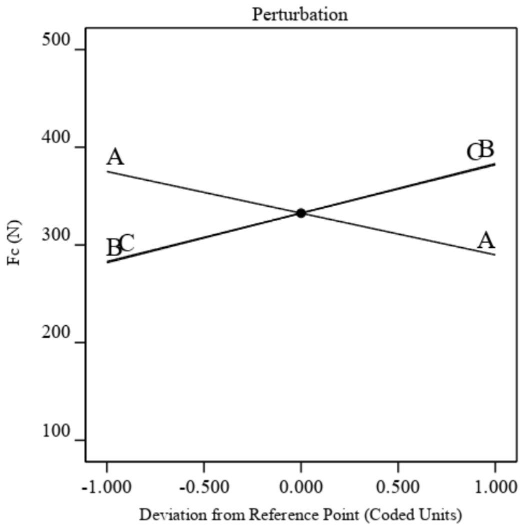

(b) HPC

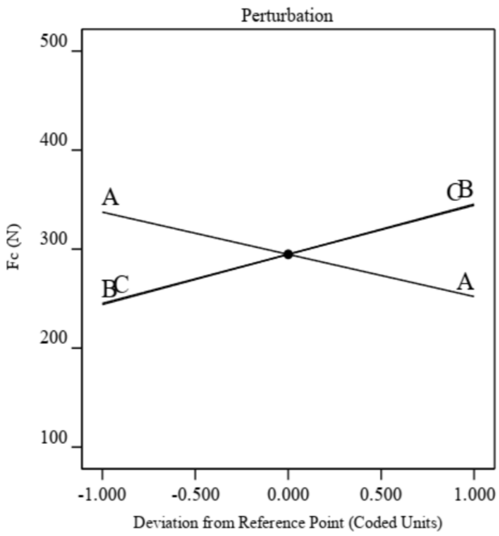

(c) RHPC

Fig. 4.4 Perturbation plots for cutting force under (a) Dry, (b) HPC and (c) RHPC conditions [A: cutting velocity, B: table feed, C: depth of cut]

Again, Fig. 4.10 shows the response surface plots of R_a vs. f and V_c for dry, HPC, and RHPC aided milling, respectively. The surface plots clearly show that R_a increases with increasing f and decreases with increasing V_c like F_c, regardless of cutting circumstances. This tendency may be based on the argument that f is directly related to chip thickness, and as chip thickness increases, chip tool contact length increases, resulting in increased friction, which negatively affects surface quality; a similar characteristic was observed in a study conducted by Mia [2017]. Simultaneously, the reverse relationship between V_c and R_a is linked to reduced friction and less development of BUE, resulting in a better surface with lower roughness. Surface roughness rises with greater f and a_p, which is the result of thicker chips forming with sharp edges, as seen in Fig. 4.11. It is also worth noting that the HPC aided milling had a lower cutting force (F_c) and surface roughness (R_a) than the dry cutting condition, while RHPC had the lowest cutting force (F_c) and surface roughness (R_a).

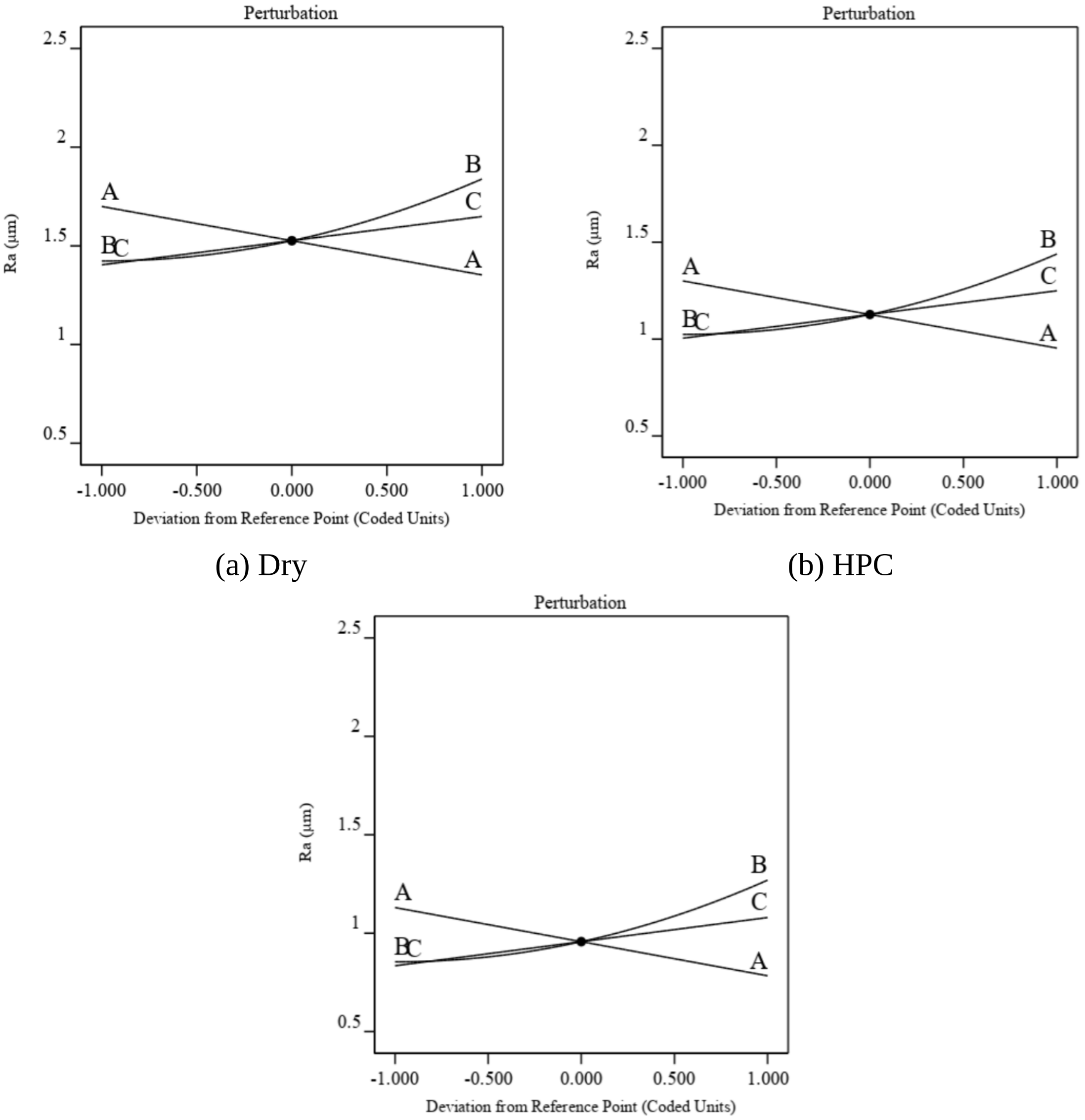

(c) RHPC

Fig. 4.5 Perturbation plots for surface roughness under (a) Dry, (b) HPC and (c) RHPC conditions [A: cutting velocity, B: table feed, C: depth of cut]

However, as compared to HPC, RHPC is more effective in reducing the mentioned responses. Because dry milling lacks cutting fluids, the convective heat transformation rate is zero, resulting in the bulk of heat being retained at the cutting zone for a longer period, reducing machinability. The exterior nozzle in traditional HPC is kept static and stationary, incapable of precision impingement of high-pressure cutting fluids (greater than 80 bar). However, converting nonrotational fluids to rotational fluids is projected to dramatically increase the cooling efficiency since such type rotating fluids carry out more heat than nonrotational fluids by significantly lowering hydraulic loss based on the principle provided by Weigand and Beer [1992]. The rotating impact on cutting fluids increases the rate of forced convective heat transfer in RHPC compared to the non-rotational supply of cutting fluids which results in better control of cutting zone temperature. So, RHPC enhances tool life with minimal tool wear and BUE, resulting in a smooth surface with reduced cutting forces (F_c). As a result, RHPC assisted milling is proposed to minimize cutting temperature, cutting force, and surface roughness.

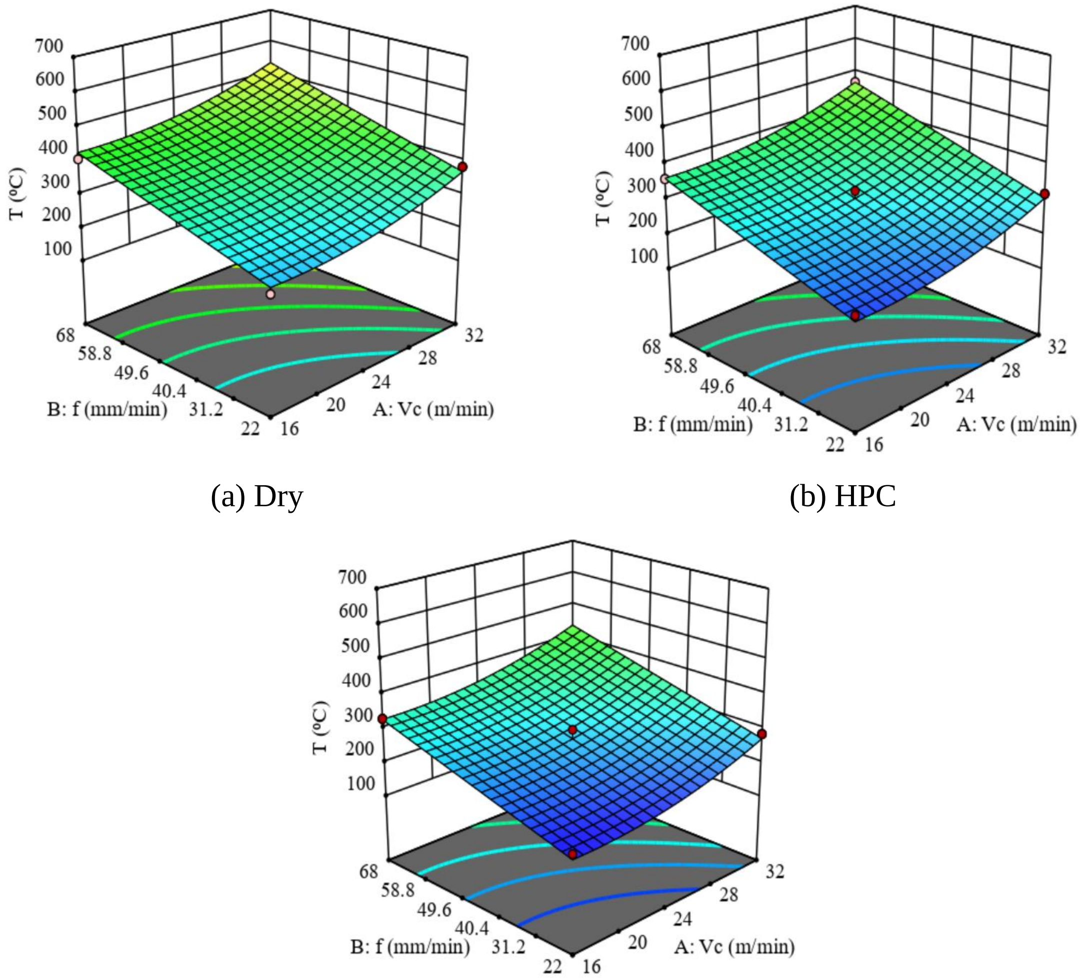

(a) Dry

(b) HPC

(c) RHPC

Fig. 4.6 3D response surface plots showing the interaction effects of V_c and f on T at 0.75 mm depth of cut under (a) Dry, (b) HPC, and (c) RHPC

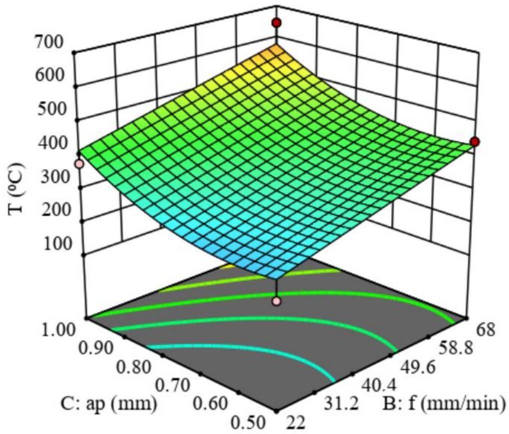

(a) Dry

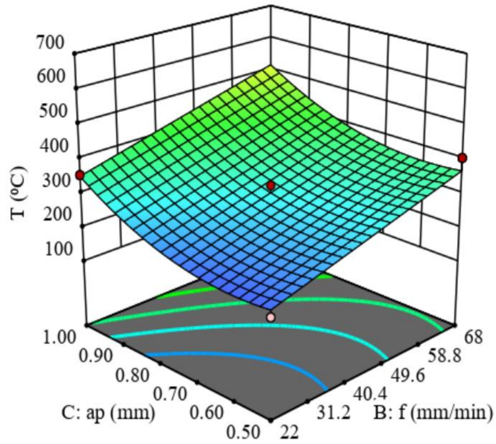

(b) HPC

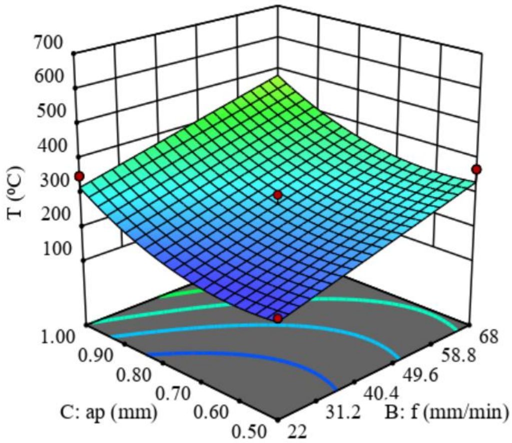

(c) RHPC

Fig. 4.7 3D response surface plots showing the interaction effects of a_p and f on T at 24 m/min cutting velocity under (a) Dry, (b) HPC, and (c) RHPC

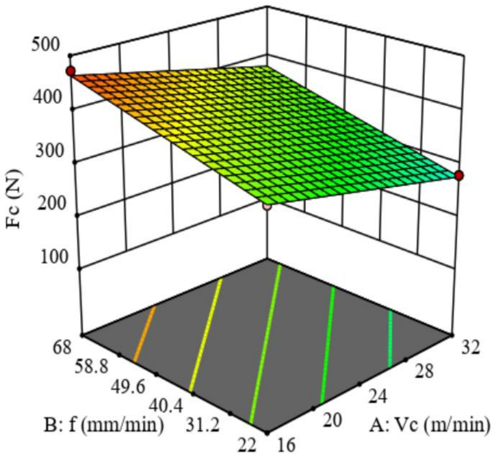

(a) Dry

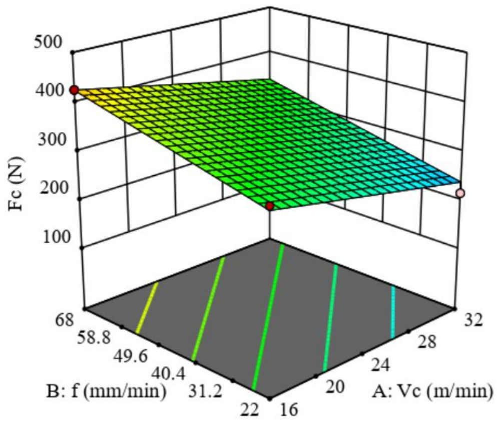

(b) HPC

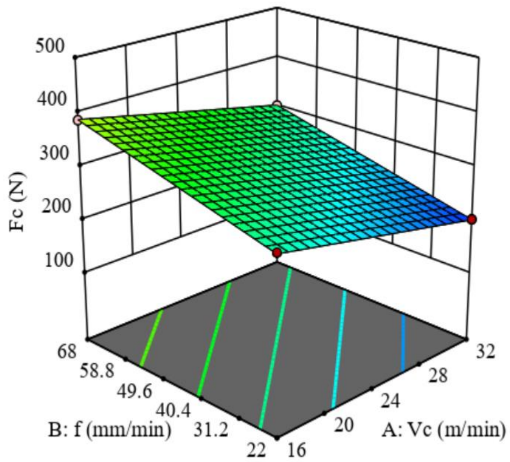

(c) RHPC

Fig. 4.8 3D response surface plots showing the interaction effects of V_c and f on F_c at 0.75 mm depth of cut under (a) dry, (b) HPC, and (c) RHPC

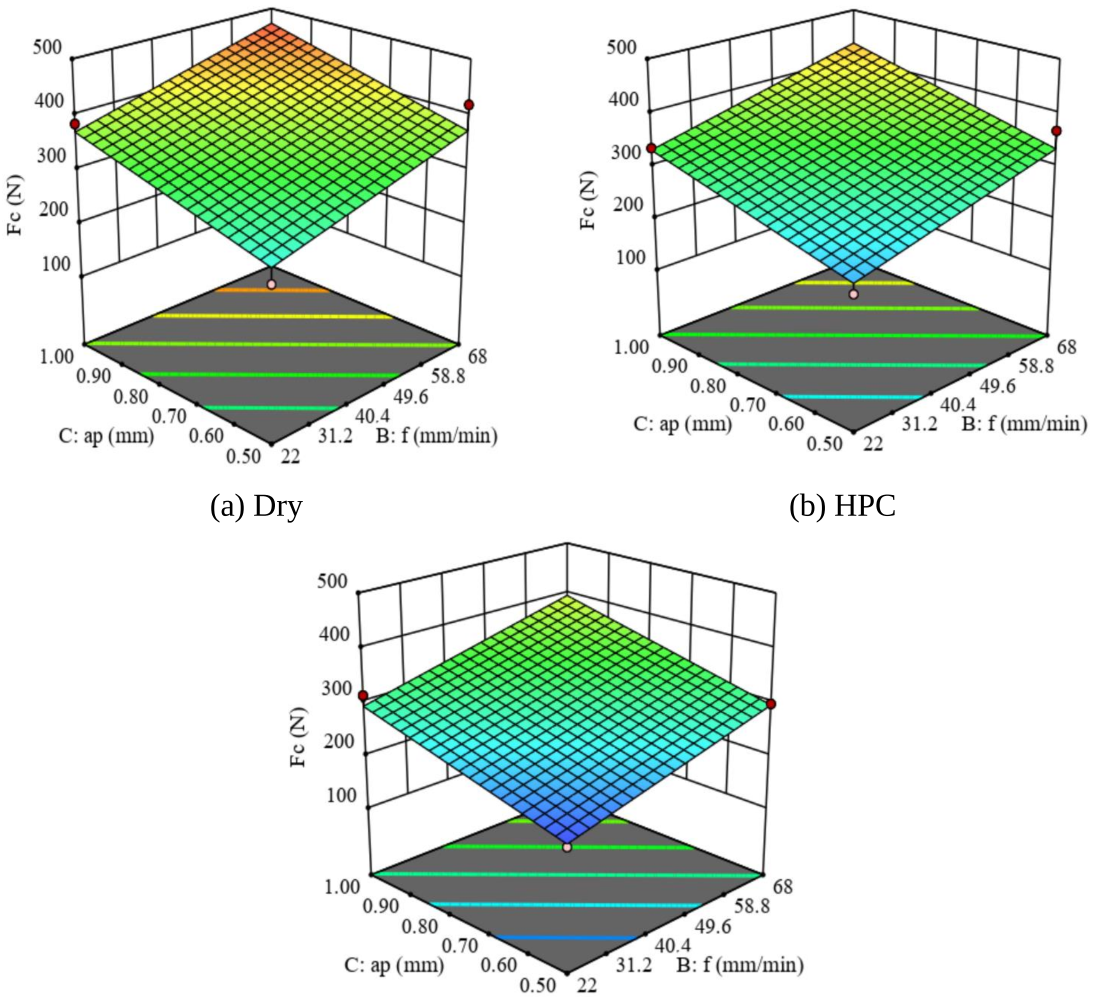

(c) RHPC

Fig. 4.9 3D response surface plots showing the interaction effects of a_p and f on F_c at 24 m/min cutting velocity under (a) Dry, (b) HPC, and (c) RHPC

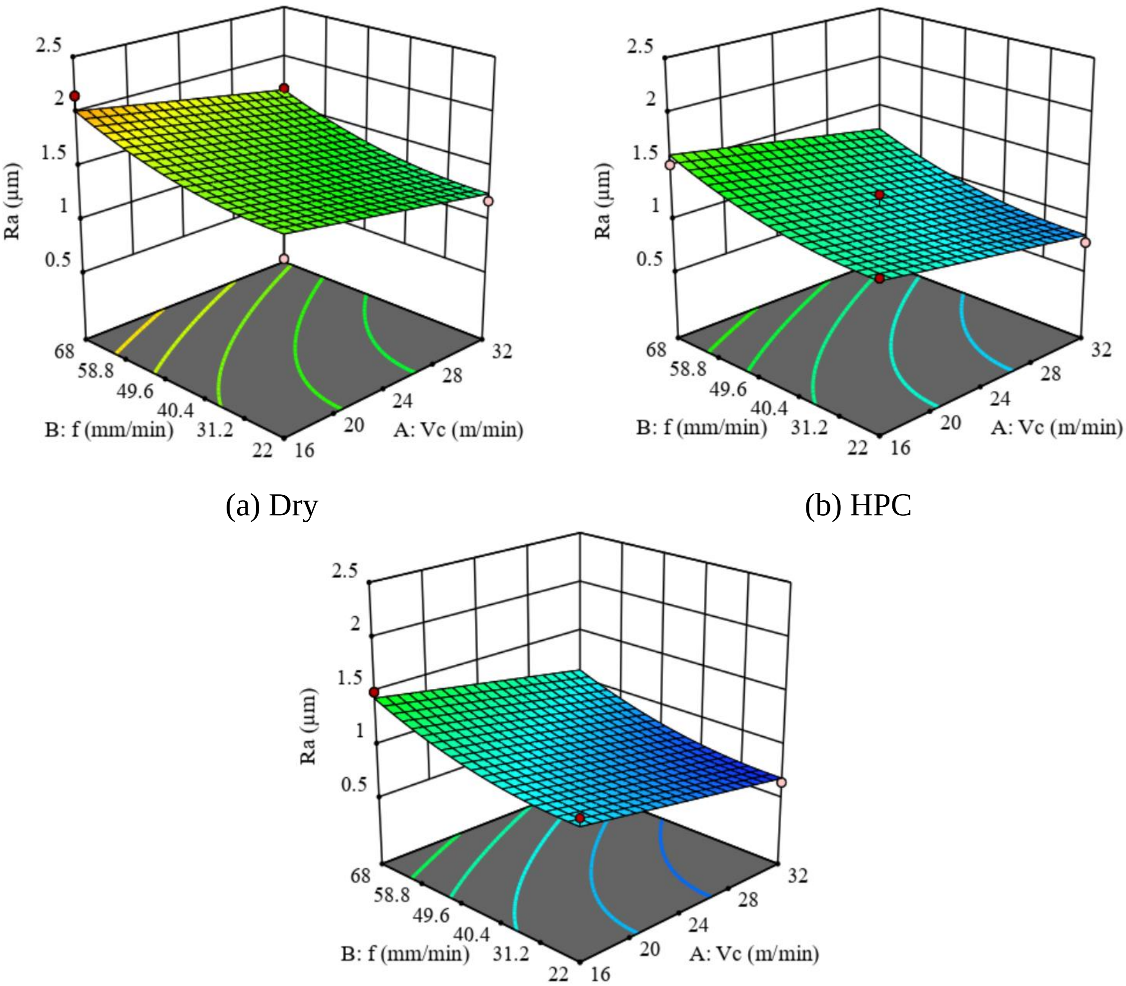

(a) Dry

(b) HPC

(c) RHPC

Fig. 4.10 3D response surface plots showing the interaction effects of V_c and f on R_a at 0.75 mm depth of cut under (a) Dry, (b) HPC, and (c) RHPC

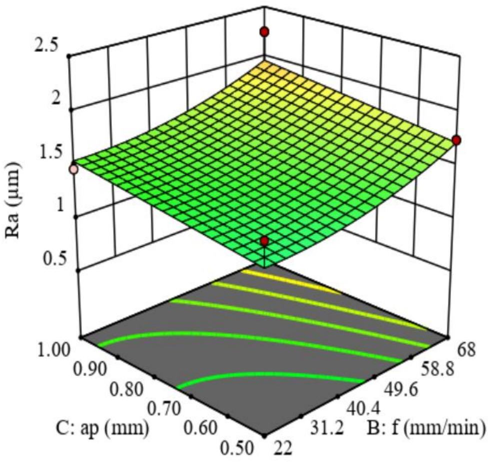

(a) Dry

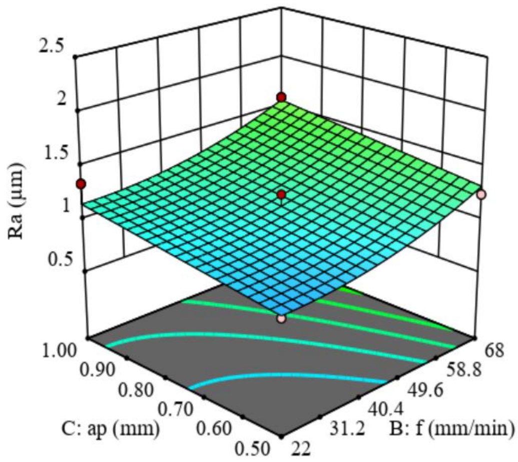

(b) HPC

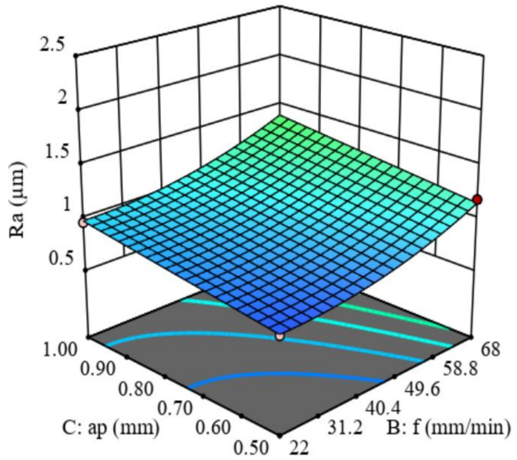

(c) RHPC

Fig. 4.11 3D response surface plots showing the interaction effects of a_p and f on R_a at 24 m/min cutting velocity under (a) Dry, (b) HPC, and (c) RHPC

Nobody can thrive in today's highly competitive market without reducing costs while simultaneously enhancing product quality. Optimizing process inputs to lower production costs without sacrificing the quality of the machined part is the primary objective of today's manufacturing business. Different multi-response optimization (MRO) techniques are available in literature but in this study, the desirability approach (DA) has been chosen as the optimization tool because of its simplicity and less time-consuming nature with better accuracy. At the beginning, conversion of the selected responses to dimensionless behavior (D_i) ranging from 0~1 is carried out to prevent calculation complexity (Ehrgott M., 2005). The weighted desirability values of each response are multiplied together to produce composite desirability (D), as illustrated in Eqn. (4.13).

$$D = (D_{i1}^{w_1} \times D_{i2}^{w_2} \times \dots \dots \times D_{im}^{w_m})^{\frac{1}{m}} \tag{4.13}$$

Where, D_i is the individual desirability for each i^{th} response and m is the number of responses. Generally, optimization has three objectives: maximization, minimization, or achieving the target. But in our experiment, all responses are required to minimize as possible. As a result, the best possible parameter values with the highest D will be chosen. The current study minimizes milling responses (T, F_c, and R_a) using an RSM-based desirability approach (DA), assuming equal weight and importance considering cutting velocity, feed rate, and depth of cut as the key process parameters for intermittent milling. The optimization criteria (goals) and constraints are listed in Table 4.6. The solution with the highest desirability value (D_i) for any given response within the range of process parameters is rated as the best solution (Sahu and Andhare 2019). In this study, multi-response optimization has been achieved at 32 m/min cutting velocity (V_c), 22 mm/min table feed rate (f), and 0.60 mm depth of cut (a_p) under RHPC with the maximum desirability 1.0. The achieved minimal values of T, F_c, and R_a are 251.9ºC, 169.8 N, and 0.60 µm, respectively at the optimum parameter settings. Finally, the revealed optimization findings are graphically depicted in Fig. 4.12. Validation has been performed by comparing the computed optimum values of responses with real experimental test results at the optimum parameter settings, and the findings are shown in Table 4.7.

Table 4.6 Optimization criteria and constraints for desirability approach

Inputs/responses	Goal	Lower limit	Upper limit	Lower weight	Upper weight	Importance
V_c	Within range	16	32	1	1	3
f	Within range	22	68	1	1	3
a_p	Within range	0.5	1	1	1	3
CC	Within range	Dry	RHPC	1	1	3
T (ºC)	Minimize	178.07	647	1	1	3
F_c (N)	Minimize	189	480.7	1	1	3
R_a (µm)	Minimize	0.64	2.25	1	1	3

Table 4.7 Validation test results

Results	V_c, m/min	f mm/min	a_p, mm	CC	T (ºC)	F_c (N)	R_a (µm)
Experimental	32	22	0.60	RHPC	252	170	0.60
Calculated	32	22	0.60	RHPC	277	185	0.67
% of error					9.03	8.11	10.03

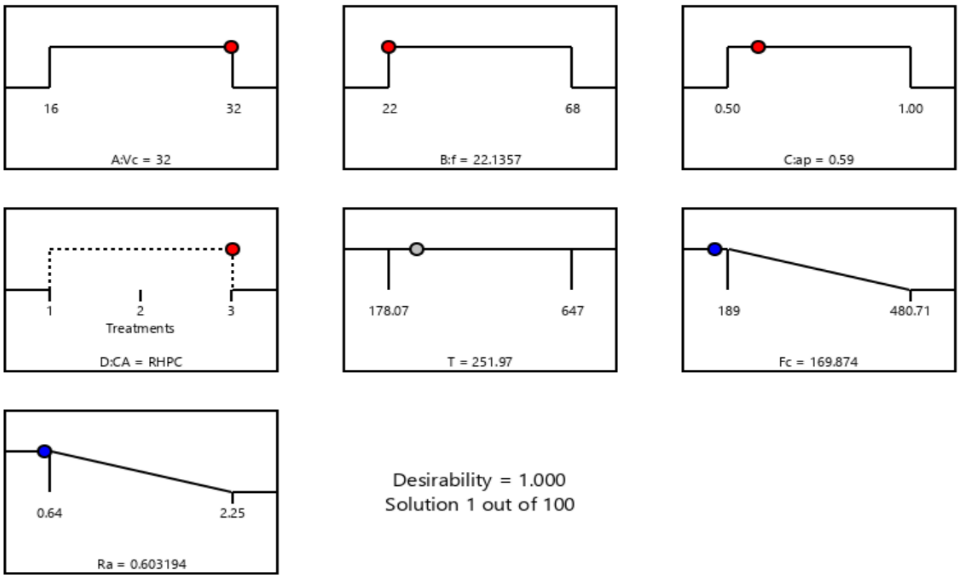

Fig. 4.12 Ramp graphs of optimization results with desirability value

4.2 Temperature Modelling using FEM

Finite element modelling (FEM) is a powerful tool for simulating any process and evaluating its performance in its intended operating environment. For the present work, 3D FEM analysis has been carried out by using the commercial software ABAQUS 6.14 with the explicit solver for more accuracy. The first step of modelling is to create the solid domain of workpiece and tool with the actual measurements and proper specifications. The thermos-physical properties of the used workpiece and tool are summarized in Table 4.8. For simulation, the size of the work material has been taken as 35mm×12mm×10mm. The element type for both Ti-6Al-4V alloy and end mill tool has been considered as C3D8RT which is an 8-node thermally coupled brick element type with trilinear displacement and temperature with reduced integration, and enhanced hourglass control. Fig. 4.13 shows the formed models of workpiece and tool with proper assemble and meshing. Hex-shaped mesh elements are chosen for discretizing the used work material and tool into 1,75,000, and 26,112 elements, respectively. For the visualization of mechanical and thermal changes with variables, the analysis step has been selected as Dynamic, temp-disp, explicit type. The uncut chip layer thickness has been taken at 0.50 and 1.00 mm. The ambient temperature of the milling process is set to 25°C.

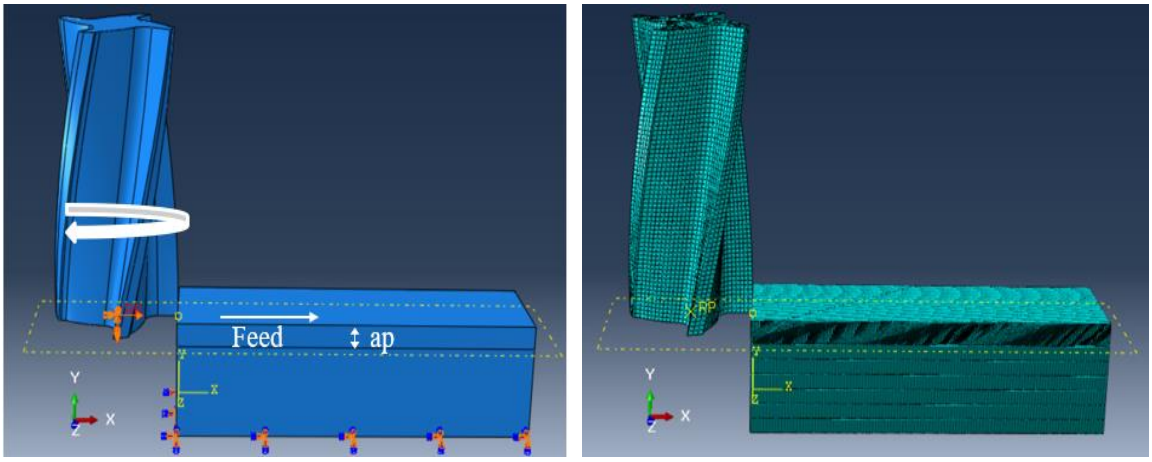

(a) Assemble model (b) Mesh model

Fig. 4.13 Simulation domain with boundary conditions of the milling process

The workpiece has been considered as a static body (ENCASTRE) while tool is dynamic with two different motions- linear motion of tool in x-direction and clockwise rotational motion, depicted in Fig. 4.13.

Table 4.8 Physical, mechanical, and thermal properties of Ti-6Al-4V alloy and HSS cutting tool

Material	Density (Kg/m^3)	Young's Modulus (GPa)	Poisson's ratio	Specific heat (J/Kg-ºC)	Thermal conductivity (W/m-ºC)
Ti-6Al-4V	4430	114	0.34	526.3	6.785
HSS Tool	7600	233	0.30	461	20.2

The end mill cutter has been considered as a rigid body for avoiding distortion. For analyzing the thermal effects on the developed stress and strain rate under different cutting conditions can be explained by using the Johnson-Cook (J-C) plastic flow stress model. Eqn. (4.14) mathematically directly expresses the appropriate J-C model for the current study with the specific numerical values, listed in Table 4.9.

$$\sigma = (1098 + 1092\varepsilon^{0.93})\left[1 + 0.014 \ln\left(\frac{\dot{\varepsilon}}{\dot{\varepsilon_0}}\right)\right]\left[1 - \left(\frac{T-25}{1605-25}\right)^{1.1}\right] \quad (4.14)$$

Where σ, the equivalent true stress, ε is the equivalent strain, $\frac{\dot{\varepsilon}}{\dot{\varepsilon_0}}$ represents the strain rate, $\dot{\varepsilon_0}$ is the reference strain rate, and T is the temperature at the cutting zone.

Table 4.9 J-C plastic flow stress model parameters for Ti-6Al-4V alloy

J-C model	A (MPa)	B (MPa)	m	n	C	$\dot{\varepsilon_0}$ (s^{-1})	T_m (°C)	T_r (°C)
Ti-6Al-4V	1098	1092	1.1	0.93	0.014	1	1,605	25

Where, A, B, n, m, and c represent the initial yield stress, strain hardening parameter, temperature exponent, strain hardening exponent, and strain rate sensitivity of Ti-6Al-4V alloy. T_m is the melting temperature and T_r is the ambient temperature. For analyzing the chip serration in milling, the J-C damage model has been selected following the earlier research works [Zhang et al. 2015]. J-C enhanced the model by including a fracture model based on cumulative damage, which is applicable for progressive damage to high strain rate applications such as milling. Damage parameters for the used Ti-6Al-4V alloy are collected in Table 4.10 and the mathematical expression of J-C fracture model is presented in Eqn. (4.15).

$$\varepsilon^f = \left[-0.09 + 0.25\exp(-0.5)\frac{\sigma_m}{\bar{\sigma}}\right]\left[1 + 0.014 \ln\left(\frac{\dot{\varepsilon}}{\dot{\varepsilon_0}}\right)\right]\left[1 + 3.87\frac{\theta-25}{1605-25}\right] \quad (4.15)$$

Where, ε^f is the equivalent plastic strain rate, $\frac{\sigma_m}{\bar{\sigma}}$ is the triaxiality factor, σ_m is the hydrostatic pressure and σ is the von mises stress. The first, second, and third bracketed terms in the model represent the effect of stress triaxiality, strain rate, and local heating, respectively.

Table 4.10 J-C damage model parameters for Ti-6Al-4V alloy

J-C damage model	D1	D2	D3	D4	D5	$\dot{\varepsilon_0}$ (s^{-1})	G_f (mJ/mm^2)
Ti-6Al-4V	-0.09	0.25	-0.5	0.014	3.87	1	20

Where, D1~D5 refers to damage factors, $\frac{\sigma_m}{\bar{\sigma}}$ is the ratio of average normal stress to von-mises stress, $\dot{\varepsilon_0}$ symolizes the reference strain rate. Damage initiation follows standard damage law [Zhang et al. 2015], as depicted in Eqn. (4.16).

$$\gamma_d = \frac{\Delta\varepsilon}{\varepsilon^f} \tag{4.16}$$

Where, γ_d is the damage initiation parameter, $\Delta\varepsilon$ is the accumulated strain rate at each increment step. Based on this model, damage initiation follows damage evolution law and the damage criteria is met when $\gamma_d = 1$. Damage evolution law can be quantitatively expressed in two terms: equivalent plastic displacement ($\bar{v}_P$) or fracture energy dissipation (G_f). This law describes how the material degrades after the damage criteria met or the degradation of material stiffness. Eqn. (4.17) can be used to calculate the damage parameter.

$$D_m = \frac{\bar{v}_p}{\bar{v}_f} \tag{4.17}$$

Where, D_m is the damage parameter, $\bar{v}_p$ and $\bar{v}_f$ symbolizes the equivalent plastic displacement at any point until failure and equivalent plastic displacement at failure, repectively. Actual damage occurs within this range ($0 < \bar{v}_p \leq 1$) of equivalent plastic displacement. When the material stiffness is fully degraded then $\bar{v}_p = \bar{v}_f$ i.e, material is removed from the calculation and chip forms. In cutting process, after the damage initiation the stress-strain curve of material is no longer able to describe the actual material's property. In this study, for avoiding such problem of mesh dependency and excess distortion of material fracture energy dissipation (G_f) was considered [Hiller Borg et al. 1976]. Fracture energy dissipation (G_f) has been calculated as a function of fracture toughness (f_{tough}), Young's modulus (E) and poison's ratio (υ), depicted as in Eqn. (4.18) [Zhang et al. 2015]:

$$G_f = f_{tough}^2 \frac{(1 - \vartheta^2)}{E} \tag{4.18}$$

The value of fracture toughness depends on the size of distorted elements but in milling the size of chips (the location of damage initiation and propagation) is very smaller so the use of f_{tough} is not realistic. Gamboa and Carolina [2021] used directly the value of G_f within the range of 15 mJ/mm^2 to 75 mJ/ mm^2 in turning Ti-6Al-4V alloy and recommended 20 mJ/mm^2 to 33.67 mJ/ mm^2 for better results in respect of chip serration. Following that in this study, 20 mJ/mm^2 has been selected as the value of G_f. The contact behavior at the tool-chip interfaces influences the variation of cutting temperature because maximum portion of the formed shear stress and frictional stress are fully converted into heat energy. In FEM, the value of inelastic heat fraction (η) has been assumed 0.9 that indicates that 90% dissipated energy is converted into heat. In this study, the mechanical and thermal interactions are modeled with the surface-to-surface contact. Surface to surface contact is characterized by master surface (tool) and slave surface (uncut chip layer of work material). The portion of heat distribution in both surfaces has been assumed equal (0.50) [Wu and Zhang 2014]. The contact areas are divided into two regions- the sliding/friction region and the sticking/cutting region. Both regions follow Coulomb's friction law which is popularly used in cutting simulation [Wu and Zhang 2014]. Based on this law, shear stress (σ_s) is equal to material shear strength ($\tau_{strength}$) at the sticking region while frictional stress (σ_f) is equal to the product of the coefficient of friction (μ) and stress to normal direction (σ_n) at the sliding region. Coulomb's friction law for cutting and sliding regions are mathematically expressed in Eqns. (4.19~4.20).

$$\sigma_s = \sigma_f = \tau_{strength}\,; \quad 0 \leq \text{length of cut} \leq \text{contact length} \tag{4.19}$$

$$\sigma_f = \mu\sigma_n\,; \quad \text{length of cut} \geq \text{contact length} \tag{4.20}$$

The coefficient of friction for dry, HPC and RHPC are assigned to be 0.2, 0.11, and 0.09, respectively as referred to this prior study [Gariani et al. 2017]. 100% of the frictional energy is converted into heat and the coefficient of heat conductance between tool and work material has been considered to be 10^8 W/m^2-°C which is imposed for the distance in the contact pair of 10^{-7} m [Klocke et al. 2017]. In this proposed model, conduction is considered the dominant heat transfer mechanism in dry milling and convection is ignored but in the case of HPC and RHPC, convective heat transfer coefficient (h) and surface film thickness coefficient (G) at the tool surface are incorporated, as previously described [Jamaludin 2017]. The cooling mechanism's effectiveness has been determined by the heat transfer coefficient and the formation of a lubricating coating on the cooled surfaces. Because of its high pressure (80 bar), forced convective heat transfer has been used to analyze the cooling impact. The forced convective heat transfer coefficient (h) is affected by the following characteristics of coolant flow such as Nusselt number (Nu), Reynolds number (Re), and Prandtl number (Pr), as well as the jet outlet shape, that are represented in Eqn. (4.21).

$$h = f(Re, Pr, Nu, shape) \tag{4.21}$$

Eqns. (4.22~4.24) mathematically express Nu_{jet}, Re_{jet}, Pr_{jet} for the used cylindrical shaped nozzle with a circular outlet [Saha 2018].

$$Nu_{jet} = \frac{hd}{K_{jet}} \tag{4.22}$$

$$Re_{jet} = \frac{\rho V_{jet} d}{\mu} \tag{4.23}$$

$$Pr_{jet} = \frac{\mu C_p}{K_{jet}} \tag{4.24}$$

Where, d (mm), the diameter of the nozzle, ρ (Kg/m^3), V_{jet} (m/s), μ (N-s/m^2), K_{jet} (W/m-°C) symbolize the density, velocity, dynamic viscosity, thermal conductivity of the sprayed jets, respectively. The velocity (V_{jet}) of the high-pressure coolant jets can be calculated by using the following Eqn. (4.25). [Hadzley et al. 2013]:

$$V_{jet} = (\frac{2P_s}{\rho})^{0.5} \tag{4.25}$$

Where, P_s (N/m^2) is the pressure of the jets at the stagnation point, after defining the flow characteristics of the sprayed fluid jets on the heated surface, the surface film thickness (G) is needed to calculate using Eqn. (4.26) [Hadzley et al. 2013].

$$G = \frac{d}{r}[\frac{1 - 1.1\frac{d}{r}}{1 + 0.1\left(\frac{H}{d} - 6\right)\frac{d}{r}}] \tag{4.26}$$

Where r and $\frac{H}{d}$ are the radial distance from the jet stagnation point and the jet to horizontal surface vertical dimensionless distance. Finally, for high-pressure coolant jets, the average Nusselt number can be calculated by using Eqn. (4.27). [Saha 2018]:

$$\overline{Nu} = 2GRe^{0.5}Pr^{0.42}(1 + 0.005Re^{0.55})^{0.5} \tag{4.27}$$

All the characteristic values related to heat transfer coefficient (h) and surface film coefficient (G) are summarized in Table 4.11.

Table 4.11 Characteristic values of high-pressure coolant jets in HPC and RHPC

Parameters	HPC	RHPC
No. of nozzle	1	4
Dia. of nozzle outlet, d (mm)	2.0	0.50
Radial distance from stagnation point, r (mm)	17.3	14
Jet to horizontal surface vertical dimensionless distance $(\frac{H}{d})$	20	20
Velocity of the jet, V_{jet} (m/s)	11.05	44.37
Pressure of the jet, P_s (N/m^2)	80×10^6	80×10^6
Reynolds number (Re)	162	320
Surface film coefficient (G)	0.1136	0.307
Sink temperature	25℃	25℃
Heat transfer coefficient (h)	20563.7	27372.7

Following the described calculation steps, a new interaction 'surface film condition' has been updated with the boundary conditions for milling with HPC and RHPC. In simulation, the temperature values are collected by choosing the tool-chip inter-face nodes and Fig. 4.14. shows that the lower level of depth of cut, feed rate, and cutting velocity are associated with the lowest cutting temperature, while the opposite relationship is seen for the higher level of depth of cut, feed rate, and cutting velocity. The highest value of cutting temperature has been recorded for dry milling at 32 m/min cutting velocity, 68 mm/min feed rate, and 1.0 mm depth of cut, that may be attributed by the increased heat accumulation at the cutting zones due to negligible heat dissipation by convection and poor thermal conductivity of Ti-6Al-4V alloy.

In HPC and RHPC, the heat reduction is accredited by two folds: carrying away heat from cutting zone through forced convection of high-pressurized coolant jets and suppressing heat generation by minimizing friction through forming an effective oil film layer between interfaces. To better understand the real changing behavior of average cutting temperature during milling it is mandatory to analyze the actual effects of process parameters in depth. As part of that, the effect of cutting velocity on the average cutting temperature at the fixed feed rate 68 mm/min and 1.0 mm depth of cut is graphically depicted in Fig. 4.15.

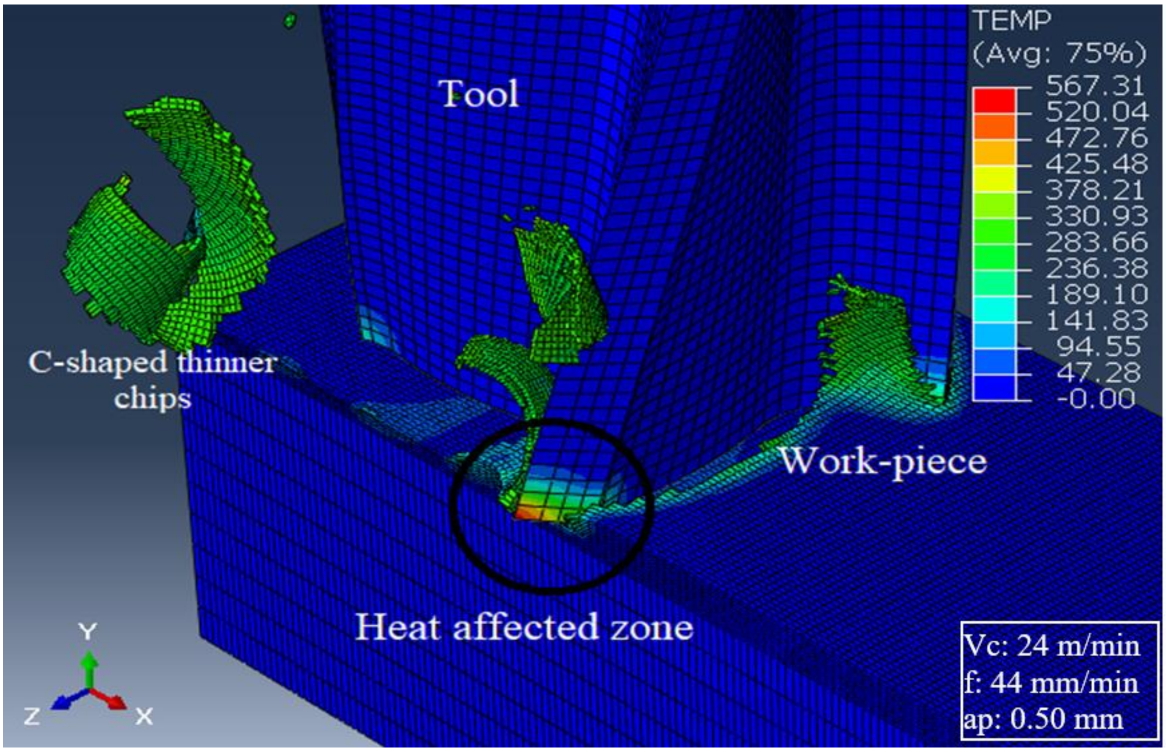

(a)

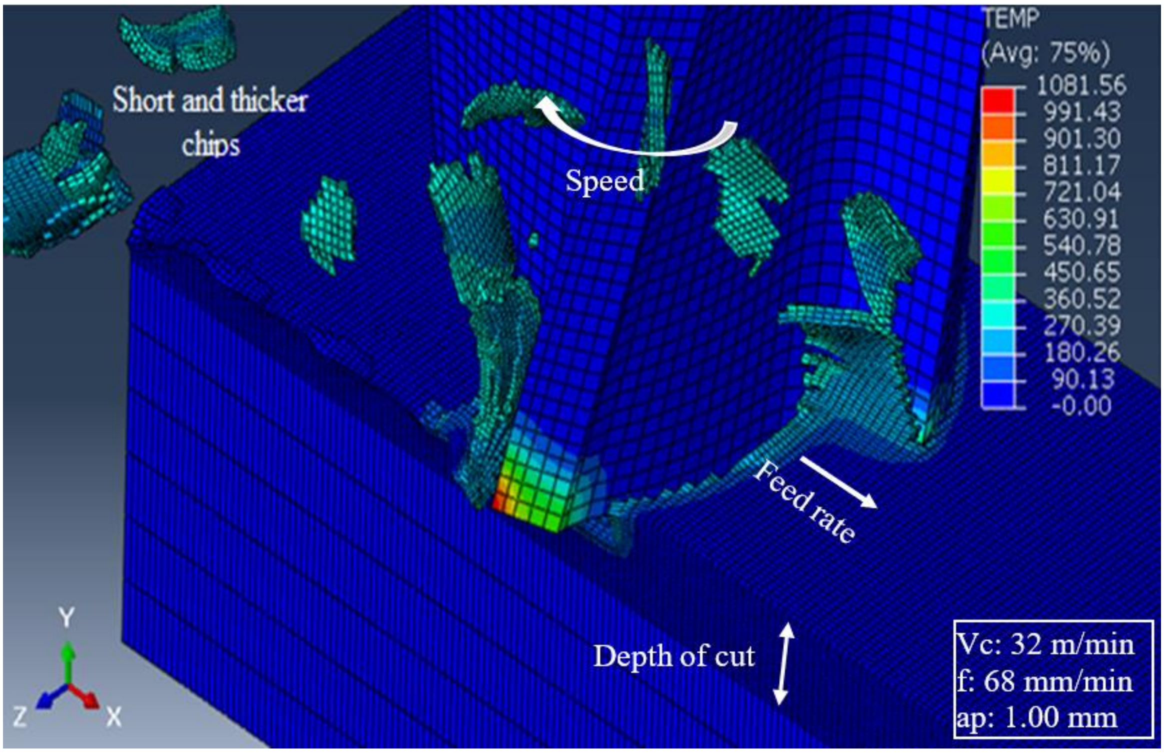

(b)

Fig. 4.14 Variation of average cutting temperature with changing process parameters under dry milling of Ti-6Al-4V alloy

When milling at cutting velocity 32 m/min instead of 24 m/min, cutting temperature increased that may be linked to a high MRR, which necessitates more specific cutting energy and momentum energy. During milling, the majority of those energies are transformed to heat energy, which leads to higher temperature. Moreover, from the J-C plastic flow model it can be elucidated that the higher strain rate in shear formation zone is responsible for such temperature rise. Similarly, Fig. 4.16 shows, a larger feed rate results in a higher temperature. The higher feed rate (68 mm/min) increased the average cutting temperature by 6.87~7.93% at constant cutting velocity 32 m/min and 1.0 mm depth of cut that may be the synergistic effects of higher friction with increased chip-tool contact length. Moreover, it can be noted that HPC and RHPC reduced the temperature over dry milling by as much as 11% ~31% and 20%~42%, respectively that dictates the significance of RHPC in reducing temperature.

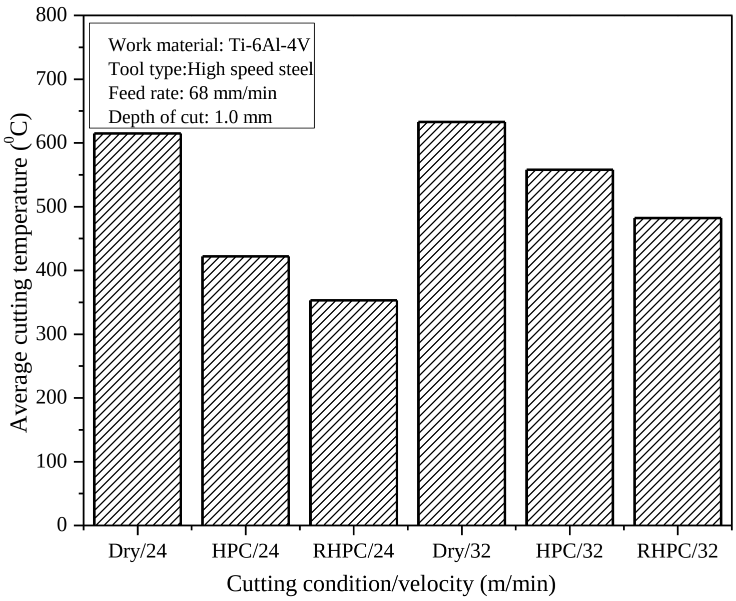

Fig. 4.15 Effect of cutting velocity on cutting temperature under different cooling conditions

Fig. 4.17 shows the effect of depth of cuts on changing the average cutting temperature at the fixed cutting velocity 24 m/min and 68 mm/min feed rate under all cooling approaches. In milling under dry, HPC, and RHPC conditions, increasing the depth of cut by 50% causes a rise in cutting temperature of 42%, 11.3%, and 8.61%, respectively, according to the simulation results in Table 4.13. The cause could be attributed to the fact that deeper cuts with larger chip loads require more energy to shear chips from the work piece, which raises temperature and is in line with earlier observations [Wu and Zhang 2014].

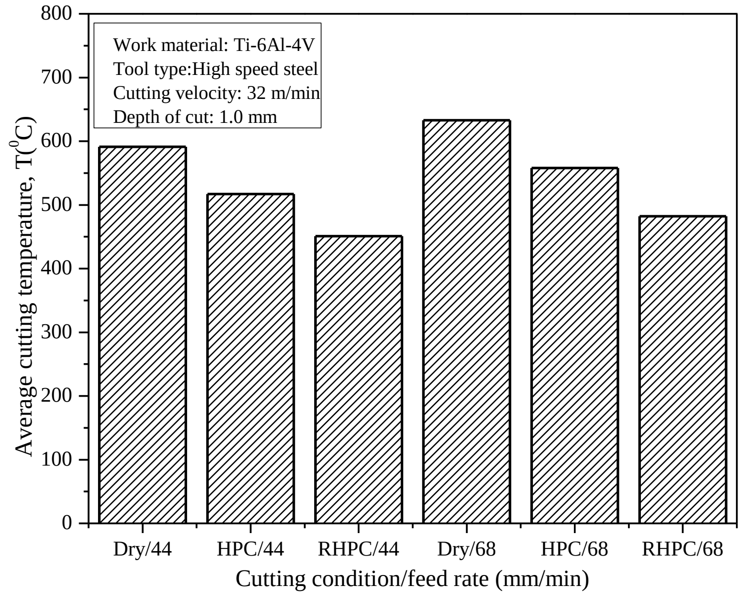

Fig. 4.16 Effect of feed rate on cutting temperature under different cooling conditions

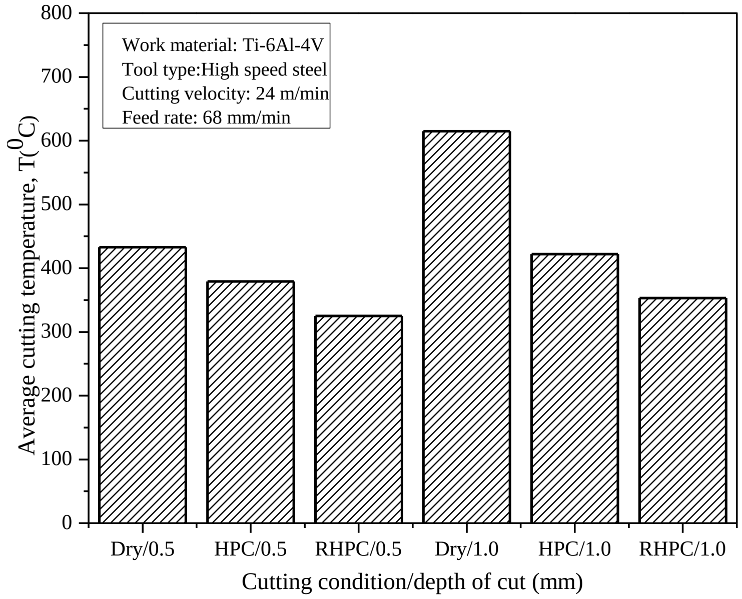

Fig. 4.17 Effect of depth of cut on cutting temperature under different cooling conditions

4.3 Modelling of Cutting Forces

Cutting force is an important metric for assessing the stability of a machining process especially at high speed, and it is linked to other responses such as power, torque, stress, tool wear, tool failure, and surface quality [Altintas 2000]. As a result, it is critical to understand the force system characteristics encountered during a specific machining operation. One goal of this research is to create an adaptable mechanistic force model that can be used to predict in a commonly encountered scenario. In this research, it is tried to model cutting for slot milling of Ti-6Al-4V alloy with a flat end mill tool under dry and high-pressure cooling (HPC). The proposed mechanistic models for the estimation of cutting forces in milling Ti-6Al-4V alloy with the consideration of the cooling effect of high-pressure coolant jets comprises of three major steps- defining cutting forces using average force method [Altintas 2000], calibrating the cutting force coefficients following oblique cutting model [Srinivasa and Shunmugam 2013], and finally, explaining the cooling effect by incorporating the modified Oxley-Johnson Cook flow stress model [Lalwani et al. 2009]. The basic assumptions of the proposed model are as follows:

i. Four flute cylindrical solid flat end mill tool with uniform helix angle.

ii. Oblique cutting model with non-zero inclination angle.

iii. Semi-static serrated chip formation [Chen et al. 2018].

iv. Consideration of both cutting and rubbing force coefficients.

v. No cutter run out along with negligible vibration and chatter.

vi. No heat loss i.e., adiabatic shear was considered at the heat sources.

vii. Integration of hardening, strain rate and thermal effects [Lalwani et al. 2009].

To minimize the initial impact load, helical design of solid end mill tools is preferred. To evaluate the cutting forces, it is a common practice to discretize the tool into a number of dz elements along the tool axis in z-direction with uniform helix angle (as shown in Fig. 4.18). Now, the forces (tangential (dF_t), radial (dF_r) and axial (dF_a)) acting on the small segment of oblique cutting edge dz can be expressed as the function of force coefficients and uncut chip thickness (h_c), as shown in Eqns. (4.28~4.30). [Altintas 2000].

$$dF_{t,j}(\theta, z) = [K_{tc}.\, h_c(\theta_j, z) + K_{te}]dz \tag{4.28}$$

$$dF_{r,j}(\theta,z) = [K_{rc}.h_c(\theta_j,z) + K_{re}]dz \quad (4.49)$$

$$dF_{a,j}(\theta,z) = [K_{ac}.h_c(\theta_j,z) + K_{ae}]dz \quad (4.30)$$

$K_{tc}, K_{rc},$ and K_{ac} represent specific cutting force coefficients whereas $K_{te}, K_{re},$ and K_{ae} notifies rubbing force coefficients in tangential, radial, and axial directions, respectively.

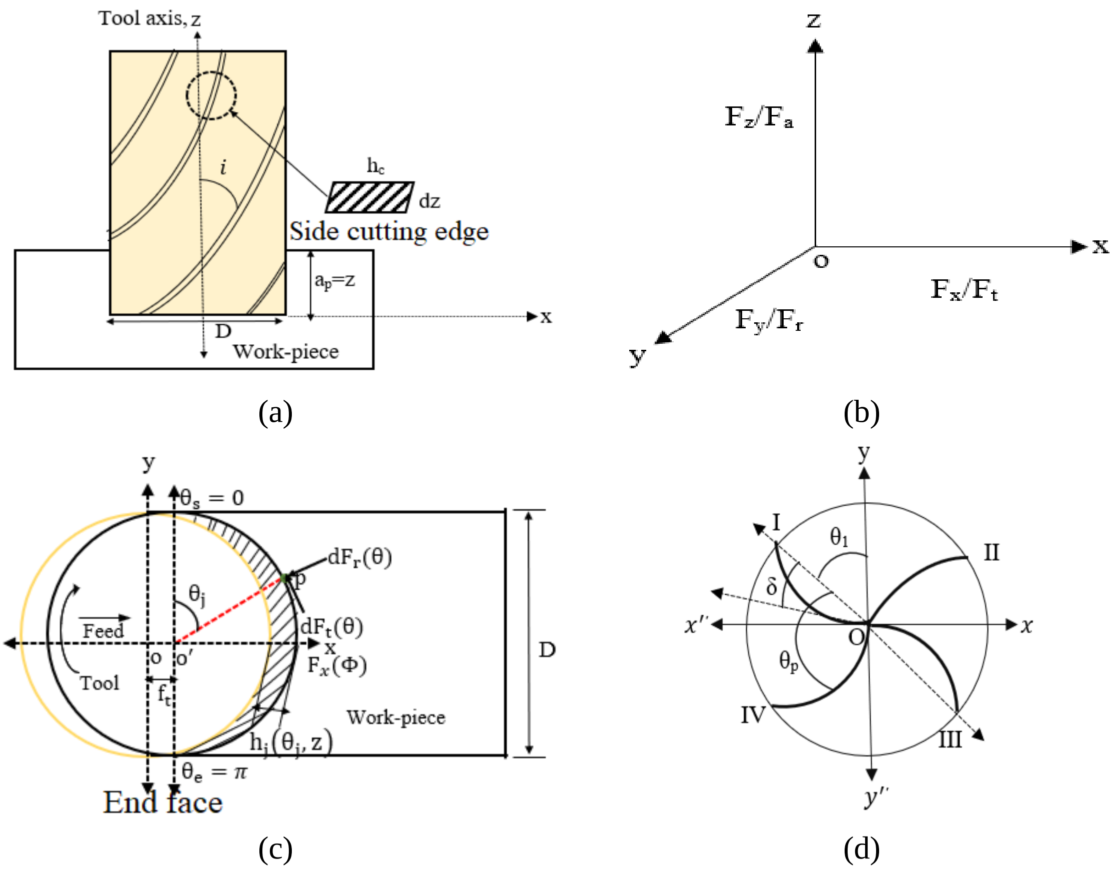

Fig. 4.18 Geometry of chip formation in slot milling

θ_j and z are the instantaneous radial and axial immersion of the cutting tool, and $h_c(\theta_j, z)$ is the instantaneous uncut chip thickness for the j^{th} tooth that is shown in Eqn. (4.31) [Srinivasa and Shunmugam 2013]:

$$h_c(\theta_j,z) = f_t \sin\theta_j(z) \ \text{ where } f_t\text{(mm/tooth) is the feed/tooth} \quad (4.31)$$

Fig 4.18 shows that complex geometry of the cutting tool which is related with different angles such as, helix angle (i), lag angle (δ), and pitch angle (θ_p) that affect the instantaneous positioning of tool. The mathematical expressions for angular positioning of any jth cutting edge are shown in Eqns. (4.32~4.33) [Kao et al. 2015]:

$$\theta_j(z) = \theta_1 + (j-1)\theta_p - \delta = \theta_1 + (j-1)\frac{2\pi}{N} - 2\tan(i)\frac{z}{D}; \quad (4.32)$$

where, N is the number of teeth, θ_1 is the angular positioning of flute 1, and D is the diameter of the tool.

After differentiating Eqn. 7.5 w.r.t. z we can get, $\frac{d\theta}{dz} = -\frac{2\tan(i)}{D}$; (4.33)

$$\therefore dz = -\frac{D}{2\tan i}d\theta$$

To generalize the modelling of cutting forces, the differential forces such as dF_t, dF_r, and dF_acan be resolved into cartesian coordinates x, y and z directions (as shown in Fig. 4.18) considering the tool center as the origin. The transformation of three different cutting forces can be written as follows (Eqn. 4.34) [Srinivasa and Shunmugam 2013]:

$$\begin{Bmatrix} dF_{x,j}(\theta,z) \\ dF_{y,j}(\theta,z) \\ dF_{z,j}(\theta,z) \end{Bmatrix} = \begin{Bmatrix} dF_{t,j}(\theta,z) \\ dF_{r,j}(\theta,z) \\ dF_{a,j}(\theta,z) \end{Bmatrix} \begin{bmatrix} -\cos\theta_j(z) & -\sin\theta_j(z) & 0 \\ \sin\theta_j(z) & -\cos\theta_j(z) & 0 \\ 0 & 0 & 1 \end{bmatrix} \quad (4.34)$$

After substituting the value of dF_t, dF_r, dF_a, and $h_j(\theta_j, z)$ into Eqn. 4.34 the model can be expressed as follows:

$$dF_{x,j}(\theta,z) = \{[-K_{tc}.f_t\sin\theta_j(z).\cos\theta_j(z) - K_{te}.\cos\theta_j(z)] + [-K_{rc}.f_t\sin^2\theta_j(z) - K_{re}.\sin\theta_j(z)]\}dz \quad (4.35)$$

$$dF_{y,j}(\theta,z) = \{[K_{tc}.f_t\sin^2\theta_j(z) + K_{te}.\sin\theta_j(z)] + [-K_{rc}.f_t\sin\theta_j(z).\cos\theta_j(z) - K_{re}.\cos\theta_j(z)]\}dz \quad (4.36)$$

$$dF_{z,j}(\theta,z) = [K_{ac}.f_t\sin\theta_j(z) + K_{ae}]dz \quad (4.37)$$

Now, by replacing 'dz' by $(-\frac{D}{2\tan i}d\theta)$ the Eqn.s (4.35~4.37) can be transformed into the following Eqns. (4.38~4.40):

$$dF_{x,j}(\theta,z) = \{[-K_{tc}.f_t\sin\theta_j(z).\cos\theta_j(z) - K_{te}.\cos\theta_j(z)] + [-K_{rc}.f_t\sin^2\theta_j(z) - K_{re}.\sin\theta_j(z)]\}dz \quad (4.38)$$

$$dF_{y,j}(\theta,z) = -\frac{D}{2\tan(i)}\{[K_{tc}.f_t\sin^2\theta_j(z) + K_{te}.\sin\theta_j(z)] + [-K_{rc}.f_t\sin\theta_j(z).\cos\theta_j(z) - K_{re}.\cos\theta_j(z)]\}d\theta \quad (4.39)$$

$$dF_{z,j}(\theta,z) = -\frac{D}{2\tan(i)}[K_{ac}.f_t\sin\theta_j(z) + K_{ae}]d\theta \quad (4.40)$$

After that, integrating the eqns. (4.38~4.40) within the boundary conditions (Start angle, $\theta_s = 0$ and end angle, $\theta_e = \pi$) of slot milling (down type), we can get the total force for j^{th} tooth, as follows [Altintas 2000]:

$$F_{x,j}(\theta, z) = \int_{\theta_s=0}^{\theta_e=\pi} -\frac{D}{2\tan(i)}\{[-K_{tc}.f_t\sin\theta_j(z).\cos\theta_j(z) - K_{te}.\cos\theta_j(z)] + [-K_{rc}.f_t\sin^2\theta_j(z) - K_{re}.\sin\theta_j(z)]\}d\theta \quad (4.41)$$

$$F_{y,j}(\theta, z) = \int_{\theta_s=0}^{\theta_e=\pi} -\frac{D}{2\tan(i)}\{[K_{tc}.f_t\sin^2\theta_j(z) + K_{te}.\sin\theta_j(z)] + [-K_{rc}.f_t\sin\theta_j(z).\cos\theta_j(z) - K_{re}.\cos\theta_j(z)]\}d\theta \quad (4.42)$$

$$F_{z,j}(\theta, z) = \int_{\theta_s=0}^{\theta_e=\pi} -\frac{D}{2\tan(i)}[K_{ac}.f_t\sin\theta_j(z) + K_{ae}]d\theta \quad (4.43)$$

$$F_r(\theta_j, z) = \int_{\theta_s=0}^{\theta_e=\pi} dF_{r,j}(\theta, z)\ ;\ r=x,\ y,\ z \quad (4.44)$$

Finally, the cutting force expressions can be written as in Eqns. (4.45~4.47) by considering full axial immersion, $z = \frac{D}{2\tan(i)}$:

$$F_{x,j}(\theta, z) = \frac{z}{2}f_t\pi.K_{rc} + 2z.K_{re} \quad (4.45)$$

$$F_{y,j}(\theta, z) = -\frac{z}{2}f_t\pi.K_{tc} - 2z.K_{te} \quad (4.46)$$

$$F_{z,j}(\theta, z) = -2zf_t.K_{ac} - z\pi.K_{ae} \quad (4.47)$$

As per the Eqns. (4.28~4.30), the average force components per tooth are dependent on the value of chip load (h_c (θ_j, z)). Now, the average cutting forces for N number of flutes in one revolution can be expressed as follows [Altintas 2000]:

$$\bar{F}_x(\theta, z) = -\frac{Nzf_t.K_{rc}}{4} - \frac{Nz.K_{re}}{\pi} \quad (4.48)$$

$$\bar{F}_y(\theta, z) = \frac{Nzf_t.K_{tc}}{4} + \frac{Nz.K_{te}}{\pi} \quad (4.49)$$

$$\bar{F}_z(\theta, z) = \frac{Nzf_t.K_{ac}}{\pi} + \frac{Nz.K_{ae}}{2} \quad (4.50)$$

In oblique cutting, cutting forces are affected by the helix angle (i), normal rake angle (α_n), as shown in Fig. 4.19. Based on the stabler's rule [1951], helix angle (i) and chip velocity angle (ω) are equal, so α_n can be expressed as follows (Eqn. 4.51):

$$\alpha_n = \tan^{-1}(\tan\alpha \,.\, \cos i);\ \alpha,\ \text{rake angle} \tag{4.51}$$

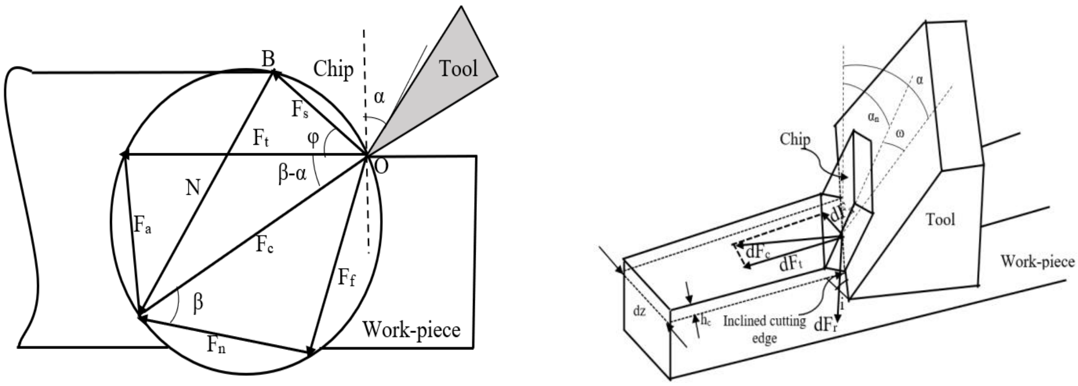

(a) Orthogonal cutting (b) Oblique cutting

Fig. 4.19 Different cutting forces in (a) orthogonal, and (b) oblique cutting

In mechanistic modelling for defining force coefficients, orthogonal to oblique transformation is generally carried out to increase its prediction accuracy. Force coefficients can be divided into cutting and non-cutting/rubbing coefficients. Earlier research conducted by Merchant [1945] reveals that both coefficients are dependent on various factors such as shear stress (τ_s), shear angle (φ_n), rake angle (α_n), chip velocity angle (ω), helix angle (i), and friction angle (β_n) that can be derived from orthogonal cutting theory. Friction angle (β_n) can be expressed as the function of friction coefficient and afterwards, shear angle (φ_n) can be calculated as follows [Sonawane and Joshi 2010]:

$$\mu = \tan\beta_n;\ \mu,\ \text{friction coefficient and } \tan\beta_n = \tan\beta.\cos\omega \tag{4.52}$$

$$\varphi_n = \frac{\pi}{4} + \frac{\beta_n}{2} - \frac{\alpha_n}{2} = C_1 + C_2(\beta_n - \alpha_n)\ ;\ C_1 \text{ and } C_2 \text{ are constants.} \tag{4.53}$$

Based on the oblique cutting principle of Armarego [1985], the three specific cutting force coefficients in tangential, radial and axial directions can be derived by using the following Eqns. (4.54~4.56), respectively.

$$K_{tc} = \frac{\tau_s[\cos(\beta_n - \alpha_n) + \tan(i).\tan(\omega).\sin\beta_n]}{\sin\varphi_n\sqrt{\cos^2(\varphi_n + \beta_n - \alpha_n) + \tan^2(\omega).\sin^2\beta_n}} \tag{4.54}$$

$$K_{rc} = \frac{\tau_s[\sin(\beta_n - \alpha_n)]}{\sin\varphi_n.\cos(i)\sqrt{\cos^2(\varphi_n + \beta_n - \alpha_n) + \tan^2(\omega).\sin^2\beta_n}} \quad (4.55)$$

$$K_{ac} = \frac{\tau_s[\cos(\beta_n - \alpha_n).\tan(i) - \tan(\omega).\sin\beta_n]}{\sin\varphi_n\sqrt{\cos^2(\varphi_n + \beta_n - \alpha_n) + \tan^2(\omega).\sin^2\beta_n}} \quad (4.56)$$

Where, the helix angle (i) was considered equal to chip velocity angle (ω) following Stabler's rule [1951]. In end milling, with decreasing the axial depth of cut, the rubbing effect of the bottom edge of the tool increases so, it is required to measure. Armarego [1985] manifested that the rubbing coefficients are independent of cutting type (orthogonal or oblique) and can be presented as follows (Eqns. 4.57~4.59) [Lin et al. 2021]:

$K_{te} = r_n.\tau_s.\tan(\frac{\pi}{4} + \frac{\alpha_n}{2})$; r_n, the nose radius of the used tool. (4.57)

$$K_{re} = 1 + \frac{\pi}{2} \quad (4.58)$$

$$K_{ae} = 0 \quad (4.59)$$

For the evaluation of force coefficients, measuring the value of shear stress (τ_s) is mandatory. Johnson-Cook [1983] provided the popular flow stress model for measuring shear flow stress as a function of the effect of shear strain, strain rate and instantaneous temperature (as shown in Eqn. 4.60) that can be used to define the required shear stress at the cutting zone.

$$\sigma_s = [\underbrace{(A + B\varepsilon^n)}_{\text{Strain hardening effect}}\underbrace{(1 + C\ln\frac{\dot{\varepsilon}}{\dot{\varepsilon}_0})}_{\text{Strain rate}}\underbrace{(1 - \left(\frac{T - T_r}{T_m - T_r}\right)^m}_{\text{Thermal softening effect}}] \quad (4.60)$$

Where, A, B, C, n, m are the constants, depend on the work material type. ε, $\dot{\varepsilon}$, and $\dot{\varepsilon}_0$ are the equivalent strain, strain rate, and reference plastic strain rate (1.0 s^{-1}), respectively. Finally, the shear stress can be determined by modifying the J-C model presented as in Eqn. (4.61) [Chen et al. 2018]:

$$\tau_s = \frac{\sigma_s}{\sqrt{3}} = \frac{1}{\sqrt{3}}[(A + B\varepsilon^n)(1 + C\ln\frac{\dot{\varepsilon}}{\dot{\varepsilon}_0})(1 - \left(\frac{T - T_r}{T_m - T_r}\right)^m] \quad (4.61)$$

T, T_m, and T_r are the instantaneous, melting and room temperature of the work-material. In dry milling, only the conductive heat transfer occurs at the tool-chip interface because of the absence of coolant. Generally, heat conduction obeys the following Eqn. (4.62):

$$\frac{\partial^2 T}{\partial x^2} + \frac{\partial^2 T}{\partial y^2} + \frac{\partial^2 T}{\partial z^2} = \frac{\rho c_p}{K} \frac{\partial T}{\partial t} \tag{4.62}$$

Where, ρ, c_p, and K are the density (Kg/m^3), specific heat (J/Kg-K), and thermal conductivity (W/m-K) of work material. But in HPC, convection is the main heat transfer mechanism between tool-chip interface and coolant jets. Finally, the cooling capacity of the used high-pressure coolant jets can be mathematically expressed as Eqn. (4.63):

$$Q_{conv} = \rho A_i V_{oil} c_{poil}(T_o - T_i) \tag{4.63}$$

Where, ρ, V_{oil}, and c_{poil} are the density (Kg/m^3), flow velocity (m/s), and specific heat (J/Kg-K) of the high-pressure coolant jets. A_i is the area of the nozzle for coolant supply. Finally, ε, and $\dot{\varepsilon}$ are unknown parameters that can be calculated from the Oxley's predictive machining theory [Lalwani et al. 2009]. Referring to Fig. 4.20, the equivalent shear strain (ε) at the shear plane is actually the half of the shear strain (γ) at the primary shear zone because of its positioning and its mathematical expression is written in Eqn. (4.64).

$$\varepsilon = \frac{\gamma}{2\sqrt{3}} = \frac{1}{2\sqrt{3}} . \frac{\cos\alpha_n}{\sin\varphi_n . \cos\ (\varphi_n - \alpha_n)} \tag{4.64}$$

The equivalent strain rate ($\dot{\varepsilon}$) at the shear plane is proportional to shear velocity (V_s) and inversely proportional to the length of shear plane (l) that is expressed in Eqn. (4.65).

$$\dot{\varepsilon} = C_0 . \frac{V_s}{\sqrt{3} l} = \frac{C_0}{\sqrt{3} l} . \frac{V_c \text{Cos}\alpha_n}{\cos(\varphi_n - \alpha_n)} \tag{4.65}$$

; V_c (m/min), cutting velocity, and C_0, strain rate constant

Based on the Oxley's theory, C_0 is the ratio of the length to thickness of the shear plane that can be determined by using following formulae (4.66) and considering the equal normal stress (σ_n) at point of shear plane and tool-chip interface [Chen et al. 2018].

$$C_0 = \frac{A + B\varepsilon^n}{2nB\varepsilon^n} [1 + \frac{\pi}{2} - 2\alpha_n - \frac{\sigma_n}{\tau_s}] \tag{4.66}$$

Where, $\sigma_n = \frac{F_n}{zh} = \frac{F_c \sin\beta_n}{zh}$ where, F_c, and h_c symbolizes the resultant force, and chip thickness before cut. In this study, instantaneous temperature of the work-piece was determined by using 3D FEM using ABAQUS.

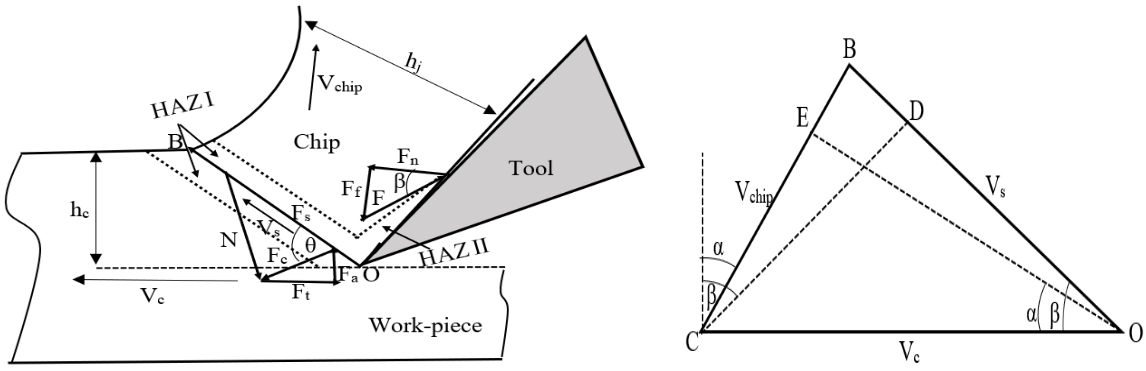

(a) (b)

Fig. 4.20 (a) Chip formation based on Oxley's theory, and (b) relationship between shear velocity and chip flow velocity with cutting velocity

4.4 Validation of the Models

Any model like empirical, numerical, or mechanistic generally manifests different degrees of prediction accuracy and it is mandatory to check its' validity. To pursue such objective in this study, the predictability of the used models has been evaluated by using absolute percentage error (APE) and mean absolute percentage error (MAPE) as expressed in Eqns. (4.67~4.68).

$$APE = \frac{|Y_{actual} - Y_{predict}|}{Y_{actual}} \times 100\% \tag{4.67}$$

$$MAPE = \frac{1}{N}\sum_{i=1}^{N} APE_i \tag{4.68}$$

Where, N is the total number of trial runs, Y_{actual} symbolizes the actual experimental value and $Y_{predict}$ represents the predicted value of responses determined by the used models such as RSM, FEM, and mechanistic. RSM model was used to evaluate three quantitative measures of milling performances namely cutting temperature (T), cutting force (F_c), and surface roughness (R_a). Table 4.12 summarizes the RSM models' predictability which was checked by computing APE and MAPE for 24 randomly selected trials from the BBD design matrix (as ref. to Table 4.2). MAPE obtained by using RSM for F_c are 4.45 %, respectively, whereas the values for T and R_a are 6.60% and 6.26 %. The lower value of MAPE for T, F_c, and R_a manifest the higher consistency between the experimental and RSM predicted results.

Table 4.12 APE and MAPE for predicted values of cutting temperature, cutting force, and surface roughness by RSM

Trial	V_c, m/min	f, mm/min	a_p, mm	CC	T (°C)	T_p (°C)	APE	F_c (N)	F_{cp} (N)	APE	R_a (µm)	R_{ap} (µm)	APE
1	24	68	1.00	RHPC	404	465	15.1	378	395	4.61	1.32	1.39	5.30
2	24	68	0.50	RHPC	371	318	14.3	298	296	0.72	1.18	1.15	2.54
3	24	68	1.00	HPC	491	542	10.4	416	433	4.14	1.59	1.56	1.89
4	16	45	1.00	Dry	480	487	1.43	481	463	3.70	1.63	1.82	11.66
5	32	45	1.00	Dry	617	591	4.26	377	378	0.30	1.32	1.48	12.12
6	24	68	0.50	Dry	443	480	8.36	419	372	11.19	1.74	1.72	1.15
7	24	22	1.00	RHPC	351	322	8.40	314	294	6.41	0.96	0.98	2.08
8	32	45	0.50	RHPC	299	331	10.6	213	202	5.06	0.74	0.66	10.81
9	24	22	1.00	Dry	378	384	1.70	384	370	3.83	1.47	1.55	5.44
10	16	45	0.50	RHPC	249	227	8.99	283	288	1.70	0.98	1.01	3.06
11	32	45	1.00	RHPC	488	478	2.02	308	302	1.99	1.00	0.91	9.00
12	24	22	0.50	RHPC	180	174	3.52	189	194	2.90	0.72	0.73	1.39
13	24	68	1.00	Dry	647	628	2.96	458	471	2.91	2.25	1.96	12.89
14	32	45	0.50	Dry	484	443	8.44	289	279	3.67	1.35	1.23	8.89
15	24	22	0.50	HPC	184	186	1.51	213	232	8.87	0.88	0.90	2.27
16	16	45	1.00	HPC	413	419	1.49	435	425	2.39	1.44	1.42	1.39
17	32	45	1.00	HPC	518	523	0.96	333	339	1.81	1.24	1.08	12.90
18	16	45	1.00	RHPC	356	374	5.19	377	387	2.56	1.30	1.25	3.85
19	32	45	0.50	HPC	320	375	17.3	270	240	11.06	0.84	0.83	1.19
20	24	22	0.50	Dry	209	236	12.9	243	271	11.52	1.53	1.30	15.03
21	16	45	0.50	HPC	259	272	4.86	316	326	3.01	1.14	1.18	3.51
22	24	22	1.00	HPC	355	334	5.85	335	331	1.04	1.34	1.15	14.18
23	24	68	0.50	HPC	405	395	2.46	368	334	9.22	1.24	1.32	6.45
24	16	45	0.50	Dry	323	339	5.02	363	364	0.26	1.58	1.56	1.27
MAPE							6.60			4.45			6.26

Similarly, validation of finite element modelling for predicting cutting temperature in milling Ti-6Al-4V alloy at various cutting velocities, feed rates, and depth of cuts was conducted. Table 4.13 manifests that the MAPE values of cutting temperature for dry, HPC and RHPC are 5.01%, 8.38%, and 11.3%, respectively which is acceptable based on the prior findings by researchers [Wu and Zhang 2014]. From the error results analysis it has been noticed that the prediction accuracy of FEM is higher for dry milling compared to other twos that may be attributed by the fact of considering uniform surface film thickness coefficient over the cutting edges of the tool for both HPC and RHPC but in reality, uniformity is lacking. Moreover, a certain error may exist in the temperature measuring thermocouple system during milling with high-pressure coolant jets. Another observation was that lower values of cutting temperature was achieved in simulation compared to experimental results for all cutting conditions that may be attributed by the consideration of stable machining neglecting the machining disturbances such as vibration, chattering and tool run out during simulation. For clear visualization of the mismatch between the experimental and predicted results of cutting temperature Fig. 4.21 was plotted. The comparative prediction accuracy of RSM model and FEM in respect of experimentally measured cutting temperature for some random cutting conditions is graphically presented in Fig. 4.22. The MAPE value of FEM model was achieved 6.63% while this value was found slightly higher in RSM model with 8.10% that ultimately reveals the higher accuracy of FEM which is also agreed with the findings of a prior study [Zhang et al. 2015].

Table 4.13 Experimental and numerically predicted results of average cutting temperature using FEM with their corresponding APE

Test No.	V_c (m/min)	f (mm/min)	a_p (mm)	Dry			HPC			RHPC		
				T (℃)	T_n (℃)	APE	T (℃)	T_n (℃)	APE	T (℃)	T_n (℃)	APE
1	24	44	0.5	356	333	6.50	303	294	2.97	283	264	6.50
2	24	68	0.5	443	433	2.25	405	379	6.40	371	325	12.5
3	24	44	1.0	539	517	3.90	471	405	14.0	392	334	14.0
4	24	68	1.0	647	615	4.90	491	422	14.0	404	353	12.6
5	32	44	0.5	484	439	9.30	320	315	1.25	299	271	9.20
6	32	68	0.5	556	551	1.25	443	386	12.8	393	331	14.8
7	32	44	1.0	617	591	4.20	565	517	7.30	488	451	7.60
8	32	68	1.0	687	633	7.80	609	558	8.30	559	482	13.0
MAPE						5.01			8.38			11.3

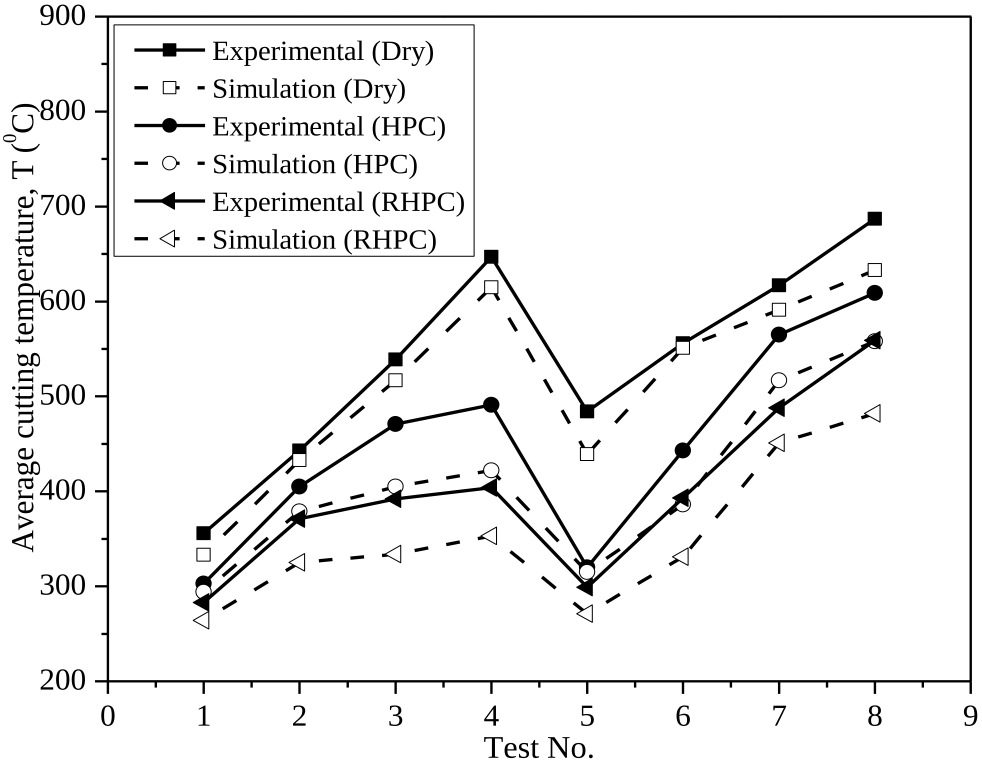

Fig. 4.21 Validation of simulated results compared to its corresponding experimental results

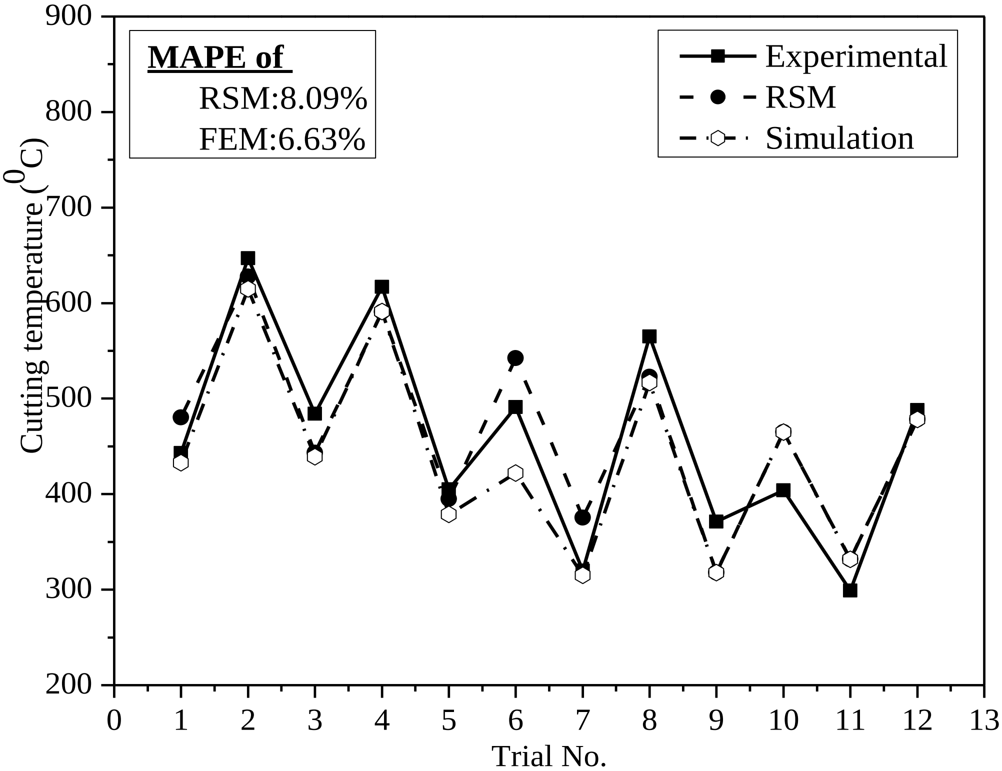

Fig. 4.22 Comparative analysis of prediction accuracy of RSM and FEM results

To validate the accuracy of the proposed mechanistic model of cutting forces, a series of slot milling tests are carried out with and without high-pressure coolant jets. The cutting conditions used for slot milling tests with the experimental and predicted results from the proposed model are summarized in Table 4.14. The normal rake angle (α_n) and the mean friction angle (β_n) has been determined by using Eqns. (4.51~4.52), where friction coefficient (μ) is considered 0.2 and 0.11 for dry and HPC [Gariani et al. 2017]. Finally, the shear angle has been obtained by using Eqn. (4.53) considering $C_1 = \frac{\pi}{4}$ and $C_2 = 0.5$ based on the minimum energy principle provided by Merchant [1945]. The measured values of different angles can be specified as follows: $\alpha_n = 4.33°, \beta_n^{Dry} = 11.3°, \beta_n^{HPC} = 6.28°, \emptyset_n^{Dry} = 41.52°, \emptyset_n^{HPC} = 44.03$. Three separate cutting forces have been calculated after measuring the values of all necessary unknown parameters using the above mathematical formulas. For instance, the following values of the six cutting force coefficients are reported when dry milling the Ti-6Al-4V alloy at 32 m/min cutting velocity, 44 mm/min feed rate, and 1.0 mm depth of cut: K_{tc}=2333MPa, K_{rc}=1404 MPa; K_{ac}= 428 MPa; K_{te}=16.04; K_{re}=2.57; and K_{ae}=0.

Table 4.14 Experimental and predicted values of cutting forces at different cutting conditions

Trial No.	V_c (m/min)	f (mm/min)	a_p (mm)	Cooling Conditions	Experimental Result				Predicted Result			
					F_t (N)	F_r (N)	F_a (N)	F_c (N)	F_{tm} (N)	F_{rm} (N)	F_{am} (N)	F_{cm} (N)
1	24	22	1.0	Dry	233	126	279	385	263	107	258	384
2	24	22	1.0	HPC	198	120	242	335	220	102	197	312
3	32	22	1.0	Dry	201	115	255	343	245	125	216	350
4	32	22	1.0	HPC	180	117	222	309	228	105	204	323
5	32	44	0.5	Dry	159	128	205	289	190	119	176	285
6	32	44	0.5	HPC	147	93	207	270	172	90	175	261
7	32	44	1.0	Dry	217	173	256	377	270	169	216	385
8	32	44	1.0	HPC	192	120	246	334	234	110	213	335

Fig. 4.23 shows the experimental and mathematically predicted values of resultant cutting forces where slight differences were noticed with MAPE 2.6% that may be attributed by the following facts such as no chatter, vibration, cutter runout is considered in the model. Moreover, the variable rake angle of the helical tool during the intermittent cutting is not considered for the simplicity of the model that may also contribute some misalignments between the predicted results and real data. For checking the prediction accuracy between RSM and mechanistic modelling in respect to actual results of cutting forces some random

data are taken into consideration and summarized the APE and MAPE of RSM and mechanistic modelling in Table 4.15. From the comparative analysis, it has been observed that the accuracy of the proposed mechanistic model is higher than RSM model.

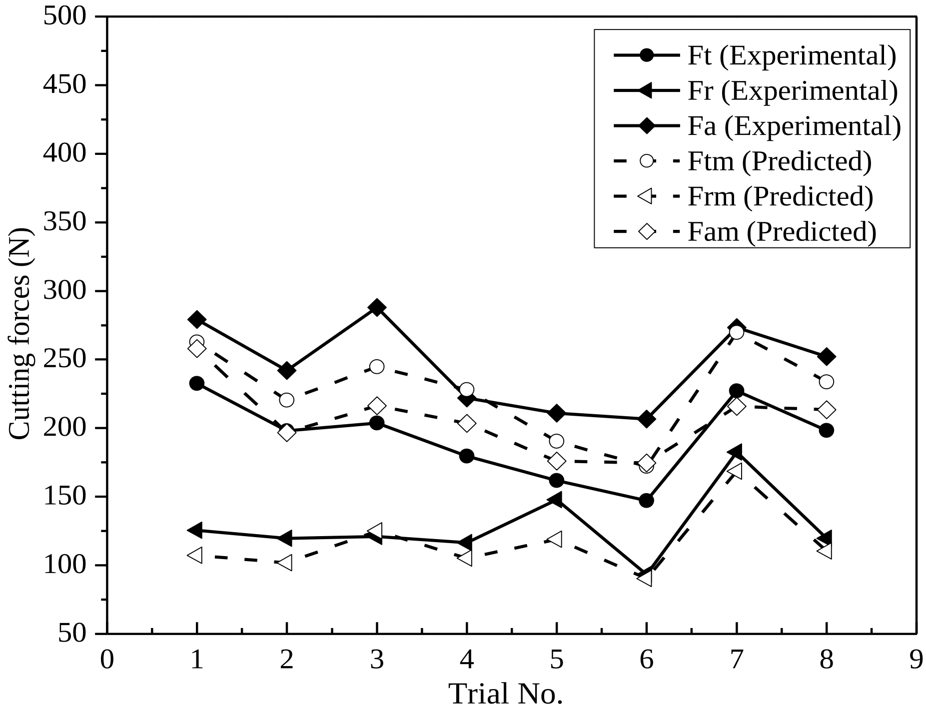

Fig. 4.23 Experimental and predicted values of cutting forces

Table 4.15 Comparative analysis of prediction accuracy of RSM and FEM models

Trial No.	V_c (m/min)	f (mm/min)	a_p (mm)	Cooling Conditions	F_c (N)	F_{cp} (N)	F_{cm} (N)	APE_{RSM}	APE_{ME}
1	24	22	1.0	Dry	385	370	384	3.90	0.35
2	24	22	1.0	HPC	335	331	312	1.19	6.74
3	32	44	0.5	Dry	289	279	285	3.46	1.38
4	32	44	0.5	HPC	270	240	261	11.11	3.20
5	32	44	1.0	Dry	377	378	385	0.27	2.08
6	32	44	1.0	HPC	334	339	335	1.50	0.30
MAPE								3.60	2.34

Chapter-5

Conclusions and Recommendations

5.1 Conclusions

The purpose of this research is to design and develop rotary applicator for supplying high-pressure coolant jets in milling Ti-6Al-4V alloy in respect of machinability enhancement. An external rotary applicator has been experimentally and numerically investigated for milling this alloy. The main contributions of this research are as follow:

i. An efficient external rotary applicator for supplying uninterrupted coolant jets towards the end mill cutter during milling has been designed and developed. Using integrated Taguchi-CFD analysis, the optimum design parameters have been achieved as 80 bar pressure, 3.0 L/min oil flow rate, and 0.50 mm nozzle dia. while volumetric flow rate has been noticed as the most dominant factor followed by nozzle dia., and oil flow pressure in enhancing cooling rate.

ii. In RHPC, the circulating jets simultaneously speed up the rate of convective heat transfer that ultimately enhances the machinability of Ti-6Al-4V alloy.

iii. Compared to dry milling, cutting temperature is reduced by 24.11% and 37.56% in HPC and RHPC, respectively. Similarly, cutting force and surface roughness are reduced by 21.53% and 41.33% in RHPC over dry milling, respectively. Less BUE, less chattering with steady machining conditions, and a lower coefficient of friction due to the creation of a superior oil lubricating film between tool-chip-work interfaces boost to achieve such favorable results in RHPC.

iv. At higher levels of cutting velocity, feed rate, and depth of cut, the conversion of a greater quantity of specific cutting energy into heat energy raises cutting temperature. On the other hand, thermal softening with lower BUE, reduced friction, and shorter tool-chip contact length, reduce cutting force and surface roughness at greater velocity with lower feed rate and depth of cut.

v. Compared to dry and HPC, 53% and 24% higher tool life is observed in RHPC, respectively. In RHPC, proper cooling and lubrication effects seem to be the prime reasons behind this.

vi. From statistical analysis, it is noticed that feed rate is the most dominant factor in changing responses followed by depth of cut, and lastly by, cutting velocity. Using CDA, 32 m/min cutting velocity, 26 mm/min table feed rate, and 0.60 mm depth of cut has been found as the optimal process parameters for minimizing the stated responses as a whole.

vii. Three dimensional (3D) finite element modelling (FEM) using ABAQUS/Explicit has been conducted to predict the cutting temperature accurately during end milling of Ti-6Al-4V alloy with a complex shaped end mill tool. In this investigation, approximately 6.60% mismatch has been observed between the experimental and simulated results.

viii. An integrated mechanistic model has been used to predict cutting forces as a function of velocity, feed rate, depth of cut, cooling condition, and tool’s helix angle. The proposed model's MAPE was only 2.60% that is highly accepted. Comparative assessment amongst three different modelling reveals the empirical model as the least accurate prediction methods.

5.2 Recommendations

Some limiting facts of this research are recommended as scopes for further research:

i. Only HSS end mill tools have been used in this study; the effect of coated or uncoated carbide tools is not specified; this may be incorporated in future research. Furthermore, additional research can be conducted with brief analyses of various micro and macro aspects of chips, tool materials, and residual stress.

ii. Different weight calculation methods such as principal component analysis (PCA), criteria importance through inter-criteria correlation (CRITIC), analytical hierarchy process (AHP), entropy method, standard deviation method can be incorporated to perform sensitivity analysis.

iii. In mechanistic modelling, the effect of unstable machining conditions such as vibrations, chattering, tool run out are not considered, that may be added to extend the applicability of the proposed model.

References

Alagan, N. T., Zeman, P., Mara, V., Beno, T., Wretland, A. "High-pressure flank cooling and chip morphology in turning Alloy 718", CIRP Journal of Manufacturing Science and Technology, Vol. 35, pp. 659-674, 2021.

Altintas, Y., Spence, A., & Tlusty, J. "End milling force algorithms for CAD systems", CIRP annals, Vol. 40, No. 1, pp. 31-34, 1991.

Altintas, Y. "Modelling approaches and software for predicting the performance of milling operations at MAL-UBC", Machining science and technology, Vol. 4, No. 3, pp.445-478, 2000.

Ahmed, L. S., Govindaraju, N., & Pradeep Kumar, M. "Experimental investigations on cryogenic cooling in the drilling of titanium alloy", Materials and Manufacturing Processes, Vol. 31, No. 5, pp. 603-607, 2016.

Andriya, N., Rao, P. V., & Ghosh, S. "Dry machining of Ti-6Al-4V using PVD coated TiAlN tools", In Proceedings of the World Congress on Engineering, WCE, July, 2012.

Antony, J. "Design of experiments for engineers and scientists", Elsevier, 2014.

Asiltürk, I., Neşeli, S., Ince, M.A. " Optimization of parameters affecting surface roughness of Co28Cr6Mo medical material during CNC lathe machining by using the Taguchi And RSM methods", Measurement, Vol. 78, pp. 120-128, 2016.

Astakhov, V. P., & Shvets, S. "The assessment of plastic deformation in metal cutting", Journal of Materials Processing Technology, Vol. 146, No. 2, pp. 193-202, 2004.

Astakhov, V. P., & Godlevskiy, V. "Delivery of metalworking fluids in the machining zone. In Metalworking Fluids (MWFs) for Cutting and Grinding", pp. 79-134. Woodhead Publishing, 2012.

Attanasio, A., Ceretti, E., Rizzuti, S., Umbrello, D., & Micari, F. "3D finite element analysis of tool wear in machining", CIRP annals, Vol. 57, No. 1, PP. 61-64, 2008.

Aramcharoen A, Shaw KC. "An Experimental Investigation on Cryogenic Milling of Inconel 718 and its Sustainability Assessment". Procedia CIRP, Vol. 14, pp. 529-534, 2014.

Aramcharoen, A. "Influence of cryogenic cooling on tool wear and chip formation in turning of titanium alloy", Procedia CIRP, Vol. 46, pp. 83-86, 2016.

Aristimuño, P., Lazcano, X., Sela, A., Basagoiti, R., & Arrazola, P. J. "An optimization methodology for material databases to improve cutting force predictions when milling martensitic stainless steel JETHETE-M152", Procedia CIRP, Vol. 77, pp. 287-290, 2018.

Arizmendi, M., Fernández, J., de Lacalle, L. L., Lamikiz, A., Gil, A., Sánchez, J. A.,Campa, F.J., & Veiga, F. "Model development for the prediction of surface topography generated by ball-end mills taking into account the tool parallel axis offset. Experimental validation", CIRP annals, Vol. 57, No. 1, pp. 101-104, 2008.

Armarego, E.J.A. & Whitfield, R.C. "Computer based modelling of popular machining operations for force and power prediction", CIRP annals, Vol. 34, No.1, pp.65-69, 1985.

Arrazola, P. J., Özel, T., Umbrello, D., Davies, M., & Jawahir, I. S. "Recent advances in modelling of metal machining processes", CIRP Annals, Vol. 62, No. 2, pp. 695-718, 2013.

Azeem, A., Feng, H. Y., & Wang, L. "Simplified and efficient calibration of a mechanistic cutting force model for ball-end milling", International Journal of Machine Tools and Manufacture, Vol. 44, No. 2-3, pp. 291-298, 2004.

Bai, X., Li, C., Dong, L., & Yin, Q. "Experimental evaluation of the lubrication performance of different nanofluids for minimum quantity lubrication (MQL) in milling Ti-6Al-4V", The International Journal of Advanced Manufacturing Technology, Vol. 101, No. 9, pp. 2621-2632, 2019.

Bayoumi, A. E., Yucesan, G., Kendall, L. A. "An analytic mechanistic cutting force model for milling operations: a theory and methodology", Transactions of ASME: Journal of the Engineering and Industries, Vol. 116, pp. 324–330, 1994.

Bermingham, M. J., Kirsch, J., Sun, S., Palanisamy, S., & Dargusch, M. S. "New observations on tool life, cutting forces and chip morphology in cryogenic machining Ti-6Al-4V", International Journal of Machine Tools and Manufacture, Vol. 51, No. 6, pp. 500-511, 2011.

Bermingham, M. J., Palanisamy, S., Kent, D., & Dargusch, M. S. " A comparison of cryogenic and high-pressure emulsion cooling technologies on tool life and chip morphology in Ti–6Al–4V cutting", Journal of Materials Processing Technology, Vol. 212, No. 4, pp. 752-765, 2012.

Bermingham, M. J., Palanisamy, S., Morr, D., Andrews, R., & Dargusch, M. S. "Advantages of milling and drilling Ti-6Al-4V components with high-pressure coolant", The International Journal of Advanced Manufacturing Technology, Vol. 72, Nos.1-4, pp. 77-88, 2014.

Boswell, B., & Chandratilleke, T. "Air-cooling used for metal cutting", American Journal of Applied Science, Vol. 6, No. 2, pp. 251-262, 2009.

Braghini Junior, A., & Diniz, A. E. "Tool wear and tool life in end milling of 15–5 PH stainless steel under different cooling and lubrication conditions", The International Journal of Advanced Manufacturing Technology, Vol. 43, No. 7, pp. 756-764, 2009.

Braham-Bouchnak, T., Germain, G., Morel, A., & Furet, B "Influence of high-pressure coolant assistance on the machinability of the titanium alloy Ti555–3", Machining

Science and Technology, Vol. 19, No.1, pp. 134-151, 2015.

Budak, E., Altintas, Y., & Armarego, E. J. A. "Prediction of milling force coefficients from orthogonal cutting data", Transactions of the ASME Journal of Manufacturing Science and Engineering, Vol. 118, pp. 216–224, 1996.

Budak, E., Ozturk, E., & Tunc, L. T. "Modelling and simulation of 5-axis milling processes", CIRP annals, Vol. 58, No.1, pp. 347-350, 2009.

Caggiano, A., Napolitano, F., & Teti, R. "Dry turning of Ti6Al4V: tool wear curve reconstruction based on cognitive sensor monitoring", Procedia CIRP, Vol. 62, pp.209-214, 2017.

Campatelli, G., & Scippa, A. "Prediction of milling cutting force coefficients for Aluminum 6082-T4", Procedia CIRP, Vol. 1, pp. 563-568, 2012.

Chen, Y., Li, H. and Wang, J. "Predictive modelling of cutting forces in end milling of titanium alloy Ti6Al4V", Proceedings of the Institution of Mechanical Engineers, Part B: Journal of Engineering Manufacture, Vol. 232, No. 9, pp.1523-1534, 2018.

Cheng, P. J., Tsay, J. T., & Lin, S. C. "A study on instantaneous cutting force coefficients in face milling", International Journal of Machine Tools and Manufacture, Vol. 37, No.10, pp. 1393-1408, 1997.

Chetan, B. C., Behera, S., Ghosh, S., & Rao, P. V. "Wear behavior of PVD TiN coated carbide inserts during machining of Nimonic 90 and Ti6Al4V superalloys under dry and MQL conditions", Ceramics International, Vol. 42, No. 13, pp. 14873–14885, 2016.

Childs, T. H., Maekawa, K., Obikawa, T., & Yamane, Y. "Metal machining: theory and applications", Butterworth-Heinemann, 2000.

Courbon, C., Kramar, D., Krajnik, P., Pusavec, F., Rech, J., & Kopac, J. "Investigation of machining performance in high-pressure jet assisted turning of Inconel 718: an experimental study", International Journal of Machine Tools and Manufacture, Vol. 49, No. 14, pp. 1114-1125, 2009.

Courbon, C., Sajn, V., Kramar, D., Rech, J., Kosel, F., & Kopac, J. "Investigation of machining performance in high pressure jet assisted turning of Inconel 718: A numerical model", Journal of Materials Processing Technology, Vol. 211, No. 11, pp. 1834-1851, 2011.

Dahlman, P., & Escursell, M. "High-pressure jet-assisted cooling: a new possibility for near net shape turning of decarburized steel", International Journal of Machine Tools and Manufacture, Vol. 44, No. 1, pp. 109-115, 2004.

Debnath, S., Reddy, M. M., & Pramanik, A. "Dry and near-dry machining techniques for green manufacturing", In Innovations in Manufacturing for Sustainability (pp. 1-27). Springer, Cham, 2019.

Deng, W. J., Xia, W., & Tang, Y. "Finite element simulation for burr formation near the exit of orthogonal cutting", The International Journal of Advanced Manufacturing Technology, Vol. 43, No. 9, pp. 1035-1045, 2009.

Dikshit, M. K., Puri, A. B., & Maity, A. "Modelling and application of response surface optimization to optimize cutting parameters for minimizing cutting forces and surface roughness in high-speed, ball-end milling of Al2014-T6", Journal of the Brazilian Society of Mechanical Sciences and Engineering, Vol. 39, No. 12, pp. 5117-5133, 2017.

Dhar, N. R., & Kamruzzaman, M. "Cutting temperature, tool wear, surface roughness and dimensional deviation in turning AISI-4037 steel under cryogenic condition", International Journal of Machine Tools and Manufacture, Vol. 47, No. 5, pp. 754-759, 2007.

Diniz, A. E., & Micaroni, R. "Influence of the direction and flow rate of the cutting fluid on tool life in turning process of AISI 1045 steel", International Journal of Machine Tools and Manufacture, Vol. 47, No. 2, pp. 247-254, 2007.

Donachie, M. J. "Titanium. A Technical Guide-Second edition", ASM International, 2000.

Dureja, J. S., Gupta, V. K., Sharma, V. S., Dogra, M., & Bhatti, M. S. "A review of empirical modelling techniques to optimize machining parameters for hard turning applications", Proceedings of the Institution of Mechanical Engineers, Part B: Journal of Engineering Manufacture, Vol. 230, No. 3, pp. 389-404, 2014.

Edkins, K. D., van Rensburg, N. J., & Laubscher, R. F. "Evaluating the subsurface microstructure of machined Ti-6Al-4V", Procedia CIRP, Vol. 13, pp. 270-275, 2014.

Ehrgott, M. "Multi-criteria optimization", Springer Science & Business Media, 2005.

Eltaggaz, A., Said, Z., & Deiab, I. "An integrated numerical study for using minimum quantity lubrication (MQL) when machining austempered ductile iron (ADI)", International Journal on Interactive Design and Manufacturing (IJIDeM), Vol. 14, No. 3, pp. 747-758, 2020.

Ezugwu, E. O., & Wang, Z. M. "Titanium alloys and their machinability—a review", Journal of materials processing technology, Vol. 68, No. 3, pp. 262-274, 1997.

Ezugwu, E. O., Bonney, J., & Yamane, Y. "An overview of the machinability of aero-engine alloys", Journal of materials processing technology, Vol. 134, No. 2, pp. 233-253, 2003.

Ezugwu, E. O., & Bonney, J. "Effect of high-pressure coolant supply when machining nickel-base, Inconel 718, alloy with coated carbide tools", Journal of materials processing technology, Vol. 153, pp. 1045-1050, 2004.

Ezugwu, E. O., Da Silva, R. B., Bonney, J., & Machado, A. R. "Evaluation of the performance of CBN tools when turning Ti–6Al–4V alloy with high-pressure coolant supplies", International Journal of Machine Tools and Manufacture, Vol. 45, No. 9, pp. 1009-1014, 2005.

Fratila, D. "Sustainable manufacturing through environmentally-friendly machining", In Green Manufacturing Processes and Systems (pp. 1-21). Springer, Berlin, Heidelberg, 2013.

Gamboa, B., Carolina. “Modelling of the fracture energy on the finite element simulation in Ti6Al4V alloy machining”, Scientific Report, Vol. 11, No. 1, pp. 1-13, 2021.

Gao, G., Wu, B., Zhang, D., & Luo, M. “Mechanistic identification of cutting force coefficients in bull-nose milling process”, Chinese Journal of Aeronautics, Vol. 26, No. 3, pp. 823-830, 2013.

Garcia, U., & Ribeiro, M. V. “Ti6Al4 V titanium alloy end milling with minimum quantity of fluid technique use”, Materials and Manufacturing Processes, Vol. 31, pp. 1–14, 2015.

García-Martínez, E., Miguel, V., Martínez-Martínez, A., Manjabacas, M. C., & Coello, J. “Sustainable lubrication methods for the machining of titanium alloys: an overview”, Materials, Vol. 12, No. 23, p. 3852, 2019.

Gariani, S., Shyha, I., Inam, F. & Huo, D. “Evaluation of a novel controlled cutting fluid impinging supply system when machining titanium alloys”, Applied Sciences, Vol. 7, No. 6, p.560, 2017.

Ghani, J. A., Haron, C. H. C., Hamdan, S. H., Said, A. Y. M., & Tomadi, S. H. “Failure mode analysis of carbide cutting tools used for machining titanium alloy”, Ceramics International, Vol. 39, No. 4, pp. 4449-4456, 2013.

Gonzalo, O., Beristain, J., Jauregi, H., & Sanz, C. “A method for the identification of the specific force coefficients for mechanistic milling simulation”, International Journal of Machine Tools and Manufacture, Vol. 50, No. 9, pp. 765-774, 2010.

Gradišek, J., Kalveram, M., & Weinert, K. “Mechanistic identification of specific force coefficients for a general end mill”, International Journal of Machine Tools and Manufacture, Vol. 44, No. 4, pp. 401-414, 2004.

Guibert, N., Paris, H., & Rech, J. “A numerical simulator to predict the dynamical behavior of the self-vibratory drilling head”, International Journal of Machine Tools and Manufacture, Vol. 48, No. 6, pp. 644-655, 2008.

Gunay, M., Kacal, A., Turgut, Y. “Optimization of machining parameters in milling of ti-6al-4v alloy using Taguchi method”, Journal of New World Science Academy, Vol. 6, pp. 428-440, 2011.

Gupta, M. K., & Sood, P. K. “Surface roughness measurements in NFMQL assisted turning of titanium alloys: An optimization approach”, Friction, Vol. 5, No. 2, pp. 155-170, 2017.

Gupta, M. K., Sood, P. K., & Sharma, V. S. “Machining parameters optimization of titanium alloy using response surface methodology and particle swarm optimization under minimum-quantity lubrication environment”, Materials and Manufacturing Processes, Vol. 31, No. 13, pp. 1671-1682, 2016.

Gupta, M. K., Mia, M., Pruncu, C. I., Khan, A. M., Rahman, M. A., Jamil, M., Sharma, V.

S. “Modelling and performance evaluation of Al_2O_3, MoS_2 and graphite nanoparticle-assisted MQL in turning titanium alloy: an intelligent approach”, Journal of the Brazilian Society of Mechanical Sciences and Engineesring, Vol. 42, No. 207, pp. 1-21, 2020.

Habak, M., & Lebrun, J. L. “An experimental study of the effect of high-pressure water jet assisted turning (HPWJAT) on the surface integrity”, International Journal of Machine Tools and Manufacture, Vol. 51, No. 9, pp. 661-669, 2011.

Hadzley, A. M., Izamshah, R., Sarah, A. S., & Fatin, M. N. “Finite element model of machining with high pressure coolant for Ti-6Al-4 V alloy”, Procedia Engineering, Vol. 53, pp. 624-631, 2013.

Hasçalık, A., & Çaydaş, U. “Optimization of turning parameters for surface roughness and tool life based on the Taguchi method”, The International Journal of Advanced Manufacturing Technology, Vol. 38, Nos. 9-10, pp. 896-903, 2008.

Hashmi, K. H., Zakria, G., Raza, M. B., & Khalil, S. “Optimization of process parameters for high speed machining of Ti-6Al-4V using response surface methodology”, The International Journal of Advanced Manufacturing Technology, Vol. 85, No. 5, pp. 1847-1856, 2016.

Hazir, E., & Ozcan, T. “Response surface methodology integrated with desirability function and genetic algorithm approach for the optimization of CNC machining parameters”, Arabian Journal for Science and Engineering, Vol. 44, No. 3, pp. 2795-2809, 2019.

Hegab, H., Umer, U., Deiab, I., & Kishawy, H. “Performance evaluation of Ti–6Al–4V machining using nano-cutting fluids under minimum quantity lubrication”, The International Journal of Advanced Manufacturing Technology, Vol. 95, No. 9, pp. 4229-4241, 2018.

Hillerborg, A., Modéer, M., & Petersson, P. E. “Analysis of crack formation and crack growth in concrete by means of fracture mechanics and finite elements”, Cement and Concrete Research, Vol. 6, No. 6, pp. 773-781 1976.

Hong, H. A. T. J. M., Riga, A. T., Gahoon, J. M., & Scott, C. G. “Machinability of steels and titanium alloys under lubrication”, Wear, Vol. 162, pp. 34-39, 1993.

Hong, S. Y., I. Markus, Jeong, Woo-cheo. “New cooling approach and tool life improvement in cryogenic machining of titanium alloy Ti-6Al-4V”, International journal of machine tools and manufacture, Vol. 41, No. 15, pp.2245-2260, 2001.

Hsu, Q. C. “Optimization of minimum quantity lubricant conditions and cutting parameters in hard milling of AISI H13 steel”, Applied Sciences, Vol. 6, No. 3, p. 83, 2016.

Hughes, J. I., Sharman, A. R. C., & Ridgway, K. “The effect of cutting tool material and edge geometry on tool life and workpiece surface integrity”, Proceedings of the Institution of Mechanical Engineers, Part B: Journal of Engineering Manufacture, Vol. 220, No. 2, pp.93-107, 2006.

Ikhlas, M., Athmane, Y. M., Hamza, B., Ahmed, K., Mohamed, E. “Prediction of surface roughness and cutting forces using RSM, ANN, and NSGA-II in finish turning of AISI 4140 hardened steel with mixed ceramic tool", International Journal of Advanced Manufacturing Technology, Vol. 97, Nos. (5-8), pp. 1931-1949, 2018.

Ingle, S. S. "The micromechanisms of cemented carbide cutting tool wear" (Doctoral dissertation), 1993.

Islam, A. K. M., Mia, M., & Dhar, N. R. "Effects of internal cooling by cryogenic on the machinability of hardened steel", The International Journal of Advanced Manufacturing Technology, Vol. 90, No. 1, pp. 11-20, 2017.

Ishak, M. H. H., Ismail, F., Che Mat, S., Abdullah, M. Z., Abdul Aziz, M. S., & Idroas, M. Y. "Numerical analysis of nozzle flow and spray characteristics from different nozzles using diesel and biofuel blends", Energies, Vol. 12, No. 2, 281, 2019.

Jamaludin, A. S., Hosokawa, A., Furumoto, T., Koyano, T., & Hashimoto, Y. "Evaluation of the minimum quantity lubrication in orthogonal cutting with the application of finite element method", International Journal of Mechanical & Mechatronics Engineering, Vol. 17, No. 1, pp. 104-109, 2017.

Jamil, M., Khan, A. M., Hegab, H., Gong, L., Mia, M., Gupta, M. K., He, N. "Effects of hybrid Al_2O_3-CNT nanofluids and cryogenic cooling on machining of Ti–6Al–4V", International Journal of Advanced Manufacturing Technology, Vol. 102, Nos. (9-12), pp. 3895-3909, 2019.

Jawaid, A., Sharif, S., & Koksal, S. "Evaluation of wear mechanisms of coated carbide tools when face milling titanium alloy", Journal of Materials Processing Technology, Vol. 99, Nos. 1-3, pp. 266-274, 2000.

Jebaraj, M., Pradeep Kumar, M., Yuvaraj, N., Mujibar Rahman, G. "Experimental study of the influence of the process parameters in the milling of Al6082-T6 alloy", Materials and Manufacturing Processes, Vol. 34, No.12, pp. 1411-1427, 2019.

Johnson, G.R. "A constitutive model and data for materials subjected to large strains, high strain rates, and high temperatures", Proceedings 7th International Symposium on Ballistics, pp.541-547, 1983.

Joshi, S. S., & Melkote, S. N. "An explanation for the size-effect in machining using strain gradient plasticity", Journal of Manufacturing Science and Engineering, Vol. 126, No.4, pp. 679-684, 2004.

Joshi, S., Pawar, P., Tewari, A., & Joshi, S. S. "Effect of β phase fraction in titanium alloys on chip segmentation in their orthogonal machining", CIRP journal of manufacturing science and technology, Vol.7, No. 3, pp. 191-201, 2014.

Kaminski, J., & Alvelid, B. "Temperature reduction in the cutting zone in water-jet assisted turning", Journal of Materials Processing Technology, Vol. 106, Nos. (1-3), pp. 68-73, 2000.

Kamruzzaman, M., & Dhar, N. R. "The effect of applying high-pressure coolant (HPC) jet in machining of 42CrMo4 steel by uncoated carbide inserts", Journal of Mechanical

Engineering, Vol. 39, No. 2, pp. 71-77, 2008.

Kamruzzaman, M., & Dhar, N. R. "The influence of high-pressure coolant on temperature tool wear and surface finish in turning 17CrNiMo6 and 42CrMo4 steels", Journal of Engineering Applied Sciences, Vol. 4, No. 6, pp. 93-103, 2009.

Kamruzzaman, M., Rahman, S. S., Ashraf, M. Z. I., & Dhar, N. R. "Modelling of chip–tool interface temperature using response surface methodology and artificial neural network in HPC-assisted turning and tool life investigation", The International Journal of Advanced Manufacturing Technology, Vol. 90, No. 5-8, pp. 1547-1568, 2017.

Kanellos, P., Karkalos, N. E., & Markopoulos, A. P. "Numerical Simulation of Machining Using a Coupled FEM-CFD Approach", Procedia Manufacturing, Vol. 41, pp. 795-802, 2019.

Kao, Y.C., Nguyen, N.T., Chen, M.S. and Su, S.T. "A prediction method of cutting force coefficients with helix angle of flat-end cutter and its application in a virtual three-axis milling simulation system",The International Journal of Advanced Manufacturing Technology, Vol.77, No. 9, pp.1793-1809, 2015.

Karas, A., Bouzit, M., & Belarbi, M. "Development of a thermal model in the metal cutting process for prediction of temperature distributions at the tool-chip-workpiece interface", Journal of theoretical and applied mechanics, Vol. 51, No. 3, pp. 553-567, 2013.

Ke, Q., Xu, D., & Xiong, D. "Cutting zone area and chip morphology in high-speed cutting of titanium alloy Ti-6Al-4V", Journal of Mechanical Science and Technology, Vol. 31, No. 1, pp. 309-316, 2017.

Kim, J. S., Kim, J. W., & Lee, S. W. "Experimental characterization on micro-end milling of titanium alloy using nanofluid minimum quantity lubrication with chilly gas", The International Journal of Advanced Manufacturing Technology, Vol. 91, No. 5, pp. 2741-2749, 2017.

Kim, S. H., Lee, S. W., Han, S., & Kim, S. M. "Numerical investigation of thermal characteristics of spray cooling with minimum quantity lubrication in milling process", Applied Mathematical Modelling, Vol. 65, pp. 137-147, 2019.

Kline, W. A., DeVor, R. E., & Lindberg, J. R. "The prediction of cutting forces in end milling with application to cornering cuts", International Journal of Machine Tool Design and Research, Vol. 22, No. 1, pp. 7-22, 1982.

Klocke, F. A. E. G., & Eisenblätter, G. "Dry cutting", CIRP Annals, Vol. 46, No. 2, pp. 519-526, 1997.

Klocke, F., Döbbeler, B., Peng, B., & Lakner, T. "FE-simulation of the cutting process under consideration of cutting fluid", Procedia CIRP, Vol. 58, pp. 341-346, 2017.

Ko, J. H., & Cho, D. W. "Determination of cutting-condition-independent coefficients and runout parameters in ball-end milling", The International Journal of Advanced Manufacturing Technology, Vol. 26, No. 11-12, pp. 1211-1221, 2005.

Ko, D. H., Ko, D. C., Lim, H. J., Lee, J. M., & Kim, B. M. "Prediction and measurement of relieved residual stress by the cryogenic heat treatment for Al6061 alloy: mechanical properties and microstructure", Journal of Mechanical Science and Technology, Vol. 27, No. 7, pp. 1949-1955, 2013.

Komanduri, R., & Hou, Z. B. "On thermoplastic shear instability in the machining of a titanium alloy (Ti-6Al-4V)", Metallurgical and Materials Transactions A, Vol. 33, No. 9, p. 2995, 2002.

Koné, F., Czarnota, C., Haddag, B., & Nouari, M. "Modelling of velocity-dependent chip flow angle and experimental analysis when machining 304L austenitic stainless steel with groove coated-carbide tools", Journal of Materials Processing Technology, Vol. 213, No. 7, pp. 1166-1178, 2013.

Kosaraju, S., & Anne, V. G. "Optimal machining conditions for turning Ti-6Al-4V using response surface methodology", Advances in Manufacturing, Vol. 1, No. 4, pp. 329-339, 2013.

Kovac, P., & Sidjanin, L. "Investigation of chip formation during milling", International journal of production economics, Vol. 51, Nos.1-2, pp. 149-153, 1997.

Kovacevic, R., Cherukuthota, C., & Mazurkiewicz, M. "High pressure waterjet cooling/lubrication to improve machining efficiency in milling", International Journal of Machine Tools and Manufacture, Vol. 35, No. 10, pp. 1459-1473, 1995.

Kumar, A. R., Roy, S., Joshi, K. K., Sahoo, A. K., & Das, R. K. "Machining of Ti-6Al-4V ELI alloy: a brief review", In IOP Conference Series: Materials Science and Engineering, Vol. 390, No. 1, p. 012112, IOP Publishing, July, 2018.

Kustas, F. M., Fehrehnbacher, L. L., & Komanduri, R. "Nanocoatings on cutting tools for dry machining", CIRP Annals, Vol. 46, No. 1, pp. 39-42, 1997.

Lai, X., Li, H., Li, C., Lin, Z., & Ni, J. "Modelling and analysis of micro scale milling considering size effect, micro cutter edge radius and minimum chip thickness", International Journal of Machine Tools and Manufacture, Vol. 48, No.1, pp. 1-14, 2008.

Lalwani, D.I., Mehta, N.K. & Jain, P.K. "Extension of Oxley's predictive machining theory for Johnson and Cook flow stress model", Journal of materials processing technology, Vol. 209, Nos. 12-13 pp.5305-5312, 2009.

Lazoglu, I., & Altintas, Y. "Prediction of tool and chip temperature in continuous and interrupted machining", International Journal of Machine tools and manufacture, Vol. 42, No. 9, pp. 1011-1022, 2002.

Łępicka, M., & Grądzka-Dahlke, M. "Surface Modification of TI6AL4V Titanium Alloy for Biomedical Applications and Its Effect on Tribological Performance-A Review", Reviews on Advanced Materials Science, Vol. 46, No. 1, 2016.

Lee, P., & Altintaş, Y. "Prediction of ball-end milling forces from orthogonal cutting data", International Journal of Machine Tools and Manufacture, Vol. 36, No. 9, pp. 1059-1072, 1996.

Li, C., Lai, X., Li, H., & Ni, J. "Modelling of three-dimensional cutting forces in micro-end-milling", Journal of Micromechanics and Microengineering, Vol. 17, No. 4, pp. 671, 2007.

Li, A., Zhao, J., Zhou, Y., Chen, X., Wang, D. "Experimental investigation on chip morphologies in high-speed dry milling of titanium alloy Ti-6Al-4V", International Journal of Advanced Manufacturing Technology, Vol. 62, Nos. (9-12), pp. 933-942, 2012.

Li, A., Zhao, J., Hou, G. "Effect of cutting speed on chip formation and wear mechanisms of coated carbide tools when ultra-high-speed face milling titanium alloy Ti-6Al-4V", Advanced Mechanical Engineering, Vol. 9, No. 7, 2017.

Li, L., Wu, M., Liu, X., Cheng, Y., & Yu, Y. "Experimental study of the wear behavior of PCBN inserts during cutting of GH4169 superalloys under high-pressure cooling", The International Journal of Advanced Manufacturing Technology, Vol. 95, No. 5, pp. 1941-1951, 2018.

Li, M., Yu, T., Li, H., Yang, L., Shi, J., & Wang, W. "Research on surface integrity in graphene nanofluid MQL milling of TC21 alloy", International Journal of Abrasive Technology, Vol. 9, No. 1, pp. 49-59, 2019.

Lin, C.J., Lui, Y.T., Lin, Y.F., Wang, H.B., Liang, S.Y. & Wang, J.J.J. "Prediction of shearing and ploughing constants in milling of inconel 718", Journal of Manufacturing and Materials Processing, Vol. 5, No. 1, p.8, 2021.

List, G., Nouari, M., G'ehin, D., Gomez, S., Manaud, J. P., & Petitcorps, Y. L., "Wear Behavior of Cemented Carbide Tools in Dry Machining of Aluminum Alloy", International Journal of Wear; Vol. 259, pp. 1177- 1189, 2005.

Liu, Z. Q., Cai, X. J., Chen, M., & An, Q. L. "Investigation of cutting force and temperature of end-milling Ti–6Al–4V with different minimum quantity lubrication (MQL) parameters", Proceedings of the Institution of Mechanical Engineers, Part B: Journal of Engineering Manufacture, Vol. 225, No. 8, pp. 1273-1279, 2011.

Machado, A. R., Wallbank, J., Pashby, I. R., & Ezugwu, E. O. "Tool performance and chip control when machining Ti6A14V and Inconel 901 using high pressure coolant supply", Machining Science and Technology, Vol. 2, No. 1, pp. 1-12, 1998.

Maier, H. J., Herbst, S., Denkena, B., Dittrich, M. A., Schaper, F., Worpenberg, S., ... & Maus-Friedrichs, W. "Towards Dry Machining of Titanium-Based Alloys: A New Approach Using an Oxygen-Free Environment", Metals, Vol. 10, No. 9, p-1161, 2020.

Mello, G. D., & Pai, P. S. "Surface roughness modelling in high speed turning of ti-6Al-4V using response surface methodology", Materials Today: Proceedings, Vol. 5,No. 5, pp. 11686-11696, 2018.

Merchant, M.E. "Mechanics of the metal cutting process. I. Orthogonal cutting and a type 2 chip", Journal of applied physics, Vol. 16, No.5, pp.267-275, 1945.

Mia, M., & Dhar, N. R. Effect of high-pressure coolant jet on cutting temperature, tool wear and surface finish in turning hardened (HRC 48) steel. Journal of Mechanical Engineering, Vol. 45, No.1, pp. 1-6, 2015.

Mia, M., & Dhar, N. R. “Optimization of surface roughness and cutting temperature in high-pressure coolant-assisted hard turning using Taguchi method”, The International Journal of Advanced Manufacturing Technology, Vol. 88, No.1-4, pp. 739-753, 2017.

Mia, M. “Multi-response optimization of end milling parameters under through-tool cryogenic cooling condition”, Measurement, Vol. 111, pp. 134-145, 2017.

Mia, M., Khan, M. A., Rahman, S. S., & Dhar, N. R. “Mono-objective and multi-objective optimization of performance parameters in high-pressure coolant assisted turning of Ti-6Al-4V”, The International Journal of Advanced Manufacturing Technology, Vol. 90, No. 1-4, pp. 109-118, 2017a.

Mia, M., Khan, M. A., & Dhar, N. R. “High-pressure coolant on flank and rake surfaces of tool in turning of Ti-6Al-4V: investigations on surface roughness and tool wear”, The International Journal of Advanced Manufacturing Technology, Vol. 90, Nos. 5-8, pp. 1825-1834, 2017b.

Mia, M., Al Bashir, M., Khan, M. A., & Dhar, N. R. “Optimization of MQL flow rate for minimum cutting force and surface roughness in end milling of hardened steel (HRC 40)”, The International Journal of Advanced Manufacturing Technology, Vol. 89, Nos. 1-4, pp. 675-690, 2017c.

Mia, M., Khan, M. A., Dhar, N. R. “Study of surface roughness and cutting forces using ANN, RSM, and ANOVA in turning of Ti-6Al-4V under cryogenic jets applied at flank and rake faces of coated WC tool”, International Journal of Advanced Manufacturing Technology , Vol. 93, No. 1, pp. 975-991, 2017d.

Mia, M., & Dhar, N. R. “Effects of duplex jets high-pressure coolant on machining temperature and machinability of Ti-6Al-4V super alloy”, Journal of Materials Processing Technology, Vol. 252, pp. 688-696, 2018.

Mia, M., Dey, P. R., Hossain, M. S., Arafat, M. T., Asaduzzaman, M., Ullah, M. S., & Zobaer, S. T. “Taguchi S/N based optimization of machining parameters for surface roughness, tool wear and material removal rate in hard turning under MQL cutting condition”, Measurement, 122, 380-391, 2018.

Mia, M., & Dhar, N. R. “Prediction and optimization by using SVR, RSM and GA in hard turning of tempered AISI 1060 steel under effective cooling condition”, Neural Computing and Applications, Vol. 31, No. 7, pp. 2349-2370, 2019.

Mohammadpour, M., Razfar, M. R., & Saffar, R. J. “Numerical investigating the effect of machining parameters on residual stresses in orthogonal cutting”, Simulation modelling practice and theory, Vol. 18, No. 3, pp. 378-389, 2010.

Mokhtar, A., & Razak, N. H. “Response Surface Methodology (RSM) Model to Evaluate Surface Roughness in Machining of Titanium Alloy (Ti-6Al–4V) Using End Milling Process”, In Recent Trends in Manufacturing and Materials Towards Industry 4.0:

Selected Articles from iM3F 2020, Malaysia (pp. 107-119). Springer Singapore, 2021.

Mouritz, A. P. "Processing and machining of aerospace metals. In Introduction to Aerospace Materials", 1st Edition, Woodhead Publishing: Cambridge, UK, pp. 154–172, 2012.

Musavi, S. H., Davoodi, B., & Niknam, S. A. "Effects of reinforced nanofluid with nanoparticles on cutting tool wear morphology", Journal of Central South University, Vol. 26, No. 5, pp. 1050-1064, 2019.

Narita, H. "A determination method of cutting coefficients in ball end milling forces model", International Journal of Automation Technology, Vol. 7, No. 1, pp. 39-44, 2013.

Nabhani, F. "Machining of aerospace titanium alloys", Robotics and Computer-Integrated Manufacturing, Vol. 17, Nos. 1-2, pp. 99-106, 2001.

Nam, J., Kim, J. W., Kim, J. S., Lee, J., & Lee, S. W. "Parametric analysis and optimization of nanofluid minimum quantity lubrication micro-drilling process for titanium alloy (Ti-6Al-4V) using response surface methodology and desirability function", Procedia Manufacturing, Vol. 26, pp. 403-414, 2018.

Nandy, A. K., Gowrishankar, M. C., & Paul, S. "Some studies on high-pressure cooling in turning of Ti–6Al–4V", International journal of machine tools and manufacture, Vol. 49, No.2, pp. 182-198, 2009.

Naves, V. T. G., Da Silva, M. B., & Da Silva, F. J. "Evaluation of the effect of application of cutting fluid at high-pressure on tool wear during turning operation of AISI 316 austenitic stainless steel", Wear, Vol. 302, Nos.1-2, pp.1201-1208, 2013.

Obikawa, T., & Yamaguchi, M. "Computational fluid dynamic analysis of coolant flow in turning", Procedia CIRP, Vol. 8, pp. 271-275, 2013.

Okafor, A. C., & Sultan, A. A. Development of a mechanistic cutting force model for wavy-edge bull-nose helical end-milling of inconel 718 under emulsion cooling strategy. Applied Mathematical Modelling, Vol. 40, No. 4, pp. 2637-2660, 2016.

Outeiro, J. C., Pina, J. C., M'saoubi, R., Pusavec, F., & Jawahir, I. S. "Analysis of residual stresses induced by dry turning of difficult-to-machine materials", CIRP annals, Vol. 57, No. 1, pp. 77-80, 2008.

Oxley, P. L. B., & Welsh, M. J. M. "Calculating the shear angle in orthogonal metal cutting from fundamental stress-strain-strain rate properties of the work material", In. Proceedings of the Fourth International Conference on Machine Tool Design and Research, pp. 73-86, 1963.

Palanisamy, S., Townsend, D., Scherrer, M., Andrews, R., & Dargusch, M. S. "High-pressure coolant application in milling titanium", In Materials Science Forum , Vol. 618, pp. 89-92. Trans Tech Publications Ltd, 2009.

Park, K. H., Yang, G. D., Suhaimi, M. A., Lee, D. Y., Kim, T. G., Kim, D. W., & Lee, S. W. "The effect of cryogenic cooling and minimum quantity lubrication on end milling of titanium alloy Ti-6Al-4V", Journal of Mechanical Science and Technology, Vol. 29, No.12, pp. 5121-5126, 2015.

Park, K. H., Suhaimi, M. A., Yang, G. D., Lee, D. Y., Lee, S. W., & Kwon, P. “Milling of titanium alloy with cryogenic cooling and minimum quantity lubrication (MQL)”, International Journal of Precision Engineering and Manufacturing, Vol. 18, No. 1, pp. 5-14, 2017.

Patil, S., Jadhav, S., Kekade, S., Supare, A., Powar, A., & Singh, R. K. P. “The influence of cutting heat on the surface integrity during machining of titanium alloy Ti6Al4V”, Procedia Manufacturing, Vol. 5, pp. 857-869, 2016.

Paschoalinoto, N. W., Batalha, G. F., Bordinassi, É. C., Ferrer, J. A. G., Lima Filho, A. F. D., Ribeiro, G. D. L., & Cardoso, C. “MQL strategies applied in Ti-6Al-4V alloy milling: comparative analysis between experimental design and artificial neural networks”, Materials, Vol. 13, pp. 1-29, 2021.

Pejryd, L., Beno, T., & Isaksson, M. “Machining aerospace materials with room-temperature and cooled minimal-quantity cutting fluids”, Part B: Journal of Engineering Manufacture, Vol. 225, pp. 74–86, 2010.

Perri, G. M., Bräunig, M., Di Gironimo, G., Putz, M., Tarallo, A., & Wittstock, V. “Numerical modelling and analysis of the influence of an air cooling system on a milling machine in virtual environment”, The International Journal of Advanced Manufacturing Technology, Vol. 86, No. 5, pp. 1853-1864, 2016.

Pervaiz, S., Deiab, I., & Darras, B. “Power consumption and tool wear assessment when machining titanium alloys”, International Journal of Precision Engineering and Manufacturing, Vol. 14, No. 6, pp. 925–936, 2013.

Pervaiz, S., Deiab, I., Rashid, A., & Nicolescu, M. “Minimal quantity cooling lubrication in turning of Ti6Al4 V: Influence on surface roughness, cutting force and tool wear”, Proceedings of the Institution of Mechanical Engineers, Part B: Journal of Engineering Manufacture, Vol. 231, pp. 1542–1558, 2015.

Pigott, R. J. U.S. Patent No. 2,653,517. Washington, DC: U.S. Patent and Trademark Office, 1953.

Podder, B., & Paul, S. “Improvement of machinability in end milling of Nimonic C-263 by application of high-pressure coolant”, International Journal of Machining and Machinability of Materials, Vol. 11, No. 4, pp. 418-433, 2012.

Pradhan, S. “Optimization of Machining Parameter Characteristics during Turning of Ti-6Al-4V using Desirability Function Analysis”, Materials Today: Proceedings, Vol. 5, No. 11, pp. 25740-25749, 2018.

Prasath, K. M., Pradheep, T., & Suresh, S. “Application of taguchi and response surface methodology (RSM) in steel turning process to improve surface roughness and material removal rate”, Materials Today: Proceedings, Vol. 5, No. 11, pp. 24622-24631, 2018.

Pusavec, F., Deshpande, A., Yang, S., M'Saoubi, R., Kopac, J., Dillon, J. r. O. W., Jawahir, I. S. “Sustainable machining of high-temperature Nickel alloy–Inconel 718: part 1–

predictive performance models", Journal of Cleaner Production, Vol.15, No. 81, pp. 255-269, 2014.

Kumar, P. M., Amarnath, K., & Sunil Kumar, M. "A review on heat generation in metal cutting", International Journal of Engineering and Management Research, Vol. 4, No. 4, pp. 193-197, 2015.

Rashid, R. A., Sun, S., Wang, G., & Dargusch, M. S. "Machinability of a near beta titanium alloy", Proceedings of the Institution of Mechanical Engineers, Part B: Journal of Engineering Manufacture, Vol. 225, No. 12, pp. 2151-2162, 2011.

Ramana, M. V., & Aditya, Y. S. "Optimization and influence of process parameters on surface roughness in turning of titanium alloy", Materials Today: Proceedings, Vol. 4, No. 2, pp. 1843-1851, 2017.

Rao, S., & Shunmugam, M. S. "Analytical modelling of micro end-milling forces with edge radius and material strengthening effects", Machining Science and Technology, Vol. 16, No. 2, pp. 205-227, 2012.

Saha, S. "Optimization of process parameters for residual stress analysis in turning alloy steel under high-pressure coolant jet condition", M.Sc. Disser-tation, Bangladesh University of Engineering & Technology ,2018.

Saha, S., Zaman, P. B., Tusar, M., Hasan, I., & Dhar, N. R. "Multi-objective genetic algorithm (Moga) based optimization of high-pressure coolant assisted hard turning of 42CrMo4 steel", International Journal on Interactive Design and Manufacturing (IJIDeM), pp.1-20, 2022.

Sahoo, S. P., Datta, S. "Dry, MQL, and Nanofluid MQL Machining of Ti–6Al–4V Using Uncoated WC–Co Insert: Application of Jatropha Oil as Base Cutting Fluid and Graphene Nanoplatelets as Additives", Arabian Journal of Science and Engineering, Vol. 45, No. 11, pp. 9599-9618, 2020.

Sahu, N. K., Andhare, A. B. "Prediction of residual stress using RSM during turning of Ti–6Al–4V with the 3D FEM assist and experiments", SN Applied Sciences, Vol. 1, No. 8, pp. 1-4, 2019.

Sen, B., Mia, M., Krolczyk, G. M., Mandal, U. K., & Mondal, S. P. "Eco-friendly cutting fluids in minimum quantity lubrication assisted machining: a review on the perception of sustainable manufacturing", International Journal of Precision Engineering and Manufacturing-Green Technology, Vol. 8, pp. 249-280, 2019.

Senthil Kumar, A., Rahman, M., & Ng, S. L. "Effect of high-pressure coolant on machining performance", The International Journal of Advanced Manufacturing Technology, Vol. 20, No.2, pp. 83-91, 2002.

Setia, S., & Chauhan, S. R. "Comparative analysis and optimization of FEM and RSM based regression model with experimental results for the dry turning of SiCp-Al7075 composite", Silicon, Vol. 13, No. 12, pp. 4681-4701, 2021.

Shanmughasundaram, P., & Subramanian, R. "Influence of graphite and machining parameters on the surface roughness of Al-fly ash/graphite hybrid composite: a Taguchi approach", Journal of Mechanical Science and Technology, Vol. 27, No. 8, pp. 2445-2455, 2013.

Shastri, A., Nargundkar, A., Kulkarni, A. J., & Benedicenti, L. "Optimization of process parameters for turning of titanium alloy (Grade II) in MQL environment using multi-CI algorithm", SN Applied Sciences, Vol. 3, No. 2, pp. 1-12, 2021.

Shin, Y. C., & Waters, A. J. "A new procedure to determine instantaneous cutting force coefficients for machining force prediction", International Journal of Machine Tools and Manufacture, Vol. 37, No. 9, pp. 1337-1351, 1997.

Shokrani, A., Dhokia, V., Muñoz-Escalona, P., & Newman, S. T. " State-of-the-art cryogenic machining and processing", International Journal of Computer Integrated Manufacturing, Vol. 26, No. 7, pp. 616-648, 2013.

Shokrani, A., Al-Samarrai, I., & Newman, S. T. "Hybrid cryogenic MQL for improving tool life in machining of Ti-6Al-4V titanium alloy", Journal of Manufacturing Processes, Vol. 43, pp. 229-243, 2019.

Singh, R., Dureja, J. S., Dogra, M., & Randhawa, J. S. "Optimization of machining parameters under MQL turning of Ti-6Al-4V alloy with textured tool using multi-attribute decision-making methods", World Journal of Engineering, Vol. 16, No. 5, pp. 648-659, 2019.

Słodki, B., Zębala, W., & Struzikiewicz, G. "Turning titanium alloy, grade 5 ELI, with the implementation of high-pressure coolant" Materials, Vol. 12, No. 5, p. 768, 2019.

Sivasakthivel, P. S., & Sudhakaran, R. "Optimization of machining parameters on temperature rise in end milling of Al 6063 using response surface methodology and genetic algorithm", The International Journal of Advanced Manufacturing Technology, Vol. 67, Nos. 9-12, pp. 2313-2323, 2013.

Söderberg, S., & Hogmark, S. "Wear mechanisms and tool life of high speed steels related to microstructure", Wear, Vol. 110, Nos. 3-4, pp. 315-329, 1986.

Sonawane, H. A., & Joshi, S. S. "Analytical modelling of chip geometry and cutting forces in helical ball end milling of superalloy Inconel 718", CIRP Journal of Manufacturing Science and Technology, Vol. 3, No. 3, pp. 204-217, 2010.

Srinivasa, Y.V. & Shunmugam, M.S. "Mechanistic model for prediction of cutting forces in micro end-milling and experimental comparison", International Journal of Machine Tools and Manufacture, Vol. 67, pp.18-27, 2013.

Stabler, G. V. "The fundamental geometry of cutting tools", Proceedings of the Institution of Mechanical Engineers, Vol. 165, No. 1, pp. 14-26, 1951.

Stampfer, B., Golda, P., Schießl, R., Maas, U., & Schulze, V. "Cryogenic orthogonal turning of Ti-6Al-4V", The International Journal of Advanced Manufacturing Technology, Vol. 111, No. 1, pp. 359-369, 2020.

Sultana, M. N., Zaman, P. B., Dhar, N. R. "Hybrid Taguchi-PCA-utility approach for simultaneous optimisation of multiple responses in turning alloy steel", Advances in Materials and Processing Technology, pp. 1-18, 2021.

Sultana, M. N., & Dhar, N. R. "Hybrid GRA-PCA and modified weighted TOPSIS coupled with Taguchi for multi-response process parameter optimization in turning AISI 1040 steel", Archive of Mechanical Engineering, Vol. 68, No.1, pp. 23-49, 2021.

Sultana, M. N., Zaman, P. B., & Dhar, N. R. "Effects of Nano-fluids Assisted MQL in Machining Processes: A Review", 6th International Conference on Mechanical, Industrial and Energy Engineering, Khulna, BANGLADESH, 19-21 December, 2020a.

Sultana, M. N., Zaman, P. B., & Dhar, N. R. "GRA-PCA coupled with Taguchi for optimization of inputs in turning under cryogenic cooling for AISI 4140 steel", Journal of Production Systems and Manufacturing Science, Vol. 1, No. 2, pp. 40-62, 2020b.

Sultana, M. N., Zaman, P. B., & Dhar, N. R. "Process Parameter optimization of Cryogenic Turning of Ni-Cr Steel using Taguchi Grey Relational Analysis", 6th International Conference on Mechanical, Industrial and Energy Engineering, Khulna, BANGLADESH, 19-21 December, 202°C.

Sultana, M. N., Dhar, N. R., & Zaman, P. B. "A Review on Different Cooling/Lubrication Techniques in Metal Cutting", American Journal of Mechanics and Applications, Vol. 7, No. 4, pp. 71-87, 2019.

Sultan, A.A. & Okafor, A.C. "Effects of geometric parameters of wavy-edge bull-nose helical end-mill on cutting force prediction in end-milling of Inconel 718 under MQL cooling strategy", Journal of Manufacturing Processes, Vol. 23, pp.102-114, 2016.

Sun J, Guo Y. "A comprehensive experimental study on surface integrity by end milling Ti–6Al-4V", Journal of materials processing technology, Vol. 209, pp. 4036–4042, 2009.

Sutherland, J. W., & Devor, R. "An improved method for cutting force and surface error prediction in flexible end milling systems", Transactions of the ASME Journal of Engineering for Industry, Vol. 108, pp. 269–279, 1986.

Syrakos, A., Varchanis, S., Dimakopoulos, Y., Goulas, A., & Tsamopoulos, J. "On the order of accuracy of the divergence theorem (Green-Gauss) method for calculating the gradient in finite volume methods", pp. 1-29, 2017.

Taylor, J. "Carbide cutting tool variance and breakage: unknown factors in machining economics", In Advances in Machine Tool Design and Research, 1967, pp. 487-504.

Taylor, C.M., Hernandez, S.G.A., Marshall, M. and Broderick, M. "Cutting fluid application for titanium alloys Ti-6Al-4V and Ti-10V-2Fe-3Al in a finish turning process", Procedia CIRP, Vol. 77, pp.441-444, 2018.

Tendolkar, A., Damir, A., Attia, H., Hendrick, P., & Diakodimitris, C. "Characterisation and optimisation of minimum quantity lubrication in milling of Ti-6Al-4V alloy using phase Doppler anemometry (PDA)", International Journal of Mechatronics and

Manufacturing Systems, Vol. 7, Nos. 4-6, pp. 296-310, 2014.

Torii, S., & Yang, W. J. "A numerical analysis on flow and heat transfer in the entrance region of an axially rotating pipe", International Journal of Rotating Machinery, Vol. 2, No. 2, pp. 123-129, 1995.

Turkes, E., Orak, S., Neseli, S., & Yaldiz, S. "Linear analysis of chatter vibration and stability for orthogonal cutting in turning", International Journal of Refractory Metals and Hard Materials, Vol. 29, No. 2, pp. 163-169, 2011.

Ucun, İ., Aslantas, K., Özkaya, E., & Cicek, A. "3D numerical modelling of micro-milling process of Ti6Al4V alloy and experimental validation", Advances in Materials and Processing Technologies, Vol. 3, No. 3, pp. 250-260, 2017.

Vardhan, M. V., Sankaraiah, G., Yohan, M., & Rao, H. J. "Optimization of Parameters in CNC milling of P20 steel using Response Surface methodology and Taguchi Method", Materials Today: Proceedings, Vol. 4, No. 8, pp. 9163-9169, 2017.

Wan, M., Zhang, W. H., Tan, G., & Qin, G. H. "New algorithm for calibration of instantaneous cutting-force coefficients and radial run-out parameters in flat end milling", Proceedings of the Institution of Mechanical Engineers, Part B: Journal of Engineering Manufacture, Vol. 221, No. 6, pp. 1007-1019, 2007.

Wan, M., Zhang, W. H., Dang, J. W., & Yang, Y. "A novel cutting force modelling method for cylindrical end mill", Applied Mathematical Modelling, Vol. 34, No.3, pp. 823-836, 2010.

Wang, F., & Wang, Y. "Investigate on effect of cryogenic cooling on oxidation wear of WC-Co carbide tool milling titanium alloy", Machining Science and Technology, Vol. 23, No. 6, pp. 906-924, 2019.

Wang, M., Gao, L., & Zheng, Y. "An examination of the fundamental mechanics of cutting force coefficients", International Journal of Machine Tools and Manufacture, Vol. 78, pp. 1-7, 2014.

Weigand, B., Beer, H. (1992) "Fluid flow and heat transfer in an axially rotating pipe subjected to external convection", International Journal of heat mass transactions, Vol. 35, No. 7, pp. 1803-1809.

Wright, P. K., & Bagchi, A. "Wear mechanisms that dominate tool-life in machining", Journal of Applied Metalworking, Vol. 1, No. 4, pp. 15-23, 1981.

Wu, B., Yan, X., Luo, M., & Gao, G. "Cutting force prediction for circular end milling process", Chinese Journal of Aeronautics, Vol. 26, No.4, pp. 1057-1063, 2013.

Wu, H. B., & Zhang, S. J. "3D FEM simulation of milling process for titanium alloy Ti6Al4V", The International Journal of Advanced Manufacturing Technology, Vol. 71, No. 5, pp. 1319-1326, 2014.

Wu, H., & Zhang, S. "Effects of cutting conditions on the milling process of titanium alloy Ti6Al4V", The International Journal of Advanced Manufacturing Technology, Vol. 77, No. 9, pp. 2235-2240, 2015.

Yang, M., & Park, H. “The prediction of cutting force in ball-end milling”, International Journal of Machine Tools and Manufacture, Vol. 31, No. 1, pp. 45-54, 1991.

Yang, Y., & Zhu, W. “Study on cutting temperature during milling of titanium alloy based on FEM and experiment”, The International Journal of Advanced Manufacturing Technology, Vol. 73, No. 9, pp. 1511-1521, 2014.

Yashiro, T., Ogawa, T., & Sasahara, H. “Temperature measurement of cutting tool and machined surface layer in milling of CFRP”, International Journal of Machine Tools and Manufacture, Vol. 70, pp. 63-69, 2013.

Yin, Q., Li, C., Dong, L., Bai, X., Zhang, Y., Yang, M., ... & Li, R. “Effects of the physicochemical properties of different nanoparticles on lubrication performance and experimental evaluation in the NMQL milling of Ti–6Al–4V”, The International Journal of Advanced Manufacturing Technology, Vol. 99, No. 9, pp. 3091-3109, 2018.

Zachert, C., Liu, H., Lakner, T., Schraknepper, D., & Bergs, T. “CFD simulation to optimize the internal coolant channels of an additively manufactured milling tool”, Procedia CIRP, Vol. 102, pp. 234-239, 2021.

Zaman, P. B., & Dhar, N. R. “Multi-objective optimization of double-jet MQL system parameters meant for enhancing the turning performance of Ti–6Al–4V alloy”, Arabian Journal for Science and Engineering, Vol. 45, No. 11, pp. 9505-9526, 2020.

Zaman, P. B., Sultana, N., & Dhar, N. R. “Quantifying the effects of cooling condition, tool type and cutting parameters on machinability of turning AISI 4140 steel using full factorial DOE”, Journal of Production Systems and Manufacturing Science, Vol. 1, No. 2, pp. 23-49, 2020.

Zaman, P. B., Sultana, M. N., & Dhar, N. R. “Multi-variant hybrid techniques coupled with Taguchi in multi-response parameter optimisation for better machinability of turning alloy steel”, Advances in Materials and Processing Technologies, pp. 1-21, 2021.

Zang, J., Zhao, J., Li, A., & Pang, J. “Serrated chip formation mechanism analysis for machining of titanium alloy Ti-6Al-4V based on thermal property”, The International Journal of Advanced Manufacturing Technology, 98, No.1, pp. 119-127, 2018.

Zeman, P., Bach, P., Trmal, G. “Tool Life of PM-HSS Cutting Tools when Milling of Titanium Alloy”, Manufacturing Technology, Vol. 17, No. 1, pp. 34-35, 2017.

Zerti, O., Yallese, M. A., Khettabi, R., Chaoui, K., & Mabrouki, T. “Design optimization for minimum technological parameters when dry turning of AISI D3 steel using Taguchi method”, The International Journal of Advanced Manufacturing Technology, Vol. 89, Nos. 5-8, pp. 1915-1934, 2017.

Zhang, Y., Outeiro, J. C., & Mabrouki, T. “On the selection of Johnson-Cook constitutive model parameters for Ti-6Al-4 V using three types of numerical models of orthogonal cutting”, Procedia CIRP, Vol. 31, pp. 112-117, 2015.

Zhang, X., Chen, Y., & Hu, J. “Recent advances in the development of aerospace materials”, Progress in Aerospace Sciences, Vol. 97, pp. 22-34, 2018.

Zhang, B., & Coddet, C. “Numerical study on the effect of pressure and nozzle dimension on particle distribution and velocity in laser cladding under vacuum base on CFD”, Journal of Manufacturing Processes, Vol. 23, pp. 54-60, 2016.

Zhang, J. Z., Chen, J. C., & Kirby, E. D. “Surface roughness optimization in an end-milling operation using the Taguchi design method”, Journal of materials processing technology, Vol. 184, Nos.1-3, pp. 233-239, 2007.

Zheng, L., Liang, S. Y., & Melkote, S. N. “Angle domain analytical model for end milling forces”, Journal of Manufacturing Science and Engineering, Vol. 120, No. 2, pp. 252-258, 1998.

Zhao, W., Gong, L., Ren, F., Li, L., Xu, Q., & Khan, A. M. “Experimental study on chip deformation of Ti-6Al-4V titanium alloy in cryogenic cutting”, The International Journal of Advanced Manufacturing Technology, Vol. 96, No. 9, pp. 4021-4027, 2018.

List of Publications

01. **Mst. Nazma Sultana** & N. R. Dhar (2023) "RSM Design-Based Hybrid Approach to Multi-Response Optimization in Milling Ti-6Al-4V Alloy: A Comparative Study", Materials Today: Proceedings. DOI: 10.1016/j.matpr.2023.03.527

02. **Mst. Nazma Sultana** & N. R. Dhar (2023) "Milling Force Modelling with High-Pressure Cooling Strategy: An Integrated Analytical Approach", Materials Today: Proceedings. DOI: 10.1016/j.matpr.2023.04.693.

03. **Mst. Nazma Sultana** & N. R. Dhar (2023) "Performance evaluation of high-pressure cooling by using external rotary liquid applicator in milling Ti–6Al–4V alloy", Heliyon, Vol. 9, No. 7, pp. 1-25, DOI: 10.1016/j. heliyon. 2023.e17671.

04. **Mst. Nazma Sultana** & N. R. Dhar (2023) "Comparative Evaluation and Sensitivity Analysis of Multi-Modelling and Optimization of Milling Ti-6Al-4V Alloy with High-Pressure Coolant Jets", Vol. 9, No. 8, DOI: 10.1016/j. heliyon. 2023.e18582

05. Ashab Shakur, **Mst. Nazma Sultana**, & N. R. Dhar. "Effect of input parameters on chip morphology in surface grinding of Al/SiC-MMC", International Journal of Advanced Manufacturing Technology. (**Accepted with revisions**)

06. **Mst. Nazma Sultana,** A. T. Shams, P. B. Zaman & N. R. Dhar (2023) "Optimization of Cutting Forces and Surface Roughness with Tool Wear Progression in End Milling of Ti- 6Al-4V alloy under Minimum Quantity Lubrication using Combo Mix Nozzle", International Journal of Nano manufacturing. (**Accepted**)

07. **Mst. Nazma Sultana**, & N.R. Dhar (2022) "A Critical Review on the Progress of MQL in Machining Hardened Steels", Advances in Materials and Processing Technology, Vol. 8, No. 4, pp. 3834-3858 DOI: 10.1080/2374068X.2022.2036041.

08. **Mst. Nazma Sultana**, Prianka B. Zaman, & N. R. Dhar (2021) Hybrid Taguchi-PCA-Utility Approach for Simultaneous Optimisation of Multiple Responses in Turning Alloy Steel", Advances in Materials and Processing Technology, Vol. 8, No. 4, pp. 3597-3614. DOI: 10.1080/2374068X.2021.1970996.

09. **Mst. Nazma Sultana**, & N. R. Dhar. (2021) "Hybrid GRA-PCA and modified weighted TOPSIS coupled with Taguchi for multi-response process parameter optimization in turning AISI 1040 steel", Archive of Mechanical Engineering, Vol. 68, No. 1, pp. 23-49. DOI: 10.24425/ame.2020.131707.

10. Prianka B. Zaman, **Nazma Sultana**, & N. R. Dhar. (2021) “Multi-variant Hybrid Techniques coupled with Taguchi in multi-response parameter optimization for better machinability of turning alloy steel”, Advances in Materials and Processing Technology, Vol. 8, No. 3, pp. 3127-3147. DOI: 10.1080/2374068X.2021.1945302.

11. Prianka B. Zaman, **Mst. Nazma Sultana**, & N. R. Dhar. (2020) “Quantifying the Effects of Cooling Condition, Tool Type and Cutting Parameters on Machinability of Turning AISI 4140 Steel using Full Factorial DoE”, Journal of Production Systems And Manufacturing Science, Vol. 1, No. 2, pp. 23-39.

12. **Mst. Nazma Sultana**, P. B. Zaman, & N. R. Dhar. (2020) “GRA-PCA Coupled With Taguchi For Optimization of Inputs In Turning Under Cryogenic Cooling for AISI 4140 Steel” Journal of Production Systems And Manufacturing Science, Vol. 1, No. 2, pp. 40-62.

13. **Mst. Nazma Sultana**, Prianka B. Zaman, N.R. Dhar. (2020) “Process Parameter Optimization of Cryogenic Turning of Ni-Cr Steel using Taguchi Grey Relational Analysis”, 6th International Conference on Mechanical, Industrial and Energy Engineering, 19-21 December, 2020, Khulna, Bangladesh.

14. **Mst. Nazma Sultana**, Prianka B. Zaman, N.R. Dhar. (2020) “Effects Of Nano-Fluids Assisted MQL in Machining Processes: A Review”, 6th International Conference On Mechanical, Industrial and Energy Engineering, 19-21 December, 2020, Khulna, Bangladesh.

15. **Mst. Nazma Sultana**, N. R. Dhar, Prianka Binte Zaman. (2019) “A Review on Different Cooling/Lubrication Techniques in Metal Cutting”, American Journal of Mechanics and Applications, Vol. 7, No. 4, pp. 71-87. DOI: 10.11648/j.ajma.20190704.11.